# Transverse Momentum and Rapidity Spectra of Negative Pions in Nucleus-Nucleus Collisions at 4.2 GeV/*c* Per Nucleon

**By**

**AKHTAR IQBAL**

**76-FBAS/PHDPHY/S16**

**Supervisor:**

**Dr. MUSHTAQ AHMAD**

**Co-supervisor:**

**Dr. KHUSNIDDIN OLIMOV**

**DEPARTMENT OF PHYSICS, FBAS,**

**INTERNATIONAL ISLAMIC UNIVERSITY,**

**ISLAMABAD**

**2019**

# Transverse Momentum and Rapidity Spectra of Negative Pions in Nucleus-Nucleus Collisions at 4.2 GeV/*c* Per Nucleon


**By**

**AKHTAR IQBAL**

**(76-FBAS/PHDPHY/S16)**


A thesis is submitted to

**Department of Physics**

For the award of the degree of

**PHD Physics**

Signature……………………………

**(Chairman, Department of Physics)**

Signature……………………………

**(Dean FBAS, IIU Islamabad)**


**DEPARTMENT OF PHYSICS, FBAS,**

**INTERNATIONAL ISLAMIC UNIVERSITY**

**ISLAMABAD**


**2019**

# Final Approval

It is certified that the work presented in this thesis having title "**Transverse Momentum and Rapidity Spectra of Negative Pions in Nucleus-Nucleus Collisions at 4.2 GeV/*c* Per Nucleon"** by **AKHTAR IQBAL** ( Reg. No. 76-FBAS/PHDPHY/S16) fulfill the requirement for the award of degree of PHD Physics from Department of physics, International Islamic University, Islamabad, Pakistan.

**Viva Voice Committee**

Chairman

**Dr. Wiqar Hussain Shah** __________________________

Supervisor

**Dr. Mushtaq Ahmad** __________________________

Co-Supervisor

**Dr. Khusniddin Olimov** __________________________

External Examiner

**Prof. Dr. Ishaq** __________________________

External Examiner

**Prof. Dr. Arshad Majid Mirza** __________________________

Internal Examiner

**Dr. Zafar Wazir** __________________________

**Dedicated**

**To**

**My Leader, My Captain and My Prime Minister**

**IMRAN KHAN**

# DECLERATION

It is hereby declared that the work presented in this thesis has not been copied from any source, neither as a whole nor a part. Furthermore, the work presented in this dissertation has not been submitted in support of any publication other than those included in this thesis, any other degree or qualification to any other university or institute and recommendable under the plagiarism rules of Higher Education Commission (HEC) Pakistan.

**AKHTAR IQBAL**

**(76-FBAS/PHDPHY/S16)**

# CERTIFICATE

It is certified that **<u>AKHTAR IQBAL</u>**, Registration No. **<u>76-FBAS/PHDPHY/S16</u>** has carried out the research work related to this thesis having title, "Transverse Momentum and Rapidity Spectra of Negative Pions in Nucleus-Nucleus Collisions at 4.2 GeV/*c* Per Nucleon" under my supervision. This work fulfills all the requirements for the award of the degree of <u>PhD Physics</u>.

______________________________


**Dr. MUSHTAQ AHMAD**

**Professor**

**Department of Physics,**

**International Islamic University,**

**Islamabad.**

# ACKNOWLEDGEMENTS

I am very much thankful to **Almighty Allah**, who is the creator of the world and source of wisdom and knowledge. **Allah** has enabled me to complete my research work with great courage and continuous efforts. It was not be possible without the help of Almighty.

Whole of my efforts would be a pack of garbage if I didn't mention the name of my worthy supervisor and Co-supervisor **Prof. Dr. Mushtaq Ahmad** and **Dr.Sc. Khusniddin K. Olimov** in this research project. It went without saying that it was the undaunted and continuous struggle of my learned supervisors, who enabled me to understand the field of High Energy Physics. It is also pertinent to mention here that the instant thesis is also a reflection of efforts, hard work and affection of my respectable supervisors. I also feel myself a lucky student, who had the privilege to work with such a skillful and seasoned supervisors, who have got no parallel in this field. I express my thanks to the staff of Laboratory of High Energies of JINR (Dubna, Russia) and of the Laboratory of Multiple Processes of Physical-Technical Institute of Uzbek Academy of Sciences (Tashkent, Uzbekistan), who took part in the processing of stereophotographs from 2-m propane ($C_3H_8$) bubble chamber of JINR.

Moreover, I would like to express my sincere thanks to all the faculty and staff members of Department of Physics IIU Islamabad. I express my heartiest thanks to my best friends Dr. Ali Zaman (IIUI), Dr. Ijaz (AWKU, Mardan), Dr. Zafar wazir (IIUI) Obaidullah Jan, Qasim Ali (CU, Islamabad) Muhammad Ibrahim Khan (USTB, Bannu) for being very supportive and co-operative throughout my research work.

**Akhtar Iqbal**

# Abstract

## Transverse Momentum and Rapidity Spectra of Negative Pions in Nucleus-Nucleus Collisions at 4.2 GeV/*c* Per Nucleon

In the present analysis, it was studied the characteristics of π-mesons in *AA* collisions at 4.2*A*GeV/*c*. In *nucleus-nucleus* interactions, it was analyzed the dependencies of characteristics of the charged pions at 4.2*A*GeV/*c* on collision centrality. There was a noticeable change in the average kinematical characteristics of the charged pions while increasing the overlap region (increasing the number of participant nucleons) of target and projectile nuclei in *nucleus-nucleus* interactions. The rapidity spectra and transverse momentum distribution of $\pi^-$–mesons were studied systematically in *nucleus-nucleus* interactions at 4.2*A*GeV/*c*. It was analyzed the changes of the $y_{c.m}$ and $p_T$ distributions of $\pi^-$–mesons with changing the collision centralities and mass numbers of the incident projectile and target nuclei. It was important to study the changes of the characteristics of produced pions by changing the collision centralities (central, semi-central and peripheral interaction) of the analyzed *nucleus-nucleus* collisions. The rapidity spectra of $\pi^-$-mesons both in experiment and model in *nucleus-nucleus* interactions at 4.2GeV/*c* were analyzed and compared. The rapidity spectra of pions were fitted by Gaussian model function. The transverse momentum spectra at different ranges and different collision centralities were fitted with different theoretical model functions to compare the experimental and simulated model data. For fitting the experimental and simulated model spectra, we used the Hagedorn Thermodynamic Model and Boltzmann Model function. The transverse momentum spectra obtained from experiment, simulated by the model (Quark Gluon String model) were fitted by these models to extract the important parameters, i.e., the spectral temperatures (inverse slope parameters). The spectral temperatures of $\pi^-$-mesons obtained in present work were compared with those of the previous works with different colliding nuclei and also at comparable incident energies.

Table of Contents

# LIST OF FIGURES

# LIST OF TABLES

## LIST OF ABBREVIATIONS

| | |
|---|---|
| JINR | Joint Institute for Nuclear Research (Dubna, Russia) |
| LHE | Laboratory of High energy |
| $\pi -$ mesons | pions |
| *A* | Nucleus |
| *AA* | Projectile-Target |
| *hA* | *hadron-nucleus* Collisions |
| *AA* | *nucleus-nucleus* Collisions |
| QGSM | Quark Gluon String |
| $P_t$ , $P_T$ | Transverse Momentum |
| $P$, $P_l$ | Total momentum, Longitudinal Momentum |
| $y_{c.m}, y_{c.m.s}$ | Rapidity in center of mass system |
| $N_{\text{part}}$ | The number of participant protons in the collision event |
| *A*GeV/*c* | Giga Electron Volt per light velocity per Nucleon |
| $\sqrt{s_{NN}}$ | Center-mass Energy |

# Chapter 1 INTRODUCTION

## 1.1 History of Pions

In particle Physics hadrons are made of different quarks and they have a strong nuclear force in between them. These hadrons are divided into two main groups. (1) Mesons: Mesons are made of quarks and anti-quarks and (2) Baryons: Baryons contain three quarks combinations. Meson is a Greek word (from Meso) which means 'middle' particle, so Mesons are subatomic particles, which are intermediate in masses between leptons and baryons. Mesons are bosons with integral spin and because of this integral spin pions obey Bose-Einstein statistics. $\pi-$ mesons are one of the lightest particle and they are considered to be very important particles in relativistic nuclear collisions. The production threshold energies for pions are very small (290 MeV for $\pi^{\pm}$ 280 MeV for $\pi^0$). Therefore pions are considered to be very important mesons for studying different nuclear properties of nuclear matter. Pions have very high multiplicity among other mesons in relativistic *nucleus-nucleus* (*AA*), *hadron-hadron* (*hh*) and *hadron-nucleus* (*hA*) collisions. Pions are denoted by the Greek word pi ($\pi$). Pions (contains first generation of quarks) were studied theoretically by Yukawa in 1935. He predicted that mesons are carrier particle in strong nuclear physics. In 1947 mesons (Pions) were discovered from the decay of strange particle (Kaon) from cosmic rays in University of Bristol, England:

$$\text{Cosmic rays}(K^+) \rightarrow 2\pi^+ + \pi^-$$

Table 1.1. Different properties of pions.

| Name | Quark contains | Mass (MeV/$c^2$) | Antiparticle | Life time (s) | Spin | *I* | $I_z$ | Decay Modes |
|---|---|---|---|---|---|---|---|---|
| $\pi^+$ | $u\bar{d}$ | 139.570 | $\pi^-$ | 2.6x10$^{-8}$ | 0 | 1 | +1 | $\mu^+ + \nu_\mu$ |
| $\pi^-$ | $\bar{u}d$ | 139.570 | $\pi^+$ | 2.6x10$^{-8}$ | 0 | 1 | -1 | $\mu^- + \nu_\mu$ |
| $\pi^0$ | $\frac{u\bar{u}+d\bar{d}}{\sqrt{2}}$ | 134.966 | Self | 8.4x10$^{-17}$ | 0 | 1 | 0 | $\gamma + \gamma$ |

In the Table 1.1 three pions with quarks contains, their masses, life time, spin, isospin, the third component and the primary decay modes of charged and neutral pions are shown. The probability of decay of charged pions are 99% in charged muon and muon anti-neutrino, and there is very small (about <<1% probability) that these charged $\pi^{-}$-mesons will be decaying into electron (or positron) and their corresponding neutrinos.

$$\pi^{\pm} \rightarrow e^{\pm} + \nu_e$$

There is a maximum probability (almost 98%) of neutral pions decays into two gammas and other decay modes of neutral pions have very less probabilities [1, 2].

## 1.2 Relativistic Nuclear Collisions and Importance of Pions

The field of relativistic heavy ion nuclear interactions is concerned with role of study and characteristic of nuclear matter in high energy and high density. This hybrid field uses the instruments and techniques of relativistic high energy physics to build our understanding about the basic characteristic and properties of nucleus. In relativistic nuclear interactions at high energies construct a strongly compressed and highly excited nuclear matter in a laboratory. At such extreme conditions different kind of new phenomena can be studied, like phase transition of hadronic matter into the pion production, density isomers, studying the interiors of neutron stars, the dynamics of supernova explosions and a deconfined state of nuclear matter. In such highly dense conditions, it is predicted theoretically a Quark-Gluon Plasma (QGP). In the QGP condition quarks and gluons are no longer considered in confinement stage, but they are freely moving at distance about ($\approx$1fermi), which is almost equal to the size of a hadron. The typical density ($\rho_0$) of nuclear matter in normal case is about 0.16 fm$^3$. In relativistic nuclear collisions the interacting energies of incident projectiles of order of few GeV (1-2 GeV), the density ($\rho$) of nuclear matter are raised by 2-3 times of normal nuclear density [3, 4].

In the figure 1.1 it is shown the nuclear phase diagram. In this diagram the horizontal axis shows baryon density and the vertical axis shows the temperature. It is not easy to understand experimentally and theoretically the nuclear matter phase diagram, but a common conjectured (like water phase diagram) is shown in the diagram. In such extreme condition governing the transitions among these phases is crucial to build a theory of the nuclear equation of state. In case of normal nuclear matter the density (0.16 $fm^3$) and temperature (near zero MeV) are at bottom left in the figure 1.1, and such condition is called the liquid-gas transition boundary. The domain of low energy nuclear physics research was extensively characterized in $20^{th}$ century. In the given figure, under the extreme conditions, the deconfined transition phase diagram can be studied by using models of strong interaction.

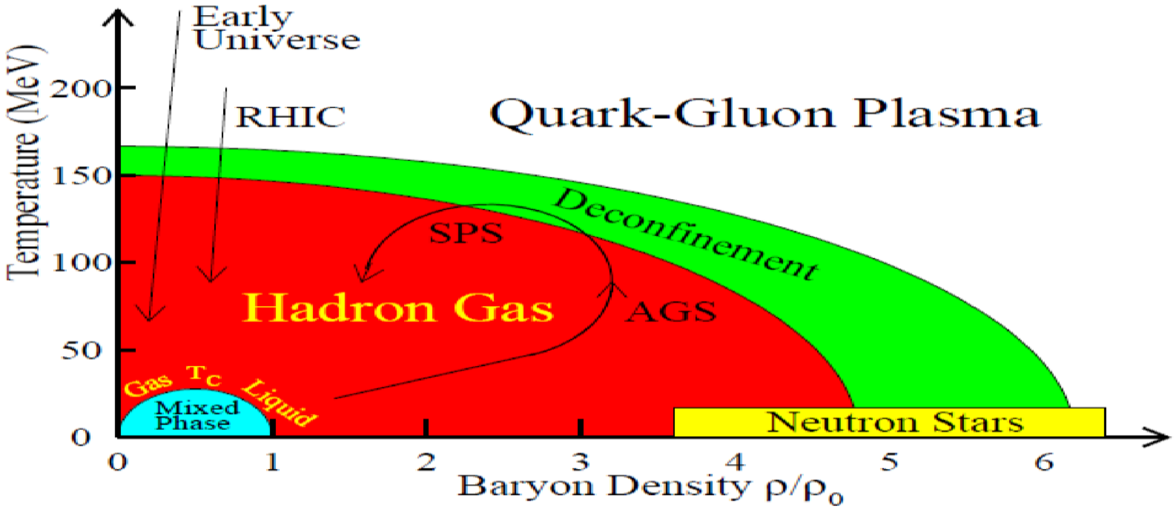


Figure 1.1. The Nuclear matter phase diagram

Using Lattice QCD calculations, with two quarks flavors the temperature of such deconfined matter at fixed baryon density, is almost 150 MeV. If the temperature is fixed (almost zero MeV) the baryon density roughly reaches to 5 times of its normal nuclear matter density and there is a deconfinement of particles in such extreme condition. It is predicted in the model of quark confinement [5-7].

A quark-gluon plasma state is created at LHC and there is about 5.5 trillion degrees Celsius temperature is achieved. There is another very high temperature (about 100 MeV) observed in heavy ions collision at the laboratory of BNL. The system is expended and then cools down from the earlier hot state, using these condition the temperature is extracted from different theoretical models. The room temperature (300K) is approximately 0.025 in eV, and 100 MeV is on the order of one trillion (~ $10^{12}$K). The next nearest man made temperature in laboratory, is the temperature achieved in thermonuclear fission process (~ $10^7$ K). The size of nuclear matter created at this temperature is very small (~ $10^3 fm^3$), but the number of individual particles can be order of a few hundreds to few thousands and statistically the equation of state (EOS) can be obtained from multiplicities of produced particles [3, 8-12].

It is very difficult job to investigate different properties of very high dense nuclear matter in relativistic nuclear interactions by direct experiment. In order to get a very high dense matter with high temperature, and also to find different parameters of the early universe, different heavy nuclei are collided with different energies are used at CERN and other laboratories. Heavy ions collisions are characterized by collisions centralities of projectile and target nuclei. These centralities are analyzed on the basis of participant protons. In LHC mostly proton-proton are studied but also, lead-lead and proton-lead collisions are studied for analysis of heavy ion. In the ALICE experiment, it is investigated Heavy ion collisions and their centralities [13-16]. Nowadays data of different particles on high energies interactions comes from the study of rapidity spectra and transverse momentum distributions of hadrons. In Heavy ion nuclear interactions most of the energies are used in creation of different particles. Similarly, in case of pions, most of incident energies are used in production of pions. Due to lower threshold energies of production of pions, energies are distributed differently among all pions. In heavy ion collisions a fireball is created. This fireball burst and produces pions and other particles. To study this fireball, spectral temperatures of pions are studied and spectral temperatures are obtained from transverse mass (energy) or transverse momentum distributions of π-mesons. It is well known fact that delta resonances have great contributions in pions production in the relativistic nuclear collisions of order of few (1-10) Giga-electron-Volt per nucleon. In the hot and compressional stage of heavy nuclei collisions, delta resonances are generated from the freezing fireball and delta resonances further produce nucleons and pions. It is cleared from these Refs. [17-20] that some pions, which are produced at these energies i.e. 1─15 GeV/nucleon from decay of delta resonances, have low transverse momentum.

### 1.3 The Participant and Spectator Model

In heavy ion relativistic interactions at relativistic energies, the participant and spectator model gives important information. In the figure 1.2, a participant and spectator model is shown. It is shown collisions of target and projectile nuclei at impact parameter of *b*. In the figure it is presented interaction between two heavy nuclei. A given part of incident projectile will overlap with certain portion of target particle. The average binding energy per nucleon of different element is $\approx 8MeV$ . If the incident projectile interacts with target nuclei with high energy at specific impact parameter then the overlapping part will be attached with projectile ion, and the non-interacting part of the ion will fly in same direction and with unchanged velocity. The non-interacting part of projectile ion is called projectile spectators, and similarly there will be also target spectators. The interacting part (the overlap region) of projectile and target ions is called participant region. The participant region consists of projectile and target nucleons and the participant region will usually disintegrate, and gives rise to many fragments. In the figure 1.1 a collisions of two ions are shown. A given part of these ions will meet with each other in certain portion. As can be seen from the figure 1.1 the participants region of colliding ions, and non-interacting portion of both projectile and target spectators [21, 22].

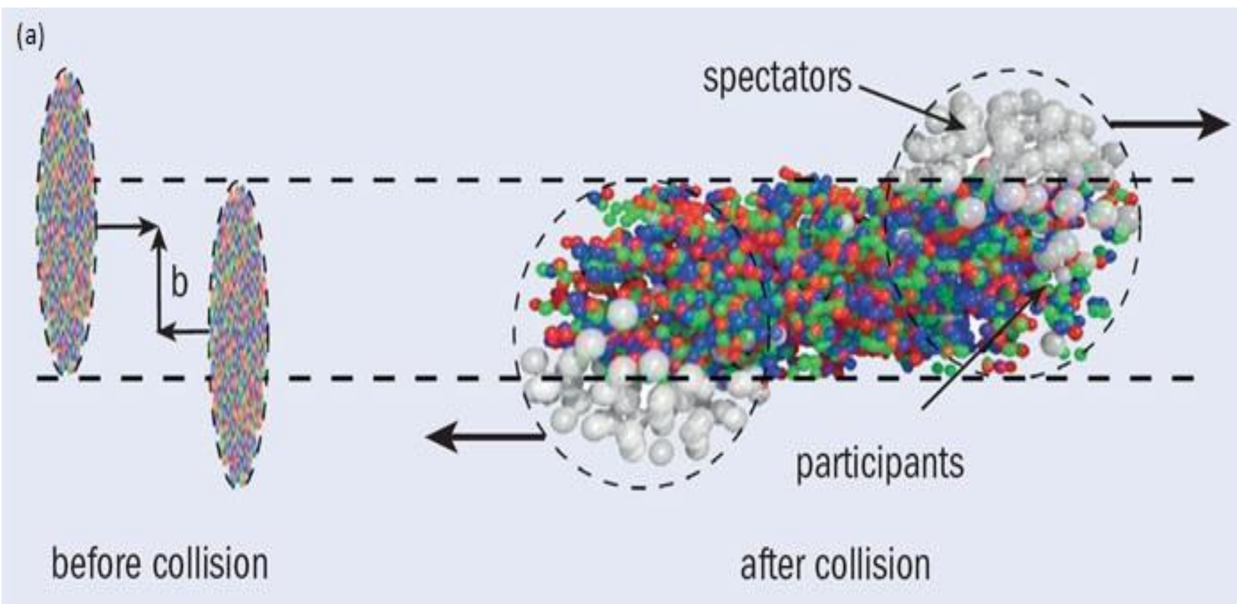


Figure 1.2. The participants and spectators model is shown. In figure it is shown interaction of projectile and target with specified impact parameter ***b***.

## 1.4 The Fireball

A participant region consists of target and projectile particles. This is also called overlap region. The participant and spectator regions are not separated clearly. When the incident projectile interacted with target nuclei then a transition region is established between these particles. The formation of transition region is directly related to the energies and masses of incident projectile and target particles. If the energy of projectile is increased then the transition region becomes smaller. The overlap region is also affected by increasing the mass number of target and projectile nuclei. Inside the overlap region the participant zone is more interesting and has more information about early universe. In heavy ion central collisions, a participant region consists of target and projectile particles, and quarks gluons plasma is formed in that region, and interact freely with each other, and this region is called a fireball [3, 22-25]. It is well known fact that in early phase of collisions, a very hot, dense and excited nuclear matter is created. This high dense nuclear matter (fireball) further produces large number of secondary particles. In this overlap region all nucleons interact very strongly with each other. In the laboratory system (fixed target experiments) at low energies (up to 10 *A* GeV), in central collisions, an excited and compressed nuclear matter is produced.

In Refs. [18] it is shown very briefly a *nucleus-nucleus* interaction can be explained by the following stages.

(i) Initial collision: it is the initial stage of target and projectile nuclei and this process takes place during the initial time of nucleons interactions i.e. ($t = \frac{2R}{\gamma_{cm} c}$).

(ii) Thermalization of overlap region: It is considered to be the second stage. In relativistic *nucleus-nucleus* collisions, when interaction takes place between target and projectile nucleons, the system is thermalized and equilibrium is established in hot and dense matter.

(iii) Expansion and cooling: It is the stage of deconfinement. A fireball is produced as a result of relativistic nuclear collisions. This fireball expands and because of expansion it becomes cool down. It is very difficult to characterize the fireball stage. Most of important calculations are performed because most of the particles are produced from direct interactions or also produced from the decay of different heavy particles. The produced products have primary information about dense and hot matter. It is very difficult to access that hot and dense matter region because of quark confinement. There are experimental procedures which can give useful information about the fireball stage.

We can extract properties of deconfined stages through different phenomenological models.

(iv) Chemical freeze-out: This stage is called the stage of hadronization. In this stage the inelastic collisions of particles stop and hadrons are produced and are distributed in different particles.

(v) Kinetic freeze out: It is the last stage before the production of secondary particles. In this stage the elastic collisions between interacting 4particles in fireball are stopped. In Refs. [18], it is explained that the separation between chemical freeze-out and kinetic freeze-out depends on the different experiment for different colliding particles and these particles are interacting with different energies. At small energies and small masses of target and projectile nuclei there is no difference between chemical freeze-out and kinetic freeze-out. Chemical freeze-out and kinetic freeze-out are almost same at our energies ($\sqrt{s_{nn}}$ = 3.14 GeV), and this separation increases when the energies are higher. After this stage secondary particles produce in collective form. The collective flow of particles is very important factor of *AA* collisions. This effect was initially studied at Bevalac experiment at low energies. In Ref. [26] it was observed that there was a strong increase in both $<\beta_T>$ and temperature at small energies i.e. about 1 Giga electron-Volt/nucleon in Lab system.

In Ref. [18] ranges of different parameters in fireball are shown at different energies, and these ranges are almost the same in low energies ($\sqrt{s_{nn}}$ = 3.14 GeV) as well. For example different parameters with different ranges are shown .i.e.

Pressure: $P$ = 100-300 $MeV(fm)^{-3}$, ($1MeV(fm)^{-3} \cong 10^{33}\,Pa$).

Temperature: $T$ = 100-500 MeV.

Volume: the volume reaches up to several thousand $fm^3$.

Density: $\rho$ = 1-10 $\rho_0$, $\rho_0$ = 0.16 $fm^3$.

Time: 10-20 $\dfrac{fm}{c}$ (about 3-6x10$^{-23}$ s).

## 1.5 Properties of Pions

It is well known fact that pions with small threshold energies are most strongly and abundantly produced particles in *hh, hA* and *AA* collisions [27]. It was roughly estimated that around (40-55) % of the produced particles are pions. In Carbon+$^{12}$C, Proton+$^{12}$C, Deuteron+$^{12}$C, Alpha+$^{12}$C and Carbon+$^{181}$Ta interactions at 4.2 *A* GeV/*c* negative, positive and neutral pions and resonances etc., are produced. It is also stated that large amount of $\pi^{-}$─mesons are obtained at $^{16}$O*p* interactions at 3.25 GeV/*c* per nucleon. Pions are produced by direct and indirect way in *AA* collisions. In case of indirect way, most of pions are considered from the decay of delta resonances. The probability of negative pions obtained from Pion + Carbon collisions at 40 GeV/*c* originate from delta resonances are about 6%. It is well known fact that the production probabilities of heavy particles ($\omega^0$, $f^0$ mesons, and $\rho^0$) are increased with increase of high energy of projectile and target particles. The investigation of pions in relativistic nuclear collisions may convey us very helpful data about the dynamic of system. It is well known fact that pions can easily isolated from different particles produced in heavy ion interactions. In most of the light or heavy ion interactions pions are produced, and pions are one of the most abundant particles among other secondary particles. Delta resonances, are secondary particles produce in nuclear collisions, and delta resonances further decay to give pions and other nucleons [28-32].

In the laboratory of LHE, Joint Institute of Nuclear Research (JINR, Dubna, Russia) large pion statistics were recorded in *hA* and *AA* interactions at intermediate energies. 1-meter hydrogen and 2-meter propane ($C_3H_8$) bubble chamber are used to obtained data of produced pions from ionized tracks. In *hA* and *AA* collisions, it is already mentioned that production of delta resonances play very significant role in pions multiplicities at low energies [33-35].The prompt production of $\Delta$ resonances in nuclear collisions at low energies (1 - 15 GeV) and its decay to pions enhances the low transverse momentum of pions. It is already mentioned that pions, obtained from excited nuclear matter and these pions have important information about excited nuclear matter, and further these information can be helpful in dynamic of system. Therefore, it will be very interesting, to investigate different characteristic of pions in relativistic *hA* and *AA* interactions. In relativistic nuclear interactions, there are different ways of pions production but there are two ways in which the probabilities of pions are higher as compare to other ways of pions production.

(i) Direct production: it is that process in which pions are directly produced from interaction of projectile and target nuclei. The projectile energy must be greater than threshold energy of pions. The direct productions of negative pions have following equations.

$$nucleus + nucleus \rightarrow nucleus + pions$$
$$nucleus + nucleus \rightarrow nucleus + nucleus + pions + pions.....$$

(ii) From Delta resonance decay or indirect production: in this scenario a delta resonance is produced due to *AA* collisions and delta resonance are short lived baryons. This excited delta resonance decays later on to produce pions. The multiplicities of pions are also dependent on energies of interacting projectile and target nuclei. At Dubna energies most abundantly produced delta baryons are $\Delta$(1232 GeV/$c^2$) resonances. Here 1232 is the mass of delta resonance.

$$nucleus + nucleus \rightarrow N(\Delta)^* \rightarrow nucleus + pions.....$$

It is important to mention that there is an asymmetric ratio between negative and positive pions production at different masses of target and projectile nuclei, and also on each beam of energy of incident nuclei. It is studied that at energy from (2 – 8) *A*GeV it is reduced from 1.79 to 1.39, and this value reduces up to $\approx 1$ in Super-Proton Synchrotron SPS at CERN experiment[36].

There are two important parameters (density and temperature) in relativistic nuclear collisions. These parameters give important information about Equation of State (EOS) [3, 12]. To investigate the spectral temperature of these hadrons, using theoretical models, slopes of transverse momenta, and slopes of energy spectra are studied. In relativistic *AA* collisions most of incident energies of projectile are used in production of secondary particles (delta resonances, rho mesons, pions etc.). In Ref. [37], the spectral temperatures of negative $\pi^-$ are obtained from collisions of *d*C, HeC, and CC interactions at 4.2 GeV/*c*. In these collisions fitting of non-invariant c.m.s. energy distribution of negative pions on Maxwell-Boltzmann spectra were used. It was studied rapidity distribution and its dependencies on angular distribution of negative mesons obtained in C─C interaction at 4.2GeV/*c* per nucleon [38]. It was investigated in that collision that rapidity distribution of negative pions is related with spectral temperature. It is very important to mention that $p_T$ spectra for $\pi^-$ obtained in *AA* interactions at 4.2 GeV/c are invariant under Lorentz transformation, while analysis of energy and longitudinal momentum longitudinal boosted under Lorentz frame [38-41]. Hence it known that transverse momentum does not change in Lorentz transformation, so it has much lesser likelihood that transverse momentum is effected by collective flow of secondary particles. In Refs. [42, 43] it is shown a rapidity distribution were studied in different transverse momentum spectra of negative pions in *AA* (p─C,(*d*─C, *d*─Ta),(C─C, C─Ta), and (*α*─C, *α*─Ta) interactions at c.m. energy i.e. $\sqrt{s_{NN}} = 3.14 GeV$ . The multiplicities of negative pions are directly related to incident energies of projectile. In central collisions multiplicities of negative pions are higher as compare to those negative pions produced at peripheral and semi-central collisions [42, 43].

In Ref. [44] it is used 7900 and 2000 statistics for rapidity spectra in C─C and C─Ta respectively at the incident projectile with momentum of 4.2*A*GeV/*c*. These statistics obtained in previous analysis were less than half as compare to the total statistics for same collisions used in our research work. It is investigated in Refs. [44], the rapidity spectrum was resembled in shape to the Gaussian function. Both spectra are changing their shape with respect to projectile and target masses and also their spectra are dependent on collision centralities. The width of rapidity spectra of extracted particles in *nucleus-nucleus* interactions, can give us important information about longitudinal flow of particles [16, 45]. The final stage scatterings processes of pions were analyzed in Refs. [16]. For a given spectral temperature obtained from secondary particles, it was found that width of rapidity spectra obtained from *nucleus-nucleus* interaction was considered to be very sensitive to a velocity of sound in medium at freeze out in Landau hydrodynamical model [46].

### 1.6 Aims and Outline of the Thesis

It is observed that at energies of order of few Giga Electron Volts, *π*─mesons are obtained most abundantly, and that's why pions are very important particles of relativistic nuclear collisions. It will be not appropriate to study negative pions without positive pions. Therefore it is important to study the characteristic and correlations of negative and positive pions and also the correlations of charged pions with production of light nuclei with momentum of 3.25*A*GeV/*c* in Oxygen-proton collisions.

In the present work it is suggested to investigate rapidity spectra and transverse momentum spectra of $\pi^-$ ─ mesons systematically in *nucleus-nucleus* (*AA*) interactions at

4.2GeV/*c* per nucleon. The fundamental point of the proposed research work is to analysis the changes of the rapidity and transverse momentum distributions of negative pions with changing the mass numbers of the target and projectile particles. Multiplicities of produced pions are changed with changing the degree of collision centrality. It will be interesting to study the changes of characteristics of produced pions by changing the collisions centralities (central, semi-central and peripheral collision) of the analyzed *nucleus-nucleus* collisions. The changes in rapidity spectra of $\pi^- -$ mesons with mass numbers of target and projectile nuclei and changes of collision centrality of interacting particles will be studied. The $y_{\mathrm{c.m}}$ spectra of negative pions both in experiment and model will be compared and fitted with theoretical model function. The rapidity distribution spectra will be fitted by Gaussian model function.

The experimental data of $p_T$ spectra of $\pi^- -$ mesons are obtained in our research work. This transverse momentum spectrum at different ranges and different collision centralities will be fitted with different theoretical model functions to compare the experimental and simulated model data. For fitting the experimental and simulated model spectra, we will use the Boltzmann function, Hagedorn Thermodynamic Model, Gaussian functions, and Simple Exponential. The transverse momentum spectra extracted from experiment, simulated model (Quark Gluon String model) will be fitted by these models to extract the important parameters, i.e., the spectral temperatures (inverse slope parameters). The spectral temperatures obtained from fitting these theoretical models on experimental $p_T$ spectra have dependencies on the mass numbers of target and projectile nuclei and also on the degree of collision centrality (the number of participant protons). These parameters extracted for $\pi^- -$ mesons in *nucleus-nucleus* interactions at 4.2GeV/*c* per nucleon will be compared with the corresponding experimental data obtained from different experiments and also with different sets of colliding nuclei at different energy. Results obtained from analysis of $y_{\mathrm{c.m}}$ distribution and $p_T$ spectra of $\pi^- -$ mesons in *nucleus-nucleus* interactions at 4.2 *A* GeV/*c* will be compared with the results available in the literature for different sets of colliding nuclei and various energies.

First chapter of this thesis presents the background knowledge related to the title of this work. The procedural details about the experimental data and the models used for simulation are described in second chapter. Then analytical discussion of the obtained results for the above mentioned collision systems and parameters are presented in chapters 3 and 4. Finally conclusions are summarized in chapter 5.

# Chapter 2 EXPERIMENTAL PROCEDURES ANDMETHODOLOGY

## 2.1 Laboratory of High Energies (LHE)

The Laboratory of High Energies (LHE), Joint Institute for Nuclear Research (JINR) was established in March 1956. This laboratory is situated in the north of Moscow, and it is around 110 km away from Moscow, Oblast. The JINR is a well-known center for particles and nuclear physics. V. I. Veksler was the first person who gave the concept of selfphasing and also he was supervisor to construct and develop new accelerator and synchrophasotron at Lebedev Physical Institute (LPI). V. I. Veksler was the first director of JINR. Veksler with his colleagues began the program of research at the synchrophasotron. The investigation of the elastic scattering processes at the minimum and maximum momentum transferred and multiple particle productions in *hadron–nucleon* interactions were the aims of the research project initially.

A.M. Baldin was the third director of LHE and he started a new research in a new field, called relativistic nuclear physics (RNP). The main purpose of this field is to study the quark structure of the nuclei. This project was started at the Laboratory of High Energies to analyze the combine production of particles in relativistic nuclear collisions.

In this center large number of research scientists, PhD scholars and staff members are working day and night. JINR has 18 member countries i.e. Russian, Armenia, Belarus, Azerbaijan, Bulgaria, Vietnam, Kazakhstan, Cuba, Georgia, South Korea, Mongolia, Moldova, Rumania, Poland, Uzbekistan, Slovak, Ukraine, Czech Republic and other countries. The main purpose of JINR is to work on theoretical and experimental fields of research and also to study, the nuclear physics, elementary particle physics, heavy ion physics, computational physics, relativistic physics, low and intermediate energy physics, condensed-matter physics, radiobiology and educational programs. The main aim of LHE, JINR is to hire leading scientist from member states and from other countries and establishes a very promising scientific group. The JINR was setup by the combination of two leading research institute, Electro-Physical Laboratory and Institute for Nuclear Problems. There is one center and seven research laboratory in Joint Institute for Nuclear Research [47].

The main part of JINR is the accelerators complex at the LHE. It was established to generate nuclear beam, polarized deuteron, deuteron and proton. The complex accelerators could accelerate the heavy and light nuclei beams up to 6 *A* GeV. It has been presented diagrammatically in figure 2.1. It consists of Nuclotron and Synchrophasotron. The Nuclotron was built in the period from 1987 to 1992. It started its function in 1993. The of JINR comprises of the following i.e.

I. Linear accelerator,
II. Synchrophasotron (Superconducting Nuclotron accelerator),
III. System of extracted beam channels,
IV. Source of heavy ions,
V. Laser source of light ions,
VI. System of slow beam extraction
VII. Electrons beam source of high charge state ions,
VIII. Internal target complex,
IX. Source of polarized deuterons.

The Helium liquefiers with the capacity of 1.6 kW each were used in cooling of superconducting elements. The Table 1.1 carries the main properties of accelerator. The main advantages of the LHE accelerator complex were due to the presence of the extraction system and a net of the external beam lines. The extraction of beams could be done from the Synchrophasotron in two directions i.e. MV-1 and MV-2, as shown in figure 1.4, leading respectively towards two experimental halls i.e. Hall 1B and experimental Hall 205.

The extraction of beams could be comparatively done in time 0.5 seconds and sent to the Hall 205. These beams becomes were forwarded through MV-1, with maximum energy and efficiency of these beams were about 95%. The beams could be extracted from MV-2 in duration of ($t < 10^{-3}$ seconds fast) or ($t = 0.35$ seconds slow). It was provided a physics setup in the experimental Hall 1B. The operation of both the extractions could take place simultaneously in the same cycle.

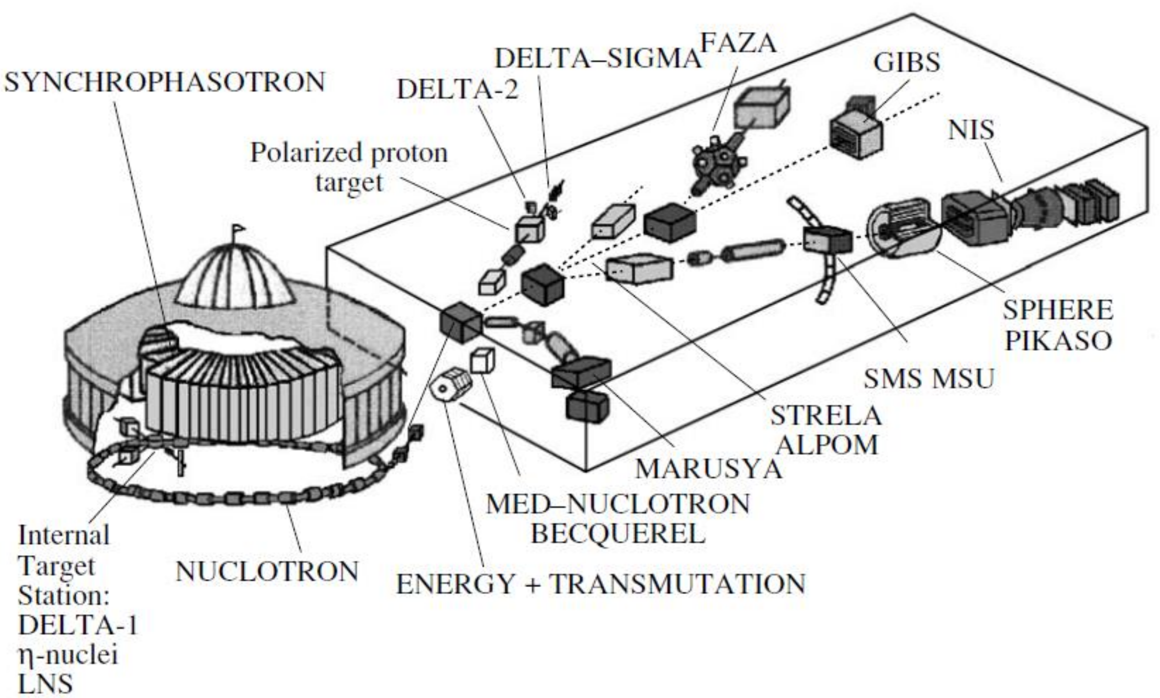


Figure 2.1. The diagrammatic show of the accelerator complex of JINR, Dubna.

Table 2.1. The comparative table of characteristic of Nuclotron and Synchrophasotron accelerators.

| Parameter | Units | Nuclotron | Synchrophasotron |
|---|---|---|---|
| Energy (max) | *A* GeV | 6 | 4.5 |
| Magnetic Field | T | 2.1 | 1.5 |
| Extraction time (max) | S | 10 | 0.5 |
| Chamber size | Cm | 12 | 120 |
| Circumference | M | 252 | 208 |

Many arrangements have been done to carry out the research at the Nuclotron. These include FAZA, MARUSYA, DELTA I and II, PIKASO, STRELA, Polarized Proton Target, GIBS, SCAN, Leading Particles, MRS and DISC as shown in figure 2.1. For details Ref. [48] can be consulted.

## 2.2 Synchrophasotron

Synchrophasotron, a type of synchrotron based particle accelerator. This accelerator has started working in 1957 for proton collisions. It had been working till 2003. Synchrophasotron was first design and constructed by Vladimir Veksler on the basis of self-phasing. The self-phasing process is mostly used in cyclic process (synchrotron accelerator). In 1944 at Dubna Russia, it was operational in USSR Academy of Sciences at the Laboratory of Lebedev Physical Institute. An Electro-Physical Laboratory (EPL) was constructed in 1953. The main purpose of EPL was to study high energy physics at Synchrophasotron. This laboratory was given name in 1956 and became part of JINR. In Synchrophasotron protons were accelerated to the energy up to 10 GeV and it was considered to be the highest energy at that time in the world. The Synchrophasotron was considered to be one of the biggest accelerator at that time. In the Synchrophasotron proton and later deuteron was accelerated up to 10 GeV and new kind of particles were observed from interactions and these new kind of particles were used in different kind of research.

The diameter of the Synchrophasotron was 60 meters. The Synchrophasotron consists of 4 huge magnets. These magnets were so big that even two cars can easily pass each other in it. These magnets are 5 meters high and 7 meters wide. The weights of magnets of Synchrophasotron are about 36000 tons [49, 50]. In figure 2.2, a small portion of Synchrophasotron is shown.


Figure 2.2. It is shown a small portion of Synchrophasotron in Laboratory of High Energy JINR, Dubna.

In the beginning the research program was used to study the elastic and inelastic processes at maximum and minimum energy-momentum transfer. This research program was initiated at JINR to study the cumulative production of different particles during nuclear collisions. It was also used to analyze production of different particles in *hA* and *AA* collisions. In this research program various new discoveries were invented in different experiments. Some of these discoveries are, anti $\Sigma^{-}$hyperon production, the phenomena in which a $\varphi^0$ meson decays into $e^-e^+$ pair, the process of slow neutron confinement, quark counting rule, quark nuclei structure. In this research program elements like 102, 113, 114, 115, 116, 118, were observed and many other processes were discovered [51].

### 2.3 Dubna Bubble Chamber

In 1952 the Bubble chamber was first constructed and operational by Donald Glaser. The basic principal of Bubble Chamber and Cloud chamber are very similar to each other. The Bubble chamber is a type of detector which detects particles on the basis of its track. The track is produced due to ionization of gas by electrically charged particles. The main principal of this chamber is, when a charged particle passes through a liquid (in superheated form and at very high pressure), bubbles were created along with track of the particle. These gas bubbles were then photographed by cameras placed at $4\pi$ around the Bubble chamber [52]. Liquid hydrogen is used as superheated liquid and the pressure is taken for this system around 5-20 atm. The whole procedure of particle detecting as follow:

i. A superheated transparent liquid and around 5 atmospheric pressure, just below its boiling point was stored at container having moveable piston.
ii. Then the pressure of system was reduced to two atmospheres by suddenly pulling of the piston. When high accelerated particles enter into the chamber, the gas is expanded just before their arrival and so the liquid becomes superheated. Each bunch of particles consists of around 10 particles.
iii. When these particles are passed through superheated liquid, then energy of these particles reduces by ionization of the superheated liquid molecules, and the superheated liquid produces tracks of bubbles and starts boiling.
iv. In bubble chamber bubbles produced and they expand for 10 ms. When the size of bubbles reaches to one mm then photographs were taken from different cameras.
v. Again the pressure of system increases and then the chamber is restored for new charged particles. This process is occurred approximately in one second.

Mostly the bubble chambers are filled with hydrogen or propane ($C_3H_8$) or mixture of neon-hydrogen or deuterium. A magnetic field by superconducting coil around (1.5-3.5) Tesla is applied around the Bubble chamber. Secondary particles that are produced from collisions form a track in bubble chamber and momentum of these particles can be obtained from these tracks, using the following relation:

$$p_{\perp} = 0.3Br \qquad (2.1)$$

Here $p_{\perp}$ (in GeV/$c$) represents momentum component which is perpendicular to the magnetic field direction, $B$ (in Tesla) is magnetic field and $r$ (in meters) represents the radius of curvature of track produced by charged particles. It can be seen in figure 2.3 tracks of different secondary particles are produced from the interaction of C-Ta interaction.

The volume of propane ($C_3H_8$) bubble chamber in LHE of JINR was about 546000 $cm^3$ (40 x 65 x 210) $cm^3$ and it is very sensitive volume. Propane ($C_3H_8$) (of 500 liters) under high pressure (about 20 atmospheres) in the chamber was kept in liquid state. The propane ($C_3H_8$) bubble chamber was operated at temperature of 58 $^0$C.

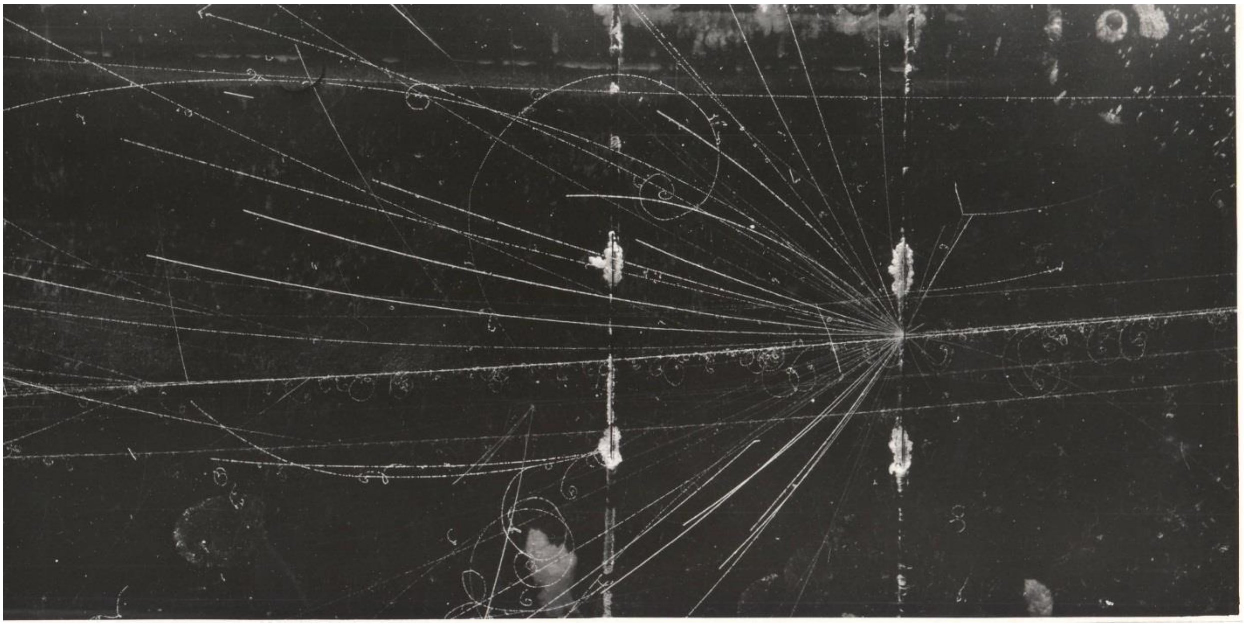

Figure 2.3. Photograph of *C+Ta* event registered by 2m propane bubble chamber.

A very strong magnetic field, (about 1.5 Tesla) was applied at perpendicular direction around the propane bubble chamber. When the moveable piston was pulled at the bottom side of the chamber, the propane reaches to a superheated form, and it is expanded in downward direction. There are 26 holes in the chamber that are illuminated to the propane bubble chamber. All 26 holes have lighting systems. There are two photographs in 4π directions and these photographs are controlled automatically. There were six cameras located at the top of the chamber, three for the front and three for the rear part of the chamber's volume, providing stereo-view of nuclear interactions and allowing 4π reconstruction of the events [53-55]. In the figure 2.4 a propane bubble chamber is shown

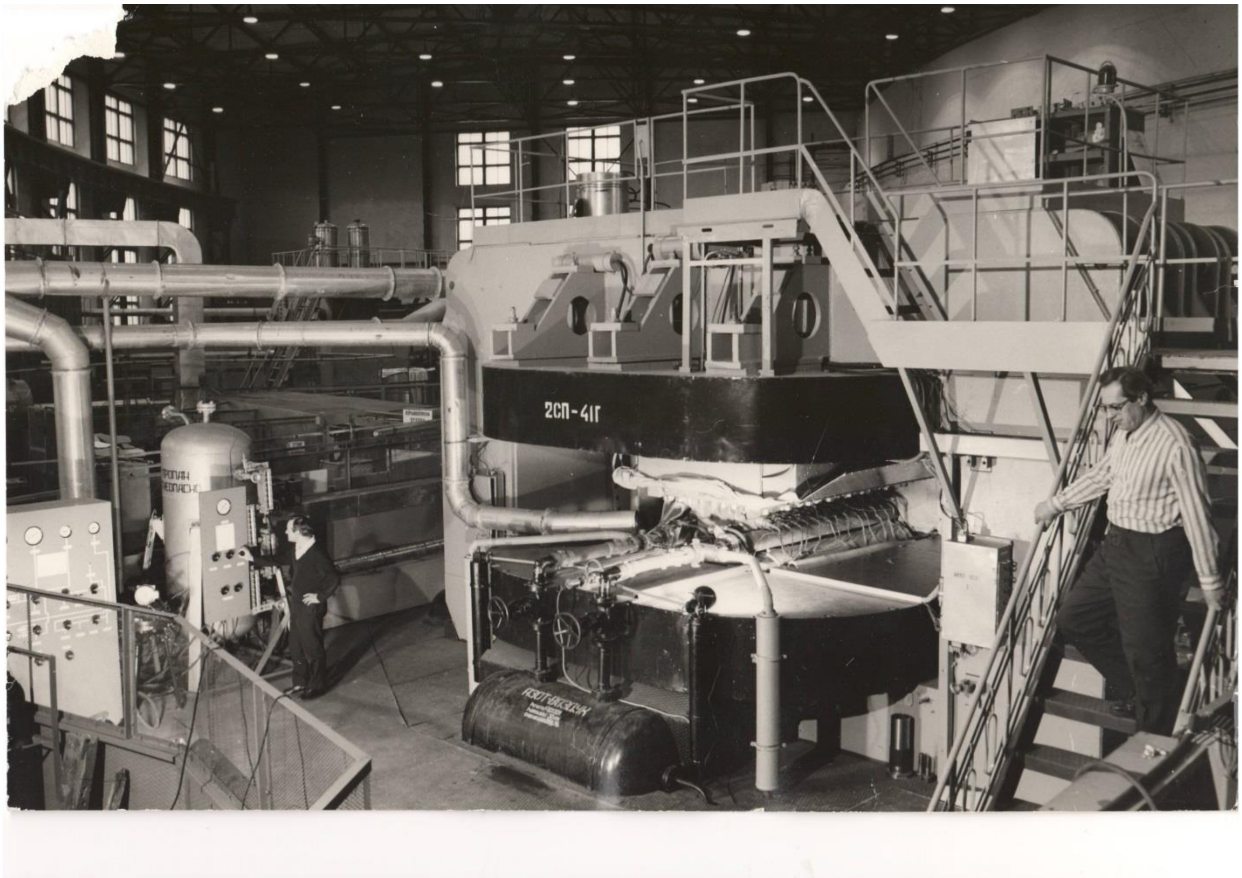


Figure 2.4. Propane Bubble chamber and its chief engineer N. Korzhev (JINR).

## 2.4 The Experiment procedure

The experimental data is present interactions are constructed from the photographs. It was used two meter Bubble chamber (propane, $C_3H_8$, PBC-500) of LHE, JINR. A constant and very strong magnetic field of 1.5Tesla is applied around the bubble chamber in perpendicular direction [29, 54-58]. To obtain the experimental data for $A$─Ta ($^{181}$Ta), three rods (1mm thickness and 93 mm separation) of Tantalum were placed in the propane chamber. A beam of nuclei ($^{2}$H, $^{4}$H, $^{16}$O and $^{12}$C) are accelerated in Synchrophasotron and then fall on target propane chamber. It is important to mention that at JINR the propane in the chamber was used as a target and a detector for analysis of produced particles. In our present analysis $^{2}$H, $^{4}$H and $^{12}$C beams are accelerated to the incident momentum of 4.2$A$GeV/$c$. The incident beams of these nuclei collide with Carbon and Hydrogen (proton) of propane molecules in the chamber and produce secondary particles. It is already mentioned that a Tantalum foil is placed inside chamber. If we want to get data of Tantalum, these nuclei are allowed to collide with Tantalum foils. These collisions events of Deuteron─C, Helium─C, Carbon─Ta, and Carbon─C interactions are first scanned, measured, reconstructed, and finally analyzed. There are approximately 52,000 (2,420 Carbon-Tantalum, 7,071 Deuteron-Carbon, 20,528 Carbon-Carbon 11,974, and Alpha-Carbon) inelastic collisions statistics were used at momentum of 4.2 GeV/*c* in our research work. There were also about 10,042 statistics of Oxygen-proton interactions at momentum of 3.25 GeV/*c* used in present work. All the secondary particles were detected and calculated under 4π geometry. There were almost 95% of produced negative particles were negative pions. The other 5% of secondary particles, produced of same curvature of the track are fast electrons and strange particles. All those pions that are produced in present analyzed collisions cannot be recorded and measured at momentum less than 70 MeV/*c* because of very small track produced in bubble chamber. All positive pions with momentum greater than 700 MeV/*c* cannot be distinguish from proton. While negative pions can easily separate, because there were no other similar kind of tracks were produced in that direction. Positive pions and protons can easily be separated from each other at (70 to 500) MeV/*c*. positive pions and protons were separated at momentum greater than 500 MeV/*c* from each other on the basis of their weights. On weights probability it was shown, that given particle is positive pions or proton. It was already known from the conservation of momentum and angular distribution of negative and positive pions and their track were coincided due to symmetric system of incident and target nuclei containing same number of protons and neutrons [59]. In Refs. [59] it was also shown that neutrons of (projectile and target) nuclei are responsible for the production of negative pions and protons are also responsible for production of positive pions. There were 0.8 degrees of average error in angles of all produced particles and there were about 11% of mean relative error in measurement of momentum [59]. In Refs. [56, 58, 60] it is described very briefly, that total interaction events were considered to be collision with carbon ($^{12}C$) nuclei of propane bubble chamber ($C_3H_8$) with following conditions:

1. Separation of number of negative and positive charges must be greater than charged of incoming projectile ($n_+ - n_- > (Z_{projectile} + 1)$),
2. Number of produced slow proton in the laboratory system (L.s.) with $P_{lab}< 0.75$GeV/*c* should be higher than 1 ($n_{proton} > 1$),

iii. Number of backward emitted proton in the laboratory system (L.s.) will be greater than zero ( $n_{proton}^{backward} > 0$ ),

iv. In case of Proton-Carbon collision the number of negative charge must me higher than 1 ( $n_{-} > 1$ ) and in case of deuteron-carbon collision the number of negative charge must be greater than 2 ( $n_{-} > 2$ ).

v. Number of negative and positive charges ( $n_{\pm}$ ) is odd for alpha-carbon collision events.

This was measured using the known cross sections [61] for Proton-Proton, Proton-Carbon, nucleons-Proton, nucleons-Carbon collisions (nucleons = *d*, $^{4}$He, and $^{12}$C) at incident *p* of 4.2*A*Giga electron-Volt/*c* and using ratios of (proton : carbon) and (nucleons : carbon) in a propane molecule [56, 60, 62, 63].Using the above criteria, around 70% of inelastic collisions events of *AA* were considered on carbon nuclei and tantalum foils and these inelastic events were separated. The remaining 30% of Deuteron─Carbon, Alpha─Carbon, and Carbon─Carbon collisions events were obtained statistically from Deuteron─Proton, Alpha─Proton, and Carbon─Proton collisions events on quasi-free protons of hydrogen atoms in $C_3H_8$ molecules. Statistics of these collisions events were calculated according to specified relevant weight formulism. According to this formulism, the relevant weight can be calculated from the number of collisions events on carbon and hydrogen atoms, and these collision events agree with the known cross sections for inelastic collisions [56, 57, 64, 65]. It was important to mention that there were about 69% of all nucleons-Carbon (nucleons = $^{2}$H, $^{4}$He or $^{12}$C nucleus) events were considered on quasi-free protons of $^{12}$C nuclei. It is because in propane ($C_3H_8$) 26 nucleons, 18 are protons of carbon nuclei [66].

## 2.5 Quark Gluon String Model (QGSM)

It is describe very briefly in [3, 9, 67, 68], that most of pions are obtained in relativistic *hA* and *AA* interactions because of low threshold energies. In these references it is mentioned that different kind of model predicts, there are large numbers of π-mesons are produced from delta resonances. It will be very important to use these models for pions production. In these simulated models the QGSM is one these models, is able to describe pion production at low energies. The QGSM describes *hA* and *AA* collisions at relativistic energies. In present research work the QGSM is used and adopted for intermediate energies. The c.m.s energy used for QGSM is,

$\sqrt{s_{nn}} \leq 4$ Gaga Electron Volt[69]. In the present work we used c.m.s. energy i.e. $\sqrt{s_{nn}} = 3.14$ GeV (The momentum of incident particle per nucleon 4.2GeV/*c*, and kinetic energy per nucleon 3.37GeV) for *hA* and *AA* interactions. So The QGSM is compatible to our energies. In QGSM we can understand the properties of pions in deuteron+$^{12}$C, helium+$^{12}$C, carbon+$^{12}$C, and carbon+$^{181}$Ta at present research work. To check the validity of this model, simulated data obtained from the model and then compared with experimental data at 4.2*A*GeV/*c*. It is already mentioned in ref. [17, 69] that QGSM is established on Regge and string phenomenological theories of secondary particles creation in *hA* and *AA* inelastic interactions.

## 2.6 Phenomenological Models Used for Description of the Pion Spectra

Thermodynamics relations are used to extract spectral temperature from produced particles at relativistic energies. These relations are derived because a source has a thermal equilibrium before hadronization. Secondary particles that are produced from the overlap region of incident projectile and target nuclei are characterized by freeze-out temperature. In relativistic interactions, in the overlap region of target and projectile nuclei, all particles stop interaction with each other in the expending fireball, and then the fireball is exploded and produce secondary particles. To obtain such temperature particles are considered to be free from fireball and temperature of these particle can give us very useful information.

Let suppose in thermal equilibrium all particles represented within specified volume, and the momentum of particles can be described by following relations [9, 23, 70]:

$$\frac{d^3N}{dp^3} = \frac{(2S_i+1)\,V}{(2\pi)^3}\left(\exp\left(\frac{E_i-\mu_i}{T}\right)\pm 1\right)^{-1} \quad \ldots\ldots\ldots\ldots\ldots\ldots\ldots\ldots\ldots\ldots \text{(2.1)}$$

$$\rightarrow \frac{(2S_i+1)\,V}{(2\pi)^3}\exp\left(\frac{\mu_i-m_i}{T}\right).\exp\left(-\frac{E_{ki}}{T}\right) \quad \ldots\ldots\ldots\ldots\ldots\ldots\ldots\ldots\ldots \text{(2.2)}$$

In following relations the arrow represents limit of classical Boltzmann-statistics, $E_i - \mu_i >> T$. $V$ represents volume of a fireball, $S_i$ is spin, $T$ is temperature, $\mu_i$ represents chemical potential of secondary particles, $E_i$, (while $E_i = \sqrt{m_i^2 + p_i^2}$ ) is energy of particle, and $E_{ki}$ ($E_{ki} = E_i - m_i$)

represents kinetic energy of the particle. In the above equation the ± signs show fermions and bosons.

We can use a specified limit i.e. $E_i - \mu_i >> T$ in the above equation (2.1) so the final equation can be obtained as:

$$\frac{d^3N}{dp^3} = \frac{d^2N}{p^2\ dp\ d\Omega} = \frac{d^2N}{pE\ dE\ d\Omega} = \mathrm{const}\cdot\exp\left(-\frac{E_k}{T}\right) \ldots\ldots\ldots\ldots\ldots \quad (2.3)$$

From the above equation the spectral temperature of secondary particles are extracted from spectral slope of energy. There are some factors that should be in mind while extracting the spectral temperatures from particles spectra. For example, it would be very difficult to find the c.m.s frame in particle collision when heavy target and light projectile interact with each other. The relativistic *AA* collisions depends on impact parameters of particles [71], and impact factor itself very difficult to determine directly. In our present research work the number of participant protons gives degree of centralities. The compressional energy obtained as a result of projectile and target interactions and it also affects pions energy and momentum spectra. The energy flows during expansion stage also affect pions multiplicity [72]. If it is supposed that delta resonances are considered to be in thermal equilibrium with surrounding particles, then pions will produce as delta resonances frozen-out. Using this assumption the two body decays of delta resonances will affect pions momentum and energy spectra[73].

The above equation that is obtained for energy spectra are also called freeze-out model. We can extract spectral temperature of negative pions using fitting of kinetic energy spectra on this equation. Equation (2.3) can be changed to simple form i.e.

$$1/(pE) \times dN/dE_k = A\exp\left(-\frac{E_k}{T}\right), \quad \ldots\ldots\ldots\ldots\ldots\ldots\ldots\ldots\ldots (2.4)$$

Here *A* is fitting parameter and it has a constant value. The equation 2.4 is also called one temperature fitting equation for kinetic energy, equation 2.4 can be written in case of two temperature fitting for kinetic energies i.e.

$$1/(pE)\times dN/dE_k = A_1\ \exp\left(-\frac{E_k}{T_1}\right)+A_2\ \exp\left(-\frac{E_k}{T_2}\right), \quad \ldots\ldots\ldots\ldots\ldots\ (2.5)$$

Here in equation (2.5) $A_1$ and $A_2$ are two fitting constant, $E$ is the energy of produced particles, and $\vec{p}$ is the momentum of particles in c.m.s, and $T_1$ and $T_2$ are temperatures that are extracted from fitting.

Thermal Model of freeze-out for hadrons in terms of kinetic energy ($E_k$) spectra is already shown above. It can be simplified if kinetic energies of hadrons are very greater than spectral temperatures of hadrons i.e. $E_k >> T$ then the Equation 2.4 can be simplified, and the normalization of total interactions of nucleons is added.

$$\frac{dN}{N\,pE\,dE_k} = A\cdot\exp\left(-\frac{E_k}{T}\right), \ldots\ldots\ldots\ldots\ldots\ldots\ldots\ldots\ (2.6)$$

Equation (2.6) is considered as one temperature function in terms of kinetic energy. For two temperatures the above equation is presented as:

$$\frac{dN}{N\,pE\,dE_k} = A_1\cdot\exp\left(-\frac{E_k}{T_1}\right)+A_2\cdot\exp\left(-\frac{E_k}{T_2}\right), \ldots\ldots\ldots\ldots\ldots\ (2.7)$$

Equation (2.7) represents simple exponential function in term of kinetic energy for two temperatures in the present work.

## 2.7 The Hagedorn Thermodynamic Model

The Hagedorn thermodynamic model predicts the extreme condition of a fireball. It is already mentioned in the introduction section that a fireball is formed when a projectile and target nuclei overlap each other. Particles inside fireball interact with each other and the fireball is then expanded. As the fireball expands the interactions between particles inside fireball is stopped and temperature of fireball is reduced. Then the fireball is exploded and hadrons are produced. The Hagedorn Thermodynamic Model [41, 74] takes into account a set of fireballs to be displaced from one another in the space of rapidity. According to Hagedorn Thermodynamic Model the $p_T$ spectra of produced particles can be written as,

$$\frac{dN}{dp_T} = \left(A \times p_T \times m_t \times K_1\right)\left(\frac{m_t}{T}\right) \approx \left(A \times p_T\right) \times \left(\sqrt{m_t T}\right) \exp\left(-\frac{m_t}{T}\right), \ldots\ldots\ldots\ldots (2.8)$$

Where $K_1$ is the MacDonald Function, The above equation is expressed in form of one temperature, In case of two temperatures this equation is written in the form of,

$$\frac{dN}{dp_T} \approx \left(A_1 \times p_t \times \left(\sqrt{m_t T_1}\right)\right) \exp\left(-\frac{m_t}{T_1}\right) + \left(A_2 \times p_T \times \left(\sqrt{m_t T_2}\right)\right) \exp\left(-\frac{m_t}{T_2}\right), \ldots\ldots\ldots (2.9)$$

Here $m_t = \sqrt{m^2 + p_T^2}$ $m_t$ is represented by transverse mass, and equations (2.8) and (2.9) are valid for condition of transverse mass i.e. $m_t >> T$. This equation can be normalized by introducing total inelastic events. So the normalized equation can be written as:

$$dN \big/ N_{ev} p_T dp_T = \left(A\sqrt{m_t T}\right) \exp\left(-\frac{m_t}{T}\right), \ldots\ldots\ldots\ldots\ldots\ldots\ldots\ldots\ldots\ldots (2.10)$$

Here $N_{ev}$, represents the normalized inelastic events, $T$ is the extracted spectral temperature, $A$ is the fitting constant. The above equation is expressed as one-temperature Hagedorn function. We can present the above formula for two temperatures, $T_1$and $T_2$ as:

$$dN \big/ N_{ev} p_T dp_T = \left(A_1\sqrt{m_t T_1}\right) \exp\left(-\frac{m_t}{T_1}\right) + \left(A_2 \cdot \sqrt{m_t T_2}\right) \exp\left(-\frac{m_t}{T_2}\right), \ldots\ldots\ldots (2.11)$$

Equation 2.11 is the two-temperature Hagedorn function.

### 2.8 The Boltzmann Model

According to The Boltzmann Model, the $p_T$ spectra of particles are obtained from the fitting of Boltzmann distribution function in terms of transverse mass. The one temperature formula can be written as:

$$ {dN}/{N_{ev}\, p_T\, dp_T} = \left(A \times m_t\right)\exp\left(-{m_t}/{T}\right) \text{ ……………………… (2.12)} $$

Equation 2.12 is shown as the one temperature formula for Boltzmann spectra. Similarly the two temperatures Boltzmann function can present as:

$$ {dN}/{N_{ev}\, p_t\, dp_t} = \left(A_1 \times m_t\right)\exp\left(-{m_t}/{T_1}\right) + \left(A_2 \times m_t\right)\exp\left(-{m_t}/{T_2}\right) \text{……... (2.13)} $$

The above equation is considered be a two temperature Boltzmann function.

## 2.9 Simple Exponential function

The simple exponential formula can be used to extract one and two temperatures of negative pions. In case of Simple Exponential formula the result of spectral temperatures will be higher than Boltzmann and Hagedorn function. The one and two temperatures pions spectra are obtained from the above expressions of Simple Exponential formula,

$$ \frac{dN}{N\, p_T\, dp_T} = A\exp\left(-\frac{p_T}{T}\right), \text{ ……………..…………….... (2.14)} $$

and

$$ \frac{dN}{N\, p_T\, dp_T} = A_1 \cdot \exp\left(-\frac{p_T}{T_1}\right) + A_2 \cdot \exp\left(-\frac{p_T}{T_2}\right). \text{ ………………… (2.15)} $$

## 2.10 Gaussian function

Investigation of rapidity spectra of pions obtained in *AA* collisions has wide range of collision energies. Rapidity spectra followed a Gaussian shape. It shown experimental rapidity spectra data of produced particles can be fitted very well to Gaussian functions [29, 44],

$$ F(y) = \frac{A_0}{\sigma}\exp\left(\frac{-(y-y_0)^2}{2\,\sigma^2}\right), \text{ ……………………… (2.16)} $$

In the equation (2.16) $y_0$ is shown as the center of Gaussian distribution, $\sigma$ is represented as the standard deviation. In the present work the standard deviation is shown as a width (cross section of interaction) of particles distributions, and $A_0$ is the fitting constant.

Now to fit $p_T$ spectra of $\pi^-$-mesons in terms of Gaussian function. The Gaussian function on the basis of transverse momentum spectra of hadrons could be written as,

$$\frac{dN}{N\,p_T\,dp_T} = A_0 \exp\left(-\frac{p_T^2}{T^2}\right), \ldots\ldots\ldots\ldots\ldots\ldots\ldots\ldots\ldots\ldots \text{(2.17)}$$

Here $A_0$ is the fitting constant. The two temperatures Gaussian function can be written as,

$$\frac{dN}{N\,p_T\,dp_T} = A_1 \cdot \exp\left(-\frac{p_T^2}{T_1^2}\right) + A_2 \cdot \exp\left(-\frac{p_T^2}{T_2^2}\right), \ldots\ldots\ldots\ldots\ldots\ldots\ldots\ldots\ldots \text{(2.18)}$$

Here in the given expression the $p_T$, $T_1$ and $T_2$ are in square form so the result of spectral temperatures obtained from fitting of Gaussian function, and it will be very greater than results of Hagedorn and Boltzmann function.

**2.11 Selection of Central, Semicentral, and Peripheral Collision Events**

In the present work it was studied different statistics limit of $p_T$ and $y_{c.m.}$– spectra of $\pi^-$-mesons. These statistics limits were studied on the basis of collision centralities of target and projectile nuclei. By studying the collisions centralities, we change in collisions parameters of target and projectile nuclei. In *AA* it is very difficult to find the impact parameter of interacting particles. Therefore number of protons participated ($N_p$) in *AA* collisions.

We have characterized three kinds of collisions events on the basis of number of participant protons i.e. peripheral, semicentral and central collisions. If number of participant protons are greater than mean multiplicity per event of participant protons then it is defined as central collision ($N_p \geq 2\langle n_{parti.prot.}\rangle$). If number of participant protons are less than mean multiplicity per event of participant protons then it will be considered as peripheral collision ($N_p \leq \langle n_{parti.prot.}\rangle$). If number of participant protons are between these two collisions events, then it will be called as a semicentral collision ($\langle n_{part.prot.}\rangle < N_p < 2\langle n_{part.prot.}\rangle$) [44].

In Refs. [28, 31, 75] it was shown that, in central collision of Carbon-Tantalum there was a complete stoppage of projectile on target nucleus, because in carbon+$^{181}$Ta collision the average number $\langle \nu^{p} \rangle$ of interacting nucleons was very close to the nucleons of projectile carbon. In Table 2.1 it is presented with in statistical errors, a percentage of *AA* collisions for experimental and QGSM model [29]. It can be shown in the Table 2.1, both experimental and model data events are coincided with each other with in errors, but in Deuteron+Carbon peripheral and semicentral collisions the QGSM data is overestimated to the experimental values [44].

Table 2.2. The percentage of peripheral, semicentral and central $d$+$^{12}$C, $^{12}$C+$^{12}$C, and $^{12}$C+$^{181}$Ta interactions per nucleon at 4.2 GeV/c relative to the total inelastic cross section ($\sigma_{in}$) [29].

| Types | Peripheral interactions, % | | Semicentral interactions, % | | Central interactions, % | |
|---|---|---|---|---|---|---|
| | Experiment | QGSM | Experiment | QGSM | Experiment | QGSM |
| $d$+$^{12}$C | 53±1 | 73±1 | 37± 1 | 15± 1 | 10±1 | 12±1 |
| He+$^{12}$C | 54 ± 1 | 54 ± 1 | 37± 1 | 38± 1 | 9 ± 1 | 8 ± 1 |
| $^{12}$C+$^{12}$C | 58±1 | 62±1 | 31± 1 | 30± 1 | 11±1 | 8±1 |
| $^{12}$C+$^{181}$Ta | 60±2 | 56±1 | 24± 1 | 29± 1 | 16±1 | 15±1 |

The further detailed information on about experimental data in relativistic *hA* and *AA* interactions (for minimum-bias interactions and on the basis of collisions centralities) using model (Quark Gluon String Model), and other theoretical models can be found from the above literature.

# *Chapter 3* Characteristic, Correlations and Transverse momentum Spectra of Negative and Positive Pions at 4.2 and 3.25 GeV/*c* per Nucleon

## 3.1 Introduction

$\pi -$ mesons are the most largely produced particles in *hA* and *AA* interactions, because of low threshold energies [25, 76]. There are two main sources of pions production in nuclear collisions, the direct production and production from decay of delta resonances [15, 16, 37, 39, 40, 44, 59, 66, 77-85]. In relativistic collisions, most part of overlap region in interactions is used in production of pions. Therefore, it would be so important to study, pions production on the basis of degree of centrality and transverse momentum distributions. This gives very useful information about kinematical properties of pions at incident projectile of energies of order few Giga Electron Volt per nucleon and higher energies in *hadrons-nucleus* and *nucleus-nucleus* interactions [75]. In this Chapter we will investigate the pion characteristic and spectra of pions in C-Ta collisions at 4.2GeV/*c* and also we will study the correlations of pions at low energy therefore we will analyze $^{16}$Op interactions at 3.25 GeV/*c*.

## 3.2 General characteristic of Negative and Positive Pions in $^{12}$C+$^{181}$TaCollisions

To study the change of the kinematical characteristic of charged pions in *AA* interactions at 4.2*A*GeV/*c* by increasing the degree of collision centrality, the number of participant protons ($N_p$) in *AA* collisions was analyzed. This analysis was already done in Refs. [28, 30-32, 44]. In our research work we distinguished the collision events by three types. We have selected these types on the basis of number of participant protons ($N_p$) compared with mean multiplicities of participant protons $\langle n_{part.prot.} \rangle$ per event. An event in which $N_p \le \langle n_{part.prot.} \rangle$ is categorized as a peripheral collision. A collision will be considered as central if $N_p \ge 2\langle n_{part.prot.} \rangle$,and the semicentral collision comes in between these two regions of multiplicities [75].

In Table 3.1 it is shown in percentage fractions (α) of selected three groups of collision events with various collisions centralities, the mean values of participant protons (<$\nu$>), the mean multiplicities of charged pions, the ratio of average number of the charged pions per one participant proton $R(\pi) = \langle n(\pi)\rangle / \langle \nu \rangle$, and the average total energy of the negative and positive pions $\left\langle \sum_i E_i(\pi) \right\rangle$ per collision event. These quantities are analyzed on the basis of three groups of collision events. In Table 3.1 it can be shown, experimental data calculated for three types of collision events (peripheral, semicentral, and central) in Carbon+Tantalum interaction. These experimental calculated values agreed very well with calculated values obtained from QGSM for Carbon+Tantalum collision [28, 31, 75].

Table 3.1.The fraction of events ($\alpha$), the average number of participant protons (<$\nu$>), the mean multiplicity per event of the $\pi^{\pm}$ (<$n(\pi)$>), the ratio $R(\pi)$=<$n(\pi)$>/<$\nu$>, the average total energy (<$\Sigma_i E_i(\pi)$>) (in MeV) of the charged pions per collision event at various centralities in $^{12}C+^{181}Ta$ collisions

| Quantity | Collision Centrality | | |
|---|---|---|---|
| | Peripheral | Semicentral | Central |
| ***α*, %** | 59 ± 1 | 24 ± 1 | 17 ± 1 |
| **<$\nu$>** | 5.0±0.1 | 19.6 ±0.2 | 33.5 ±0.3 |
| **<$n(\pi^-)$>** | 1.49 ± 0.04 | 5.31 ± 0.09 | 7.98 ± 0.13 |
| **<$n(\pi^+)$>** | 1.25 ± 0.03 | 4.90 ± 0.10 | 7.66 ± 0.15 |
| **$R(\pi^-)$** | 0.30 ± 0.04 | 0.27 ± 0.03 | 0.24 ± 0.05 |
| **$R(\pi^+)$** | 0.25 ± 0.02 | 0.25 ± 0.06 | 0.23 ± 0.08 |
| **<$\Sigma_i E_i(\pi^-)$> (**in MeV**)** | 671 ± 24 | 1817 ± 74 | 2138 ± 56 |
| **<$\Sigma_i E_i(\pi^+)$> (**in MeV**)** | 490 ± 12 | 1870 ± 33 | 2845 ± 44 |

In the Table 3.1 it can be seen, that mean multiplicities per event of both charged pions are increased by increasing the collision centrality and also it is determined that, multiplicity of negative pions are larger as compare to positive pions in the investigated three collisions groups. This is due to excess of number of neutrons over the number of protons in static target $^{181}Ta$

nuclei (108 neutrons versus 73 protons), while in case of $^{12}$C nuclei the numbers of neutrons and protons are equal.

The expected ratio of mean multiplicities of negative pions versus positive pions $<n(\pi^-)>/<n(\pi^+)>$ can be calculated by simple model formulism. According to simple model it is supposed that the number of produced charged pions is proportional to the number of neutrons and protons particles, involved in nuclear interactions. In such condition, each involved nucleon of projectile nucleus goes through a single collision with nucleon of target nucleus. Using such condition one can show that, the probability of neutron (from Projectile of $^{12}$C) with neutron (from target of $^{181}$Ta) collision is about $W(nn) \approx 0.3$, and similarly in the single proton-proton collision (one proton from projectile $^{12}$Cand one proton from target $^{181}$Ta) is about $W(pp) \approx 0.2$. The probabilities for single proton-neutron and neutron-proton collision can be calculated in same way (for Proton-neutron equal to $W(pn) \approx 0.3$ and for neutron-proton equal to $W(np) \approx 0.2$.Adding all these probabilities i.e. $W(nn)+ W(pp)+W(np)+ W(pn)$) one can find that, the total probability for single nucleon-nucleon ($nn$) is one ($W(nn) = 1$, whereas the $W(nn)$ is represented by a formula i.e. $W(nn) = W(nn)+ W(pp)+ W(np)) +W(pn)$. Using the above probabilities one can find the ratio of mean multiplicities of negative and positive pions $<n(\pi^-)>/<n(\pi^+)>$ for $^{12}$C-$^{181}$Ta system as follows.

$$\frac{\langle n(\pi^-)\rangle}{\langle n(\pi^+)\rangle} = \frac{(2\times W(nn) + W(pn) + W(np))}{(2\times W(pp) + W(pn) + W(np))} \approx 1.22 \text{----------- (3.1)}$$

Using the above method we have find values for $^{12}$C-$^{181}$Ta in three groups and also using Wounded Nucleon Model (WNM). WNM was originally proposed in Ref. [86] and further extended in Refs. [36, 75]. In this model the average multiplicity of interacting particles is considered to be in a specified proportional to the number of wounded nucleons. According to this model, those nucleons with at least one inelastic collision are called wounded nucleons. In the WNM model, particle productions in *AA* collisions are presented as superposition of independent contribution from those nucleons which have one time inelastic interaction (we have already considered them wounded nucleons) in projectile and target nuclei. Using the WNM model the value of ratio of $N(n)/N(n) = 1.44$ for Carbon-Tantalum collision energy is obtained, and using $\langle n(\pi^-)\rangle/\langle n(\pi^+)\rangle \approx 0.25$ obtained at comparable with ours collision energy from Ref.[48], we can estimate the ratio i.e. $\langle n(\pi^-)\rangle/\langle n(\pi^+)\rangle$=(1*0.25+1.44*1)/(1*1+1.44*0.25)≈1.24 in Carbon+Tantalum interaction in present interaction. Hence, it is estimated made by us using the simple model and WNM agree with each other [75].

The ratio $\langle n(\pi^-)\rangle/\langle n(\pi^+)\rangle$ proved to be 1.04 ± 0.03, 1.08 ± 0.04 and 1.20 ± 0.05 in the central, semicentral and peripheral Carbon+Tantalum interaction events. It can be seen that values are decreased by increasing the collisions centrality. In the peripheral $^{12}C+^{181}Ta$ collisions, the observed ratio $\langle n(\pi^-)\rangle/\langle n(\pi^+)\rangle$ practically coincided with the corresponding ratio estimated in Equation (3.1) according to the simple model. The observed suppression of the ratio $\langle n(\pi^-)\rangle/\langle n(\pi^+)\rangle$in the central and semicentral Carbon+Tantalum collision events as compared to the calculated ratio $\langle n(\pi^-)\rangle/\langle n(\pi^+)\rangle \approx 1.22$ could, for example, be due to the higher absorption rate of the slow negative pions produced on $^{181}Ta$ nuclei as compared to that for the slow positive pions. By increasing the collision centrality in Carbon+Tantalum collision, we expected, a rescatterings process, a process in which there is an increase in the number of slow $\pi^-$─mesons produced in secondary interactions on target $^{181}Ta$ nucleons. Hence, the suppression of the ratio $\langle n(\pi^-)\rangle/\langle n(\pi^+)\rangle$ should increase by increasing the $^{12}C+^{181}Ta$ collision centrality. It would be of great importance to mention that the cross section of absorption of the slow pions by nuclei was found to be significant for both light and heavy nuclei in the past [87-93]. As the mass number ($A$) of nucleus increases, the cross section (as roughly $A^{2/3}$) of pions absorption increases [91-93]. The cross section of absorption of the slow negative pions in nuclei (especially in heavy nuclei) is considerably larger as compared to that for positive pions due to the capture of the slow $\pi^-$ mesons by an attractive Coulomb's field of a positive target nucleus [87-89].

In Ref. [31] the number of average participant nucleon were obtained from interaction of projectile ($A$) and target ($B$) nuclei. Here we have taken ($A$) is a projectile and ($B$) is for target nuclei. A model of independent collisions of projectile and target nuclei were used for binary $AA$ (Carbon+Tantalum, Alpha+Carbon, and Carbon+Carbon) interactions per nucleon at momentum of 4.2 GeV/$c$[86, 93]. In this model it is taken only primary $AA$ collisions and it does not take cascade process of secondary nuclei in target nucleons [86, 93]. Using this model we find and calculated the average number of participant projectile ($\nu_A$), target nuclei ($\nu_B$), cross sections and the average number of binary *AA* interactions ($\nu_{AB}$)[31]. In Table 3.2 it is presented inelastic cross section ($\nu_{AB}$), ($\nu_A$), ($\nu_B$), in *AA* (Carbon+Carbon, Carbon+Tantalum, Alpha+Carbon, and Proton+ Proton) interactions with incident momentum of4.2*A*GeV/*c*.

Table3.2. Average number of *nucleon–nucleon* interactions $\langle \nu_{AB} \rangle$, the inelastic cross sections and projectile $\langle \nu_A \rangle$ and target $\langle \nu_B \rangle$ nuclei, calculated in Ref.[31] using the simple model of independent nucleon interactions [86, 93].

| Type | $^{12}C+^{181}Ta$ | $^{12}C+^{12}C$ | $^{4}He+^{12}C$ | $p+p$ |
|---|---|---|---|---|
| $\sigma^{inel}(A+B)$ (mb) | 3445 ± 140 | 830 ± 50 | 450 ± 20 | 28 ± 1 |
| $\langle \nu_A \rangle$ | 5.9 ± 0.3 | 3.8 ± 0.3 | 2.4 ± 0.2 | 1 |
| $\langle \nu_B \rangle$ | 14.0 ± 1.0 | 3.8 ± 0.3 | 2.7 ± 0.2 | 1 |
| $\langle \nu_{AB} \rangle$ | 18.0 ± 1.0 | 4.9 ± 0.3 | 3.0 ± 0.2 | 1 |
| $\langle \nu_A \rangle + \langle \nu_B \rangle$ | 20.0 ± 1.0 | 7.6 ± 0.4 | 5.1 ± 0.3 | 2 |
| $<n_{part..nucl..}>^{exper}$ | 32.5 ± 0.5 | 8.70 ± 0.04 | 5.66 ± 0.04 | 2 |

It is presented in the Table 3.2 a comparison between calculated and experimental values of average numbers of participant nuclei. In the above table it is presented that the secondary cascading processes contribution is considered to be neglected in the model. Secondary cascade processes are increasing significantly with increasing the size of collision system. By comparison the experimental and calculated number of participant nuclei in the model obtained the Table 3.2, it was considered around 10%, 13% and 38% of participant nucleons that the secondary cascading processes contribute, in Alpha+Carbon, Carbon+Carbon and Carbon+Tantalum collisions[31]. Hence, the fraction of the slow pions that are produced in secondary *AA* interactions in Carbon─Ta collisions should be significantly larger than that in $^{12}C+^{12}C$ collisions, where the contribution of the secondary nucleon-nucleon collisions (cascading) is about four times smaller than that in $^{12}C+^{181}Ta$ collisions. In cascade process the numbers of slow pions are increased by changing the degree of collision centrality in C─Ta interaction in present analyzed collision. Due to cascade pions the average momentum and energy of charged pions are decreased [75].

As observed from Table 3.1, the ratio $R(\pi)$=<$n(\pi)$>/<$\nu$> for the negative pions decreases systematically with increasing the collision centrality, whereas this ratio for the positive pions does not depend on the centrality of $^{12}$C+$^{181}$Ta collisions. As was discussed above, there was a decreased in the ratio <$n(\pi^-)$>/<$n(\pi^+)$> by increasing various centrality of $^{12}$C+$^{181}$Ta interaction.

In the Table 3.3 it is shown the average values and widths of the spectra of the full, transverse, longitudinal momenta, and emission angles of the $\pi^{\pm}$—mesons at various centralities in $^{12}$C+$^{181}$Ta interactions at 4.2 GeV/$c$ per nucleon in the laboratory frame. It is presented in the Table 3.3, the average values and widths of the spectra of the full and longitudinal momenta of the negative pions decrease significantly with an increase in degree of centrality in Carbon+Tantalum interactions. Also, the average transverse momentum of negative pions decreases systematically with an increase in degree of interaction centrality. On the other hand, as shown in Table 3.3, the average emission angle of the $\pi^-$—mesons increases significantly with increasing the $^{12}$C+$^{181}$Ta collision centrality. These observations can be explained by that, with increasing the interaction centrality, the number of binary collisions of carbon-12 nucleons with the target $^{181}$Ta nucleons increases significantly. Hence, as discussed above, the number of $\pi^-$ mesons created in secondary interactions (rescatterings) on nucleons of target $^{181}$Ta nuclei increases with increasing the degree of interaction centrality.

Table 3.3. It is shown the average values and widths of spectra of the total ($P$), transverse ($P_T$) and longitudinal ($P_l$) momenta (in MeV/$c$) and emission angles ($\Theta$) (in degrees) of the charged pions in the laboratory frame at various centralities in $^{12}$C+$^{181}$Ta collisions. Statistical errors are shown.

| Quantity | Collision Centrality | | | | | |
|---|---|---|---|---|---|---|
| | Peripheral | | Semicentral | | Central | |
| | $\pi^-$ | $\pi^+$ | $\pi^-$ | $\pi^+$ | $\pi^-$ | $\pi^+$ |
| **<$P$>** | 550 ± 11 | 476 ± 11 | 443 ± 7 | 474 ± 8 | 362 ± 6 | 462 ± 7 |
| ***DP*** | 489±15 | 459±16 | 395±10 | 420±11 | 326±10 | 399±9 |
| **<$P_l$>** | 440 ± 11 | 343 ± 11 | 325 ± 7 | 315 ± 8 | 220 ± 6 | 276 ± 7 |
| **$DP_l$** | 493±12 | 472±17 | 417±10 | 423±12 | 345±10 | 391±10 |
| **<$P_T$>** | 223 ± 4 | 240 ± 5 | 218 ± 3 | 272 ± 4 | 210 ± 3 | 290 ± 4 |
| **$DP_T$** | 176±5 | 192±5 | 164 ±4 | 218±6 | 162±4 | 242±6 |

| | | | | | | |
|---|---|---|---|---|---|---|
| **<$\theta$>** | 43.1 ± 0.8 | 51.5 ± 0.8 | 51.1 ± 0.6 | 55.4 ± 0.7 | 60.2 ± 0.7 | 60.4 ± 0.7 |
| **$D\theta$** | 35.6 ± 0.7 | 35.2 ± 0.6 | 36.2 ± 0.5 | 35.2 ± 0.5 | 38.4 ± 0.4 | 36.0 ± 0.6 |

Due to an increase of the number of negative pions obtained in secondary rescatterings on tantalum (as a target) nucleons, we observe the significant increase of the mean emission angle of the $\pi^{-}$mesons with an increase in interaction centrality. As the energy of the incoming nucleon of incident projectile ($^{12}$C) has to be shared among the larger number of the produced pions with changing interaction centrality of $^{12}$C+$^{181}$Ta, the average values and widths of the spectra of the total and longitudinal momenta of the negative pions decrease significantly by changing the collision centrality of interacting nuclei.

As seen from Table 3.3, the average value of the longitudinal momentum of $\pi^{+}$ mesons decreases significantly, whereas the average emission angle of the $\pi^{+}$-mesons increases considerably, with the increasing the $^{12}$C+$^{181}$Ta collision centrality. This is obviously (similar to the case for $\pi^{-}$ mesons) due to an increase in the number of the produced positive pions in secondary rescatterings (interactions) on target $^{181}$Ta nucleons with the increasing the $^{12}$C+$^{181}$Ta collision centrality. The larger average emission angle observed for the $\pi^{+}$-mesons compared to that for the $\pi^{-}$-mesons in Table 3.3 is probably due to the effect of the overall Coulomb's repulsive force for $\pi^{+}$ mesons as contrasted to the Coulomb's attractive force for $\pi^{-}$ mesons in a nuclear medium.

Figure3.1shows the momentum spectra of the $\pi^{\pm}$-mesons in the peripheral and central $^{12}$C+$^{181}$Ta collisions at 4.2 *A* GeV/*c* in the laboratory frame. Fig. 3.2 presents the transverse momentum distributions of the negative and positive pions in the central and peripheral $^{12}$C+$^{181}$Ta interactions at 4.2*A* GeV/*c* in the laboratory frame.

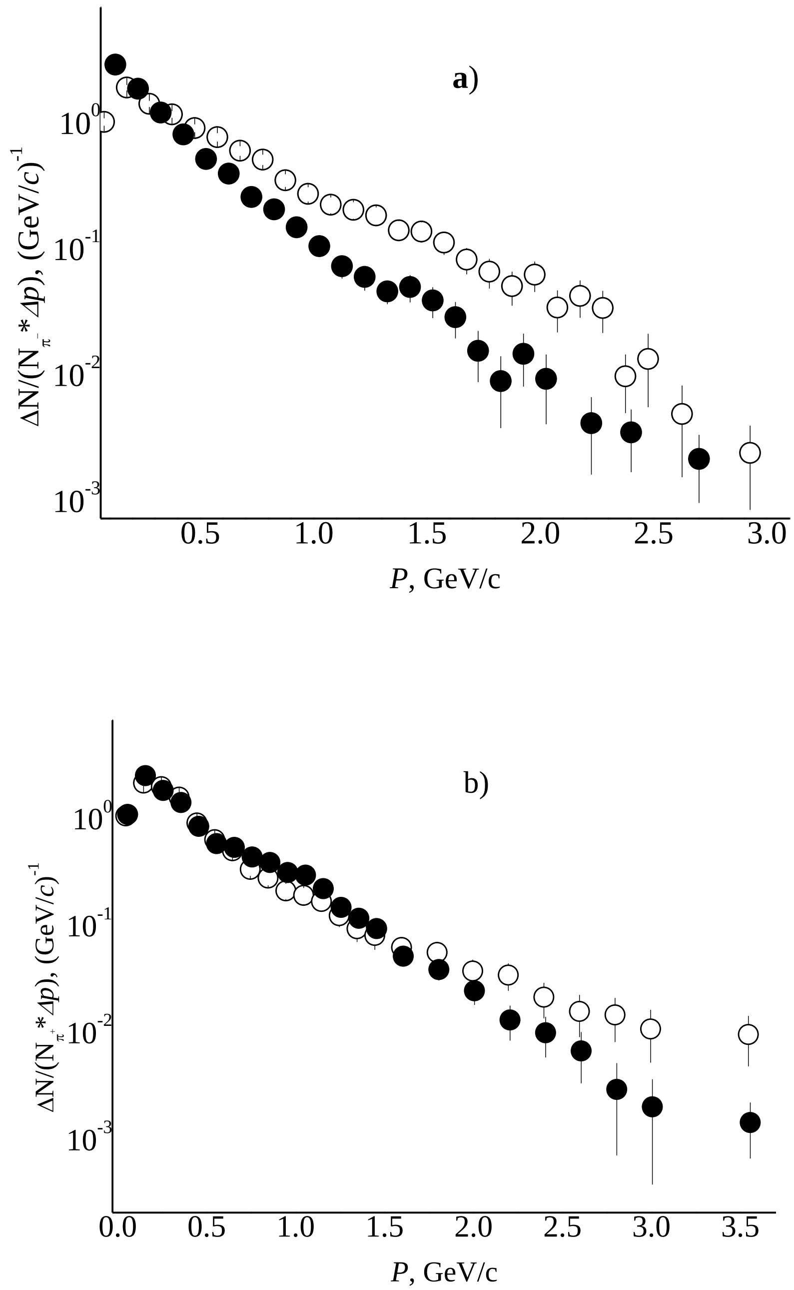


Figure 3.1. The total momentum spectra of the negative (*a*) and positive (*b*) pions in peripheral (open circles) and central (closed circles) $^{12}C + ^{181}Ta$ interaction in the present analyzed collision in the laboratory frame. Statistical errors are shown.

The emission angle distributions of the negative and positive pions in the peripheral and central $^{12}C+^{181}Ta$ collisions at 4.2 GeV/*c* per nucleon in the laboratory frame are presented in Fig. 3.1. All the distributions in figures 3.1, 3.2, and 3.3 were normalized per one pion. As observed from Figs. 3.1*a* and 3.1*b*, the fraction of the charged pions with the large momenta in the normalized full momentum distributions of the negative and positive pions decreases significantly with an increase in centrality of $^{12}C+^{181}Ta$ collisions at 4.2 *A* GeV/*c*. As seen from Figs. 3.3*a* and 3.3*b*, the fraction of the charged pions with small emission angles decreases and that with the large emission angles increases significantly for both the negative and positive pions with increasing the $^{12}C+^{181}Ta$ collision centrality. This confirms our above finding that the number of the charged pions produced in secondary interactions (rescatterings) on nucleons of target $^{181}Ta$ nuclei increases with increasing the collision centrality, which results in an increase of the average emission angle of $\pi^+$ and $\pi^-$ mesons, observed in Table 3. 3.

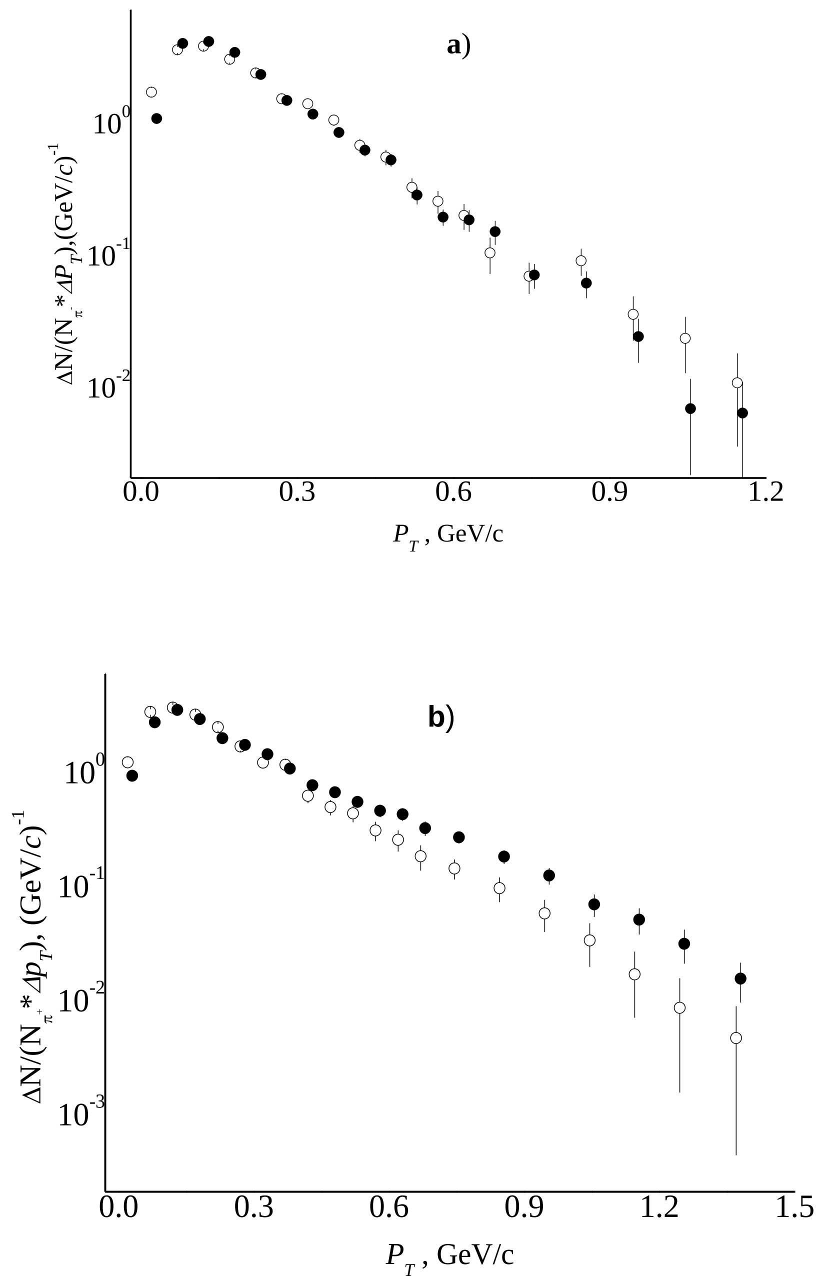


Figure 3.2. The transverse momentum spectra of the negative (*a*) and positive (*b*) pions in peripheral (open circles) and central (closed circles) $^{12}C+^{181}Ta$ collisions. The distributions are normalized per one pion.Statistical errors are shown.

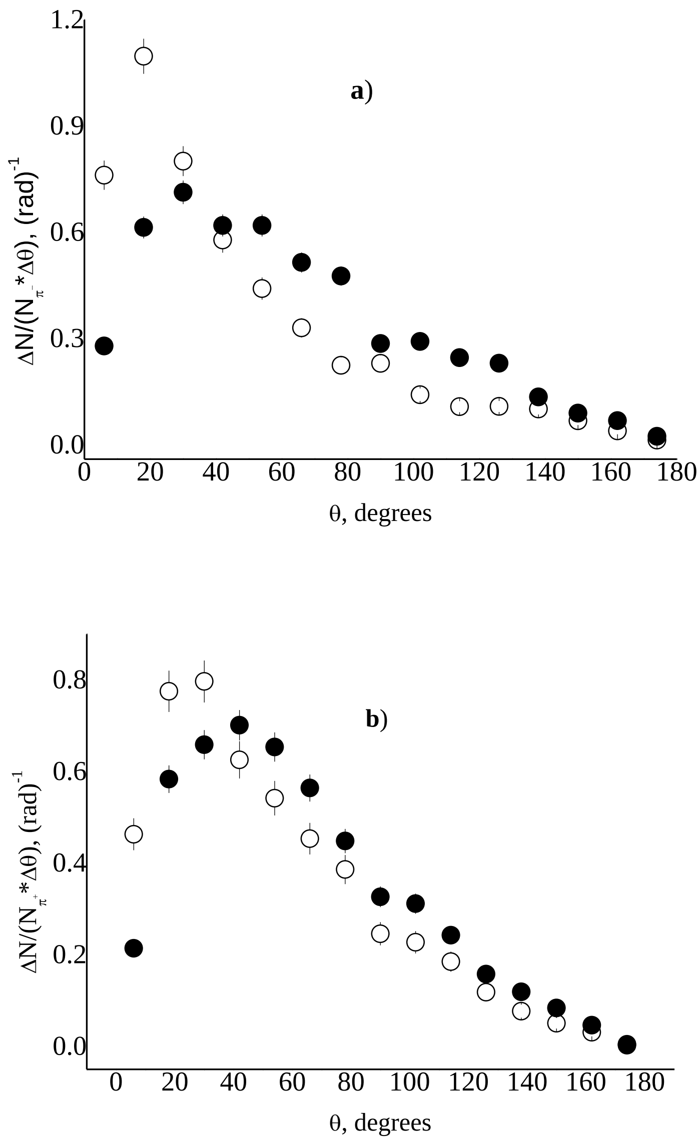


Figure 3.3. The emission angle distributions of the negative (*a*) and positive (*b*) pions in peripheral (open circles) and central (closed circles) $^{12}C+^{181}Ta$ collisions. The distributions are normalized per one pion. Statistical errors are shown.

Figures 3.3*a* and 3.3*b* show a clear difference between emission angle distributions of the charged pions created in the central and peripheral C─Ta interactions. In the peripheral interactions, as it is presented in the Figures3.3*a* and 3.3*b*, are characterized by the distinct peaks for both charged pions at the relatively small values of emission angle ($\theta \approx$ 20-30$^0$) in the laboratory frame. Whereas the peaks are broadened, lowered and shifted towards higher emission angles for the charged pions in the central CTa interactions as compared to those in peripheral interactions. It is presented in the Figures.3.3*a* and 3.3*b*, the fraction of the charged pions with lower emission angles decreases and that with the larger emission angles increase significantly in the central CTa interactions as compared to the peripheral ones. The distinct peaks observed at small emission angles in Figs. 3.3*a* and 3.3*b* in the peripheral CTa interactions are clearly due to the fast pions produced on nucleons of projectile $^{12}$C nuclei. Increase of the fraction of the charged pions with the larger emission angles in the central collisions compared to the peripheral ones are obviously due to the significant increase of the number of the relatively slow pions produced in secondary interactions (rescatterings) on the target $^{181}$Ta nucleons with increasing the collision centrality.

### 3.3 Degree of collision centrality for Negative pions in CTa collision

We obtained the spectral temperatures for negative pions in three types of collisions for CTa collision system. The experimental $p_T$ spectra of $\pi^-$ — mesons of CTa interaction obtained for three types of collisions fitted by different theoretical models.

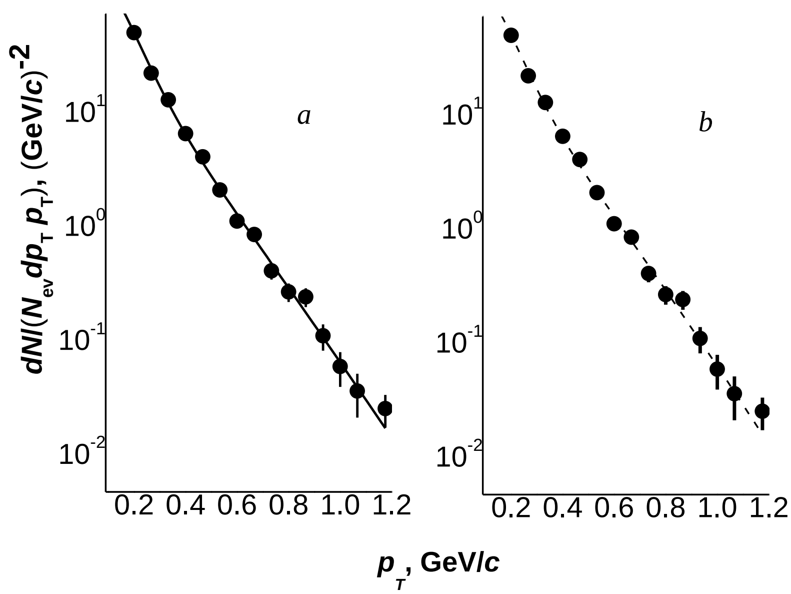


Figure 3.4. The experimental $p_T$ spectrum of the $\pi^-$ — mesons extracted in C—Ta (●) interactions at 4.2 GeV/*c*. *A* and it is fitted by the two-temperature Boltzmann (dashed line) and the two-temperature Hagedorn (solid line) functions in the $p_T$ interval of 0.1 to 1.2 GeV/c

It is already known that the numbers of produced particles are directly related to the masses of target and projectile and also their various collisions centralities. In C─Ta interaction in various degrees of collisions centralities (from peripheral to central) the number of *nucleon-nucleon* interaction increase and also multiplicities of participant nucleon increases when one moves from peripheral to central collisions. In most of central *nucleus-nucleus* interactions pion multiplicities also increases.

As can be presented in the Figure 3.4*a*, the Boltzmann function for two temperatures is fitted on $p_T$ – spectra of the $\pi^-$─mesons in central, semicentral, and peripheral Carbon-Tantalum interactions.

In Table 3.4 results obtained from the fitting of theoretical models and it can be seen that in the Table 3.4 the Hagedorn and Boltzmann functions have comparable results for three types of collisions systems while results of negative pions obtained from fitting of Simple exponential and Gaussian formula have very large values as compared to Boltzmann and Hagedorn functions.

It important to express that $R^2$ factor in Table 3.4 is expressed by the following relation:

$$R^2 = 1 - \frac{SS_E}{SS_T}$$

Here the $SS_E = \sum_{i=1}^{n} (y_i^{\exp} - y_i^{fit})^2$ represented as the sum of squared errors and $SS_T = \sum_{i=1}^{n} (y_i^{\exp} - \bar{y})^2$ is shown as the total sum of squares of experimental ( $y_i^{\exp}$ ) and model fit ( $y_i^{fit}$ ) data, respectively, and $\bar{y} = \frac{1}{n}\sum_{i=1}^{n} y_i^{\exp}$ is shown as the mean value of the experimental data. When there is smaller deviation between the experimental and model data, then $R^2$ factor approaches to 1, and thus, it shows a better fit.

Table 3.4. $T_1$ and $T_2$ temperatures obtained for $\pi^{-}$ − mesons on fitting $p_T$ spectra by various functions in various collisions centralities. The $p_{T-}$spectra is fitted from 0.1 to 1.2 GeV/*c* for various functions.

| **Fitting functions** | **Centrality Types** | $A_1$ | $T_1$ **( MeV)** | $A_2$ | $T_2$ **(MeV)** | $\chi 2/n.d.f.$ | $R^2$ |
|---|---|---|---|---|---|---|---|
| **Boltzmann Function** | Central | 67136 ± 28885 | **46 ± 4** | 1138 ± 468 | **109 ± 7** | 1.17 | 0.98 |
| | Semicentral | 50087 ± 27017 | **44 ± 5** | 1196 ± 398 | **104 ± 5** | 0.49 | 0.99 |
| | Peripheral | 5465 ± 1785 | **56 ± 5** | 120 ± 71 | **123 ± 12** | 0.93 | 0.98 |
| **Hagedorn Model** | Central | 93566 ± 49847 | **49 ± 6** | 1624 ± 740 | **119 ± 8** | 1.11 | 0.98 |
| | Semicentral | 74329 ± 53202 | **46 ± 7** | 1766 ± 629 | **112 ± 6** | 0.50 | 0.99 |
| | Peripheral | 6214 ± 2326 | **63 ± 7** | 138 ± 101 | **139 ± 16** | 0.85 | 0.99 |
| **Gaussian** | Central | 22 ± 4 | **414 ± 17** | 326 ± 38 | **182 ± 8** | 2.27 | 0.96 |
| | Semicentral | 20 ± 3 | **404 ± 13** | 213 ± 25 | **180 ± 8** | 0.86 | 0.99 |
| | Peripheral | 4 ± 1 | **441 ± 22** | 48 ± 5 | **202 ± 9** | 2.04 | 0.97 |
| **Simple Exponential** | Central | 1146 ± 285 | **71 ± 12** | 159 ± 108 | **140 ± 16** | 1.01 | 0.98 |
| | Semicentral | 714 ± 364 | **60 ± 18** | 220 ± 90 | **126 ± 9** | 0.55 | 0.99 |
| | Peripheral | 146 ± 19 | **95 ± 10** | 6 ± 10 | **193 ± 58** | 0.65 | 0.99 |

We have fitted the three types of collisions obtained for negative pions in CTa collision system by two temperatures Boltzmann function and it can be seen that the Figure 3.5 fit very well.

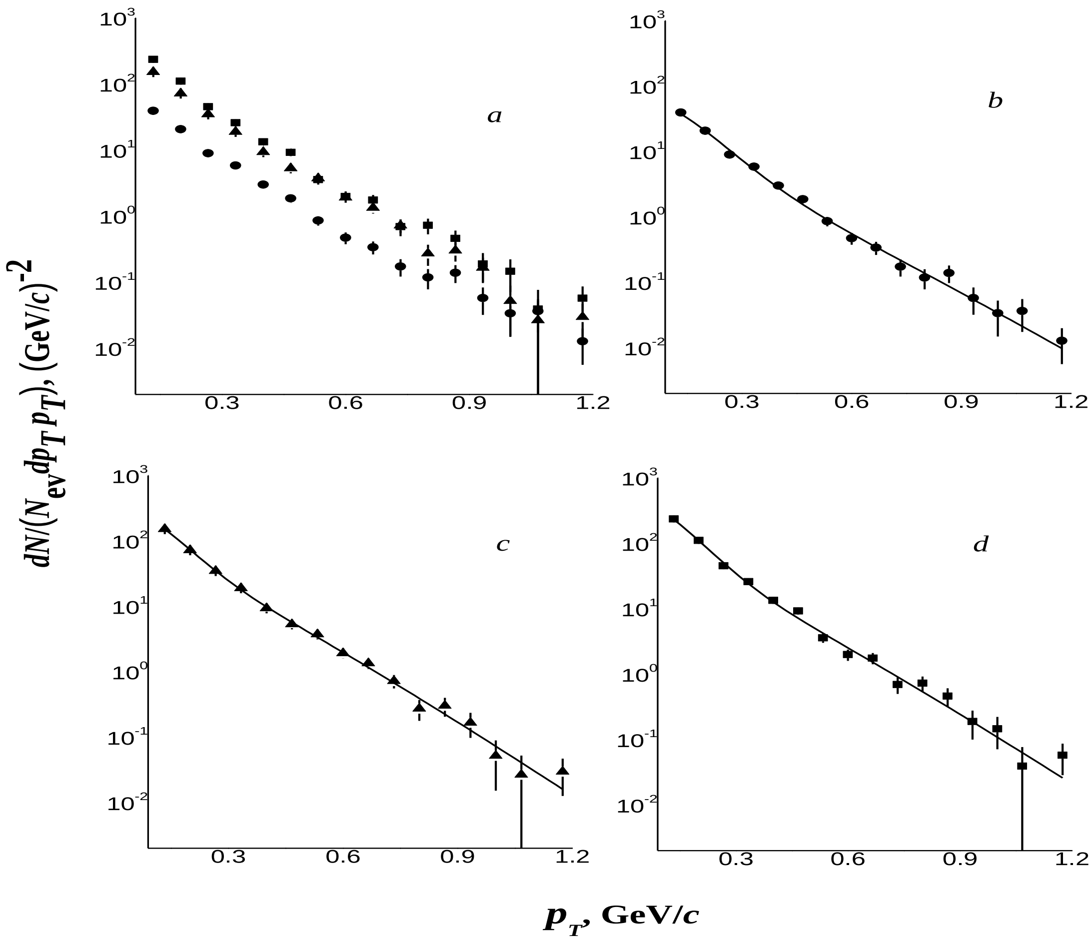


Figure 3.5. The experimental $p_T$ spectra of $\pi^-$ — mesons extracted in central (■) ((a) and (d)), semicentral (▲) ((a) and (c)), and peripheral (●) ((a) and (b)) $^{12}C$+$^{181}Ta$ collisions at 4.2 GeV/$c$ per nucleon and the corresponding fits in the $p_T$ range of 0.1 to 1.2GeV/$c$ by the two-temperature Boltzmann function (solid lines).

## 3.4 Pions correlations at 3.25 *A* GeV/*c*

The main purpose of this correlation at low energy to check the relation of charged pions at low energies. We have already checked the characteristic of charged pions for CTa interaction at 4.2*A*GeV/c and results were quite interesting. In this portion we have included our published work in which we have worked on Oxygen-proton interactions at 3.25GeV/*c* per nucleon.

We have divided the whole system of Oxygen-proton interaction at 3.25*A* GeV/*c* into two groups of charged pions:

(a) Collisions events in which there are no charged pions are produced i.e. $n_{\pi\pm} = 0$.

(b) Those collisions events in which there is at least one charged pions i.e. $n_{\pi\pm} \geq 1$.

Using these methods we will be studying the correlation in the creation of positive and negative pions[94].

Table 3.5. The percentage of collision events, of a recoil proton ($n_{RC}$) and mean number per event of light fragments with A ≤ 4. Recoil protons depend on the availability of negative and positive pions.

| Charged pions produced in an event | Fraction of events (W), % | | Types of produced particles | | | | | |
|---|---|---|---|---|---|---|---|---|
| | | $n_{RC}$ | $^1H$ | $^2H$ | $^3H$ | $^3He$ | $^4He$ |
| $<n_\pi^\pm> \geq 1$ | 55.3±0.7 | 0.59±0.01 | 1.94±0.03 | 0.37±0.01 | 0.17±0.01 | 0.16±0.01 | 0.54±0.02 |
| $n<n_\pi^\pm> = 0$ | 44.7±0.7 | 0.70±0.01 | 1.58±0.03 | 0.28±0.01 | 0.11±0.01 | 0.12±0.01 | 0.46±0.02 |

In Table 3.5 it is represented percentage of collisions events, recoil protons for two mentioned group and the mean number of produced particles per event of light fragments nuclei. It can be presented in the above Table 3.5, there are approximately 45% produced nuclei in collisions events with zero charged pions, and it was observed about 55% collisions events with at least one charged pions. It was shown in the Table 3.5 that mean multiplicities of these light nuclei with $n_{\pi\pm} \geq 1$ have larger in the group of collisions events as compared to light nuclei have zero charged pions. It is due larger amount of momentum and energy is transferred to fragmenting nucleus and there is very high destruction in such conditions. So it shows that all produced particles with at least one charged pions need higher destruction of nucleus and higher energy and momentum transferred as compare to those events having zero charged pions.

The mean values of the total charge of produced fragments are represented by ($<Q_{38}>$), here the limit of charges can be written as $3 \leq$ charge $\leq 8$ and it is already explained in the group of collisions events. In the group of collisions events having zero charged pions, the value of $<Q_{38}>$ is about 4.92 ± 0.04. For another group having at least one charged pions ($n_{\pi\pm} \geq 1$) the value of $<Q_{38}>$ is about 3.88 ± 0.04. it can be seen from the Table 3.5 the values mean multiplicities of mirror nuclei ($^3H$ and $^3He$) overlap with each other within statistical errors in both collisions events ($n_{\pi\pm} = 0$ or $n_{\pi\pm} \geq 1$). It is important to mention that, this kind of overlapping of mirror nuclei was also seen previously in inclusive Oxygen-proton reaction. It is presented in the Table 3.5 that multiplicities of recoil proton obtained from zero charged pions are higher as compared to that event where at least one charged pions are produced in Oxygen-proton collisions. It is because some parts of positive pions produced from the decay of target proton into neutron and $\pi^+$. From Table 3.5 it can be obtained the fraction of charge lost by a target proton through its inelastic exchange to reaction $p \rightarrow n + \pi^+$ and through its charge exchange $pn \rightarrow np$ with a neutron of projectile nucleus. We can obtain the fraction of a charge lost due to target proton was obtained from the given expression.

$$W(proton \rightarrow neutron) = W(n_{\pi^\pm} = 0)(1 - n_{rc}(n_{\pi^\pm} = 0)) + W(n_{\pi^\pm} \geq 1)(1 - n_{rc}(n_{\pi^\pm} \geq 1)) \text{ --------- } (3.2)$$

And the values equal to be $W(proton \rightarrow neutron) = 0.36 \pm 0.02$. In Ref. [95] in Oxygen-proton collisions the coefficient of inelastic charge exchange of target proton was obtained and it was 0.37 ± 0.01 and this that these results agrees very well with each other.

To check it from the Table 3.5, whether there is any relation between productions of light nuclei with number of charged pion production in the collision event

We observed it in the Table 3.5, the correlation between availability charged pions production and the multiplicities of light nuclei. Now to check their dependences by different method, we studied the kinematical characteristic of light fragments separately in each analyzed group of collisions events.

It is presented total momentum, transverse momentum and longitudinal momentum, and also their widths for different light nuclei fragments are shown in Table 3.6. These characteristics are obtained on absence or availability of a charged pion in Oxygen-proton collision event. In Refs. [96, 97] it is shown the kinematical characteristic multiplicities of mirror light nuclei ($^{3}$He and $^{3}$H) in oxygen-proton collisions coincidence with each other. We have united the data of these two mirror nuclei to get better results and the result can be seen in the Table 3.6.

It can be seen that mean values of total momentum and transverse momentum and their corresponding widths ($D<P>$, $D<p_T>$) do not depend within statistical errors on absence or availability of negative and positive pions in Oxygen-proton collision event. It can be seen from the table that total momentum ($P$) and $p_T$ momentum and their widths ($D<P>$, $D<p_T>$) are coincided within errors for mirror nuclei ($^{3}$H+$^{3}$He) and deuterons.

From this table it can be seen that the kinematical characteristic for deuteron and mirror nuclei ($^{3}$H+$^{3}$He) are higher than that of alpha particles. It is due to a particular character of the formation of alpha nuclei in Oxygen-Carbon collisions. There is very composite structure of projectile oxygen nucleus so the alpha particle is formed in peripheral collisions at very low excitation energy from Oxygen nucleus fragmentation in Oxygen-proton collisions.

Table 3.6. The mean values of transverse momentum, total momentum, longitudinal momentum and their widths (D) (in unit of MeV/c) for light nuclei depending on absence or availability of a charged pion.

| Quantity | Availability/Absence of charged pions in an event | Type of a fragments | | |
|---|---|---|---|---|
| | | $^2$H | $^3$H+ $^3$He | $^4$He |
| <*P*> | $n(\pi^{\pm}) \geq 1$ | 351±5 | 362±6 | 296±3 |
| | $n(\pi^{\pm}) = 0$ | 352±7 | 367±8 | 293±4 |
| D<*P*> | $n(\pi^{\pm}) \geq 1$ | 241±6 | 229±9 | 179±5 |
| | $n(\pi^{\pm}) = 0$ | 243±9 | 236±9 | 180±7 |
| $\langle P_T \rangle$ | $n(\pi^{\pm}) \geq 1$ | 253±5 | 236±4 | 189±3 |
| | $n(\pi^{\pm}) = 0$ | 257±6 | 234±6 | 189±3 |
| D$\langle P_T \rangle$ | $n(\pi^{\pm}) \geq 1$ | 207±6 | 175±7 | 143±6 |
| | $n(\pi^{\pm}) = 0$ | 215±8 | 173±8 | 149±8 |
| $\langle P_L \rangle$ | $n(\pi^{\pm}) = 0$ | 116±8 | 122±10 | 21±6 |
| | $n(\pi^{\pm}) \geq 1$ | 118±6 | 129±7 | 29±5 |
| D$\langle P_L \rangle$ | $n(\pi^{\pm}) \geq 1$ | 239±5 | 288±10 | 239±4 |
| | $n(\pi^{\pm}) = 0$ | 234±4 | 282±8 | 244±3 |

In the figure 3.6 (a) and (b) it is shown the spectra of total momentum and $p_T$ of negative and positive pions. Plots are shown for two groups of events with and without charged pions. It can be seen from these figures that in both analyzed groups ($n_{\pi\pm} = 0$ and $n_{\pi\pm} \geq 1$) spectra are coincided with each other within statistical uncertainties bars. And this shows that that process of formation of light nuclei on the basis of pions production does not have any connections [94].

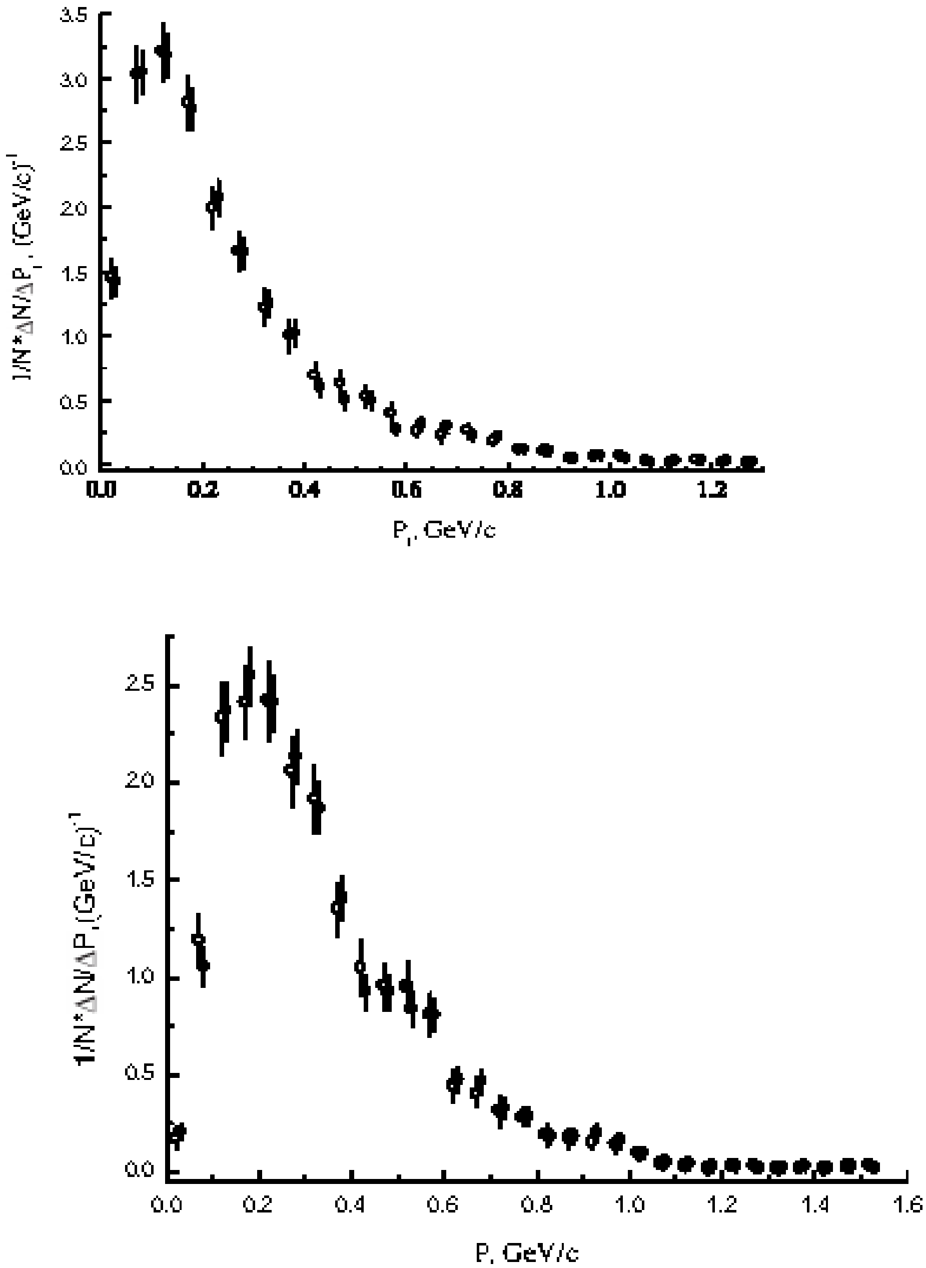


Figure 3.6. Spectra of deuterons ($^2$H nuclei) on transverse momentum (a) and total momentum (b) in $^{16}$O nucleus in collision events with absence of charge pion (•), and production of at least one charged pion (◦). For visual separation the experimental spectral points have been shifted towards left side by 5 MeV/c and to the right along the total momentum P axis for the first and second group of events, respectively.

# Chapter 4 Transverse Momentum and Rapidity Spectra of $\pi^{-}$–mesons in *AA* Collisions.

### 4.1 $p_T$ Spectra for *AA* interactions

In this chapter different results of pions transverse momentum and rapidity spectra are based on our publications [29, 30, 32, 98]. In these publications we have studied different features of pions spectra. The spectral temperatures for different ranges of $p_T$ distributions of the $\pi^{-}$ – mesons are obtained in Carbon+Tantalum, Alpha+Carbon, and Carbon+Carbon, interactions at cms energy of $\sqrt{s_{nn}}$ = 3.14 GeV (4.2 *A* GeV/*c*). For these colliding systems and selected a specified collision centralities (peripheral, semicentral and central collisions), the spectral temperatures will be extracted from the fitting of $p_T$ distributions at different ranges and at different equations (Boltzmann function and Hagedorn function (already shown in chapter 2)). It will be of more interest to check the degree of centrality of projectile and target particles, size and their overlapping region at present analyzed collisions. It will be checked is there any dependence of different overlapping region on extracted spectral temperatures?

It can be observed in the table 4.1 that the model values very nicely fit experimental values for negative pions in present work in analyzed collisions except the mean multiplicity of negative pions in Carbon+Tantalum collisions and also the $p_T$ values extracted from model underestimates the experimental $p_T$ values for all the three collisions system. The QGSM values are higher than the experimental mean multiplicity for negative pions in $^{12}C+^{181}Ta$ interactions. It is because the QGSM simply defines the nuclear effect at low energies, which are dominant in heavy ion collisions [99, 100]. It is already mentioned in Ref. [100] that there are some flaws in this model and these flaws can be removed by introducing $\pi$ – mesons absorption cross section in dense baryon medium and these absorption rate of $\pi$ – mesons should be increased.

Table 4.1. It shows participant protons, mean multiplicities per event of $\pi^-$ — mesons, transverse momentum of $\pi^-$ and the average values of rapidity in $^4$He$^{12}$C [101], $^{12}$C$^{12}$C [34, 35] and $^{12}$C$^{181}$Ta [32, 35] interactions.

| Type | | $<n_{part.prot.}>$ | $<n(\pi^-)>$ | $<p_T(\pi^-)>$ (GeV/$c$) | $<y_{c.m.}(\pi^-)>$ |
|---|---|---|---|---|---|
| $^4$He +$^{12}$C | Exp. | 2.83±0.02 | 1.02±0.01 | 0.247±0.002 | –0.090±0.007 |
| | QGSM | 2.60±0.01 | 0.99±0.01 | 0.224±0.001 | –0.082±0.007 |
| $^{12}$C+$^{12}$C | Exp. | 4.35±0.02 | 1.45±0.01 | 0.242±0.001 | –0.016±0.005 |
| | QGSM | 4.00±0.02 | 1.59±0.01 | 0.219±0.001 | 0.007±0.005 |
| $^{12}$C+$^{181}$Ta | Exp. | 13.3±0.2 | 3.50±0.10 | 0.217±0.002 | –0.34±0.01 |
| | QGSM | 14.4±0.2 | 5.16±0.09 | 0.191±0.001 | –0.38±0.01 |

In the figure 4.1 it is shown the spectra of transverse momentum and rapidity for negative pions in Carbon+Tantalum, Alpha+Carbon, and Carbon+Carbon interactions at present collisions. We can see it in the figure 4.1 that QGSM Model little below the experimental value for negative pions in analyzed collisions and also the model describes satisfactorily the experimental rapidity spectra of negative pions. However, as can be seen from Fig. 4.1(f), the double peak structure is observed in QGSM rapidity spectrum of the negative pions in $^{12}$C-$^{181}$Ta collisions. The appearance of this structure in the model is likely due to separation of heavy target fragmentation region from the central rapidity region in $^{12}$C-$^{181}$Ta collisions, the overlapping of projectile fragmentation and central rapidity regions is due to their closeness to each other in the rapidity space. The experimental broadening caused by the experimental resolution of the rapidity spectrum is obviously due to the absence of such a structure in the experimental rapidity distribution. Therefore the overlapping of both target fragmentation and central rapidity regions takes place in the experimental rapidity distribution of the negative pions. The twisted structure in figure 4.1(e) is observed in the region $p_T \approx 0.9-1.0$ GeV/$c$ of the QGSM transverse momentum spectrum of the negative pions. The statistical fluctuation of QGSM is the main cause of the appearance of this type of structure. It is fact that only few pions are produced in that region and the QGSM spectrum finishes at lower $p_T$ values compared to the experimental transverse momentum of negative pions.

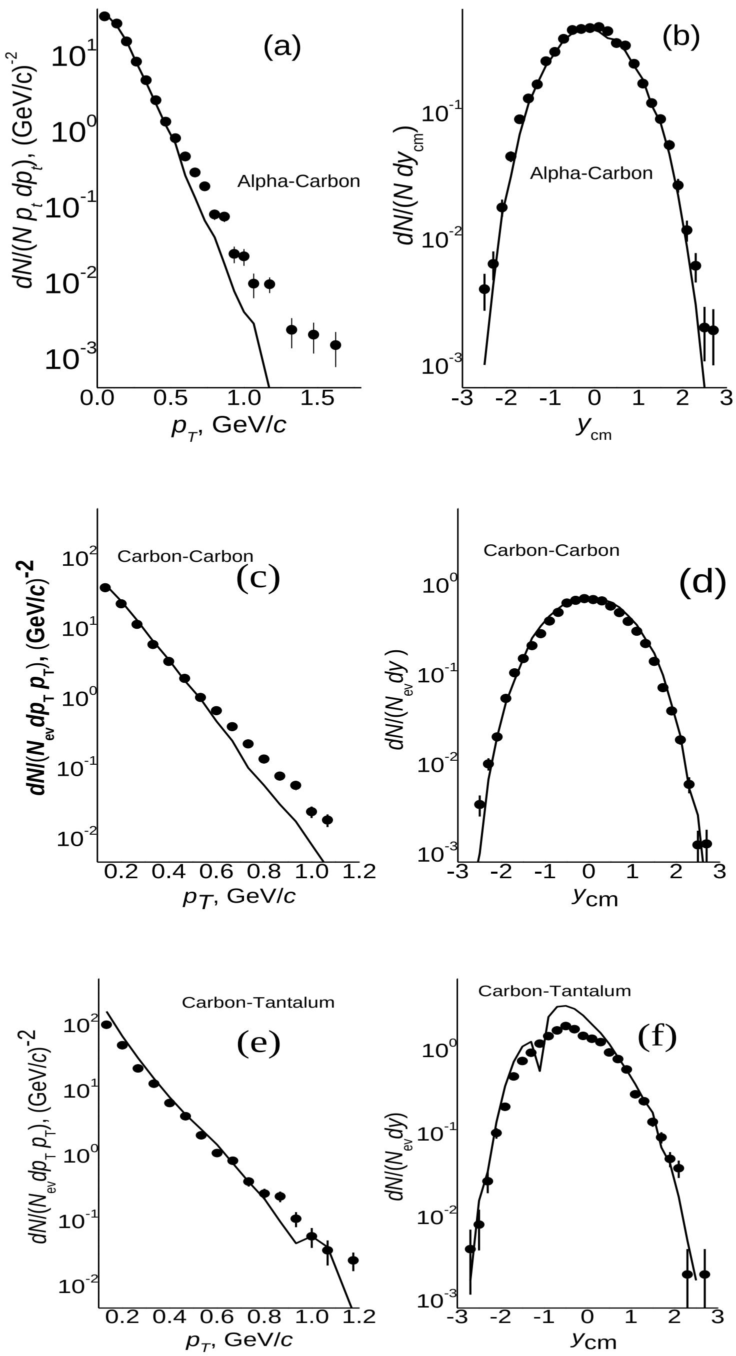


Figure 4.1. The experimental $p_{T-}$ spectra (a, c, and e) and $y_{cm}$ distributions (b, d, and f) of the π− obtained in $^{4}He^{12}C$ [101](a, b), $^{12}C^{12}C$ [32] (c, d), and $^{12}C^{181}Ta$ [28] (e, f) collisions at 4.2 GeV/*c* per nucleon. All spectra obtained are normalized per one inelastic interaction event. Solid lines represent QGSM model data.

In Table 4.2 it is shown the temperatures extracted from spectra for $\pi^-$ obtained from fitting results of Hagedorn thermodynamic model and Boltzmann functions. The extracted spectral temperatures ($T_1$, $T_2$) from $p_T$ spectra fitted (by two temperature Hagedorn and two temperature Boltzmann functions) for negative pions are lower [38], while the spectral temperatures obtained from fitting (by Maxwell-Boltzmann distribution function) of non-invariant cms energy spectra are higher. Hence, it is already mentioned that pions are mostly produced from two ways. In one temperature we wanted to show the one way of pions production. Therefore, *χ2/n.d.f.* values are very high for one temperature functions.

Table 4.2. Spectral temperatures (one temperatures and two temperatures obtained from Hagedorn and Boltzmann functions) of $\pi^-$ mesons in $^4$He-$^{12}$C, $^{12}$C-$^{12}$C, and $^{12}$C-$^{181}$Ta collisions from fitting of experimental transverse momentum spectra.

| Fitting functions | Collision type | Type | $A_1$, (GeV)$^{-1}$ | $T_1$, MeV | $A_2$, (GeV)$^{-1}$ | $T_2$, MeV | $\chi2/n.d.f.$ | $R^2$ factor |
|---|---|---|---|---|---|---|---|---|
| One Temperature Hagedorn | $^4$He$^{12}$C | Exp. | 1102 ± 65 | 97 ± 1 | --- | --- | 4.19 | 0.96 |
| | | QGSM | 1843 ± 45 | 84 ± 1 | --- | --- | 1.35 | 0.998 |
| | $^{12}$C$^{12}$C | … | 1355 ± 74 | 99 ± 1 | --- | --- | 8.17 | 0.94 |
| | $^{12}$C$^{181}$Ta | … | 5040 ± 391 | 88 ± 1 | --- | --- | 7.79 | 0.92 |
| Two Temperature Hagedorn | $^4$He$^{12}$C | Exp. | 1713 ± 186 | 83 ± 4 | 43 ± 33 | 150 ± 15 | 1.43 | 0.99 |
| | | QGSM | 1314 ± 2102 | 87 ± 10 | 702 ± 1819 | 70 ± 46 | 1.43 | 0.998 |
| | $^{12}$C$^{12}$C | … | 3097 ± 353 | 76 ± 3 | 101 ± 38 | 142 ± 7 | 1.33 | 0.99 |
| | $^{12}$C$^{181}$Ta | … | 21715 ± 4335 | 57 ± 3 | 494 ± 149 | 128 ± 6 | 0.93 | 0.99 |
| One Temperature Boltzmann | $^4$He$^{12}$C | Exp. | 974 ± 56 | 86 ± 1 | --- | --- | 6.34 | 0.95 |
| | | QGSM | 1652 ± 38 | 74 ± 1 | --- | --- | 4.05 | 0.995 |
| | $^{12}$C$^{12}$C | … | 1140 ± 62 | 89 ± 1 | --- | --- | 11.83 | 0.92 |
| | $^{12}$C$^{181}$Ta | … | 4296 ± 322 | 78 ± 1 | --- | --- | 10.03 | 0.89 |
| Two Temperature Boltzmann | $^4$He$^{12}$C | Exp. | 1811 ± 204 | 68 ± 3 | 71 ± 33 | 124 ± 8 | 1.44 | 0.99 |
| | | QGSM | 1706 ± 223 | 53 ± 7 | 822 ± 267 | 82 ± 3 | 1.35 | 0.998 |
| | $^{12}$C$^{12}$C | … | 3088 ± 326 | 65 ± 2 | 95 ± 26 | 127 ± 5 | 1.40 | 0.99 |
| | $^{12}$C$^{181}$Ta | … | 19069 ± 3229 | 50 ± 2 | 385 ± 98 | 116 ± 5 | 1.02 | 0.99 |

As we have mentioned that extracted spectral temperature are higher than our temperature. This is due to, in Ref. [77] they have included the longitudinal motion of produced negative pions which is longitudinal boosted in Lorentz frame while in our work we have used transverse momentum which is invariant in Lorentz frame [30-32].

In Figure 4.2 (a, b, c) it is shown the experimental transverse momentum fitted for three collisions system by one temperatures for $^{4}$He-$^{12}$C (a, b) and two temperatures (a, b (for $^{4}$He-$^{12}$C), c, d (for $^{12}$C-$^{12}$C), and e, f (for $^{12}$C-$^{181}$Ta)) systems, using Hagedorn Thermodynamic model and Boltzmann functions. It can be observed from Figure 4.2 (a, b), that fitting results of two temperatures Hagedorn functions and Boltzmann for total $p_T$ spectra are much better than that of one temperature function fitting. In figure 4.2 (c, d, e, and f) the experimental $p_T$ of $\pi^-$ are fitted by two temperature Hagedorn and Boltzmann functions, as it is already mentioned that one temperature fitting do not fit very well. The main reason behind two temperature fittings are pro

duction of negative pions are not only produced by direct way, but also by decay of delta resonances. In Table 4.2 represents the extracted parameters from these fitting results. The concept of two temperatures of $\pi^-$ is already observed in other experiments and various energies for different nuclei [30, 39, 40, 84]. There is another phenomenon called collective flow and the collective flow of produced pions have also very important feature of heavy ion interactions. An apparent temperature of the emitting source of transverse mass spectra or inverse slope of parameter ($T$), of produced particles were shown that it was consisted of two components: (1) the first part is called the thermal part and it is represented by ($T_{\text{Thermal}}$), and (2) this part is almost equal to the collective expansion with an average transverse velocity ($\langle\beta_t\rangle$) [102]. It is very important to mention that collective flow of negative pions and proton produced at momentum of (4.2 to 4.5) GeV/$c$ per nucleon in C-Ta, C-Cu, C-Ne, C-C and He-C interactions is already observed [103-105]. Another possibility that two temperature spectra of produced pions are also explained by two types of pions: (1) pions that are produced from hot core of overlap region at initial stage of interaction of projectile and target nuclei and (2) others pions that are generated later on from the expansion nuclear matter and then freeze-out of highly compressed matter. And we also called that compressed nuclear region a fireball. The fireball is produced mostly at central or semicentral *AA* collisions at relativistic energies. It is important to mention that the low spectral temperatures of negative pions are considered to be the mixture of expansion of nuclear matter and then freeze-out of a fireball, with “cold” $\pi$ originated from decay of resonances at a later stage of interaction. While the high temperature part of pions are coming from hard or semi *AA* collisions.

We obtained spectra temperature from invariant $p_T$ spectra and the observed two temperatures obtained for negative pions in our present analyzed collisions has the following possible reasons: (1) collective flow, (2) from decay of different resonances and (3) pions produced from hard or semi *AA* interactions. Each of these three parts has possible contribution with certain weight in $p_T$ spectra for pions and also it depends on degree of collisions centrality, mass of target and projectile nuclei.

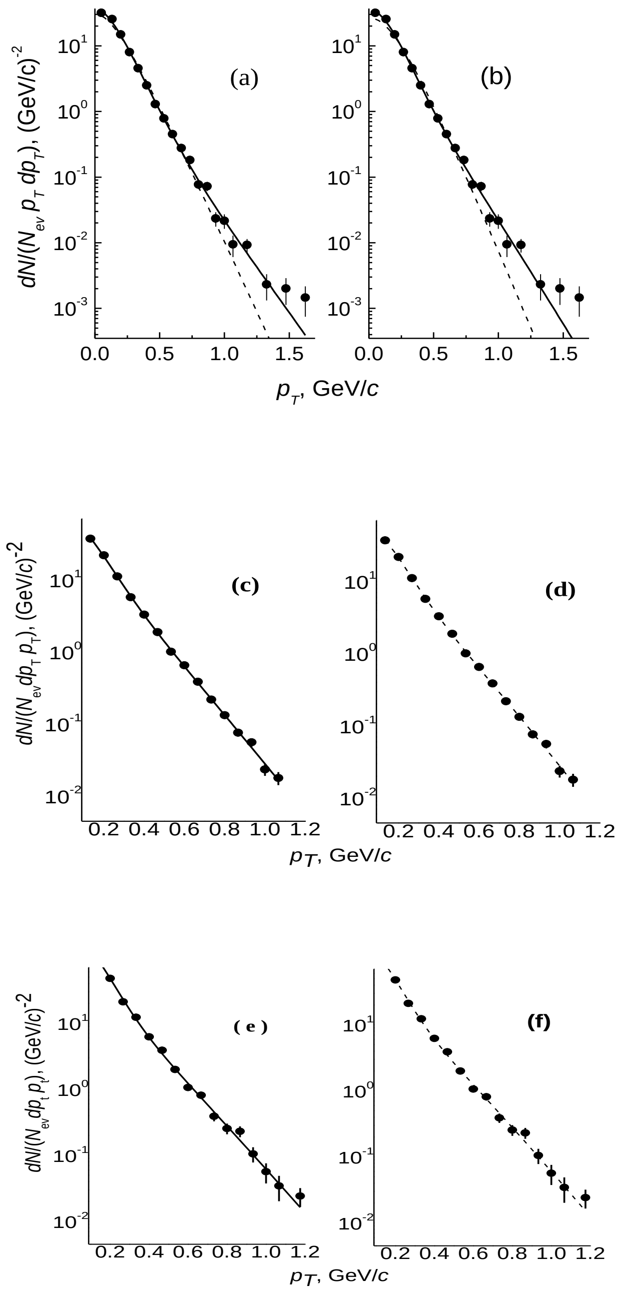


Figure 4.2. (Alpha+Carbon collision (a,b)) [101].The experimental $p_T$ spectra of the $\pi-$ fitted one temperature (dashed line) and by two temperature (solid lines), using Hagedorn (a) and Boltzmann (b) functions. (Carbon+Carbon collision (c, d)) [32]. The experimental $p_T$ spectra of the $\pi-$ fitted by two-temperature Hagedorn model (solid line) and Boltzmann function (dashed lines). (Carbon+Tantalum collision (e, f)) [28]. The experimental $p_T$ spectra of the $\pi-$ fitted by two-temperature Hagedorn model (solid line) and Boltzmann function (dashed lines).

Now to study the change in shape of transverse momentum spectra of $\pi^-$ in $^{4}He+^{12}C$ [30, 101] $^{12}C+^{12}C$ [32] and $^{12}C+^{181}Ta$ [28] interactions. It is already known that decreasing the impact parameter of colliding nuclei (projectile and target) increases the collisions centrality. And the multiplicities of produced particles also increase. The degree of collisions centrality is also defined by the number of participant protons of target and projectile overlapping nuclei. The collision centrality is also divided by three types, peripheral, semicentral and central collisions and these three types are already briefly defined in second chapter my thesis. In Table 4.3 it is defined three types of experimental collisions events for $^{4}He+^{12}C$ [30],$^{12}C+^{12}C$ [32] and$^{12}C+^{181}Ta$ [28]. In Table 4.3 it is also shown these three types of collisions events produced from QGSM. And from this table it can be seen the model satisfactorily describes the experimental collisions events. In Table 4.3 it shows there about ~ (0–15)% central collisions events in $^{12}C+^{181}Ta$ collisions and there are about~ (0–10)% central collisions events in $^{4}He+C$ and$^{12}C+^{12}C$ collisions. In Table 4.3 it is shown a comparison of spectral temperatures and their relative contributions ($R_1$and $R_2$) for present three collisions events ($^{4}He+^{12}C$ [30, 101],$^{12}C+^{12}C$ [32], and $^{12}C+^{181}Ta$ [28] collisions) and results of Ref. [37]. In Ref. [37] it is shown very less statistics as compare to the statistics used in our present work. In our present work we have used $p_T$ spectra fitted by two temperature Boltzmann and Hagedorn functions while in Ref. [37] it is used non-invariant c.m. energy spectra of $\pi^-$ for same incident energies. In Ref. [37] it is used two temperatures Maxwell-Boltzmann function as one of the fitting function to obtained spectral temperature and relative contributions ($R_1$and $R_2$). It is presented in the Table 4.3 that in our present work the spectra temperatures ($T_1$, $T_2$) of $\pi^-$ obtained by the fitting of theoretical models are lower than [37]. It is already briefly explained that the higher values of [37] is due to energy spectra of $\pi^-$ are longitudinal boosted in Lorentz frame while the $p_T$ spectra are invariant in Lorentz frame [39-41, 106].

Table 4.3. Spectral temperatures and relative contributions ($R_1$and $R_2$ ) of the $\pi-$ in $^{4}He^{12}C$[30], $^{12}C^{12}C$ [32] and $^{12}C^{181}Ta$ [28] collisions are obtained at 4.2 A GeV/c. The experimental $p_T$ spectra is fitted by two temperatures Boltzmann and Hagedorn functions for whole range of $p_T$ spectra and the corresponding

values are compared with values obtained in Ref. [37] from fitting the non-invariant c.m. energy spectra of the $\pi^-$ by Maxwell-Boltzmann distribution function.

| Fitting Function | Collision Types | $T_1$ (MeV) | $R_1$ (%) | $T_2$ (MeV) | $R_2$(%) | $\chi 2/n.d.f.$ | $R^2$ |
|---|---|---|---|---|---|---|---|
| Hagedorn | CTa | 57 ± 3 | 80 ± 22 | 128 ± 6 | 20 ± 7 | 0.92 | 0.99 |
| | HeC | 83 ± 4 | 89 ± 14 | 150 ± 15 | 11 ± 8 | 1.43 | 0.99 |
| | CC | 76 ± 3 | 85 ± 14 | 142 ± 7 | 15 ± 6 | 1.32 | 0.99 |
| Maxwell-Boltzmann | CTa | 66 ± 2 | 88 ± 3 | 159 ± 6 | 12 ± 3 | 0.58 | N/A |
| | HeC | 94 ± 6 | 85 ± 11 | 173 ± 22 | 15 ± 11 | 0.54 | N/A |
| | CC | 83 ± 3 | 79 ± 6 | 145 ± 7 | 21 ± 6 | 0.72 | N/A |
| Boltzmann | CTa | 50 ± 2 | 83 ± 20 | 116 ± 5 | 17 ± 5 | 1.02 | 0.99 |
| | HeC | 68 ± 3 | 85 ± 13 | 124 ± 8 | 15 ± 7 | 1.44 | 0.99 |
| | CC | 65 ± 2 | 85 ± 13 | 127 ± 5 | 15 ± 4 | 1.40 | 0.99 |

It can be seen from the Table 4.3 $T_1$ has dominant contribution ($R_1$ ~ 80–90%) in pions production. It is already shown in our thesis, that dominant production of negative pions is, pions produced from direct interactions. In the present analysis results are also compatible within errors with work of Backovic [37].

## 4.2 $p_T$ and Rapidity $y_{c.m}$ analysis for two temperatures in Alpha – Carbon collisions.

We performed a quantitative analysis for variation in the shape and slopes of $p_T$ spectra of $\pi^-$ with increase in collisions centrality and as result decrease in impact parameters of colliding nuclei. In order to measure the impact parameter number of participant protons $N_p$ are used, that characterizes the collision centrality. The peripheral collision events are defined for which $N_p \le \langle n_{part.prot} \rangle$, and central collisions as events for which $N_p \ge 2\langle n_{part.prot} \rangle$, where $\langle n_{part.prot} \rangle$ is average multiplicity of participant protons per event, and semi-central in between multiplicity intervals of these two [44, 106].

Table 4.3 shows the fractions with respect to total inelastic cross section of peripheral, central, and semi-central Alpha+Carbon, Carbon+Carbon, and Carbon+Tantalum events, obtained through QGSM and experimental data. It can be observed from this Table that experimental and the relevant QGSM fractions of central, semi-central and peripheral Alpha + Carbon collision events show inconsistence with one another.

In the Table 4.4 we have analyzed three types of colliding systems for Alpha+Carbon [101]. These systems are divided into three degree of collisions systems.

Table 4.4. Peripheral, semicentral, and central $^4$He$^{12}$C interactions at 4.2 *A* GeV/*c*.

| Types | Peripheral interactions (%) | | Semicentral interactions (%) | | Central interactions (%) | |
|---|---|---|---|---|---|---|
| | Experiment | QGSM | Experiment | QGSM | Experiment | QGSM |
| $^4$He+$^{12}$C | 54 ± 1 | 54 ± 1 | 37 ± 1 | 38 ± 1 | 9 ± 1 | 8 ± 1 |

Table 4.5 shows extracted parameters from fitting results of two temperature functions within interval (0.1 to 1.3 GeV/c) in central, semi-central, and peripheral Alpha+Carbon collisions. From the Table 4.5, it can be seen that for central, semi-central, and peripheral Alpha+Carbon collisions, $p_T$ spectra fitting results by two temperature Hagedorn within the fitting errors are compatible with that of two temperatures Boltzmann functions.

Table 4.5. Extracted parameters from fitting results in range, (0.1 to 1.3 GeV/c) in Alpha+Carbon interactions, for central, semi-central and peripheral collisions by two temperature Boltzmann and Hagedorn function.

| Fitting function | Collision Type | $A_1$(GeV)$^{-1}$ | $T_1$(MeV) | $A_2$(GeV)$^{-1}$ | $T_2$(MeV) | $\chi 2/n.d.f.$ | $R^2$ |
|---|---|---|---|---|---|---|---|
| Hagedorn | Peripheral | 1930±635 | 68±9 | 96±84 | 124±14 | 0.99 | 0.99 |
| | Semicentral | 5150±3215 | 58±14 | 556±238 | 111±7 | 1.54 | 0.99 |
| | Central | 6935±6371 | 60±22 | 1184±844 | 107±10 | 0.97 | 0.99 |
| Boltzmann | Peripheral | 1695±462 | 61±7 | 76±50 | 114±9 | 0.95 | 0.99 |
| | Semicentral | 4430±1878 | 54±8 | 368±139 | 103±5 | 1.53 | 0.99 |
| | Central | 6623±4098 | 55±14 | 788±466 | 100±9 | 0.98 | 0.99 |

It is also observed from Table 4.5, that extracted values of $T_1$ and $T_2$ for central and semi-central collisions are found slightly lower than that for peripheral collisions. The possible interpretation of this observation is that the considered collision system i.e. Alpha-Carbon is asymmetric ( $A_{proj} < A_{target}$ ) and that temperature is measured in terms of average kinetic energy of particles. The resultant lowered average kinetic energy (the temperature) of the negative pions for central collisions is due to fact that collision energy in central collisions on the average is distributed among large number of pions in comparison with that in peripheral collisions.

The following Figure 4.4 presents experimental $p_T$ spectra of $\pi^-$ produced in central, semi-central, and peripheral Alpha + Carbon interactions. These data were fitted with two temperatures Boltzmann function for (0.1 to 1.3 GeV/c). It can be observed from part (a) in Figure 4.4 that $p_T$ spectra of negative pions for peripheral collisions are significantly below as compared with that of central and semi-central collisions. This is due to increase in the centrality, which increases due to number of colliding nucleons. It is also seen in this figure that two temperatures Boltzmann function have very nice fitting results for $p_T$ spectra in central, semi-central, and peripheral Alpha + Carbon collisions.

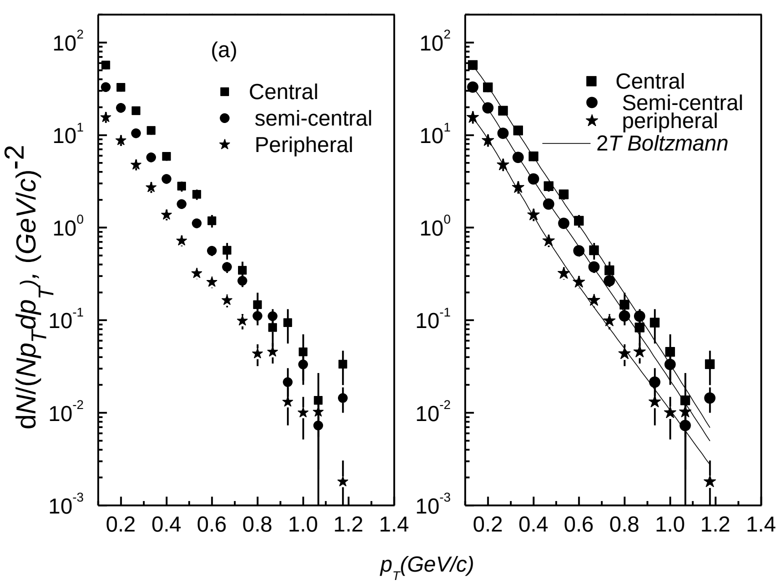


Figure 4.3. Experimental $p_T$ spectra of negative pions, in central, semi-central and peripheral Alpha + Carbon collisions (a), also fitted in the range 0.1 to 1.3GeV/*c*, with the two temperature Boltzmann function (shown by solid line in (b)).

Now for a quantitative analysis of change in shape of $p_T$ spectra of the negative pions these spectra were fitted with two temperature Boltzmann and Hagedorn functions for following three rapidity ranges: $y_{cm} \leq -0.3$, $|y_{cm.}| \leq 0.3$, and $y_{cm.} \geq 0.3$. These three rapidity regions can roughly be classified as target fragmentation region $y_{cm} \leq -0.3$, mid-rapidity region $|y_{cm.}| \leq 0.3$, and the projectile fragmentation region $y_{cm.} \geq 0.3$.

Following Table 4.6 shows the extracted parameters from fitting results of experimental $p_T$ spectra within interval (0.1 to 1.3 GeV/c) for three different rapidity ranges with two temperature Boltzmann and Hagedorn functions.

It can be observed from this Table that absolute values of extracted temperature $T_1$ proved to be consistently smaller for negative pions coming from fragmentation regions of target and projectile in comparison with those produced from mid-rapidity region.

Table 4.6. Extracted parameters from fitting results of experimental $p_T$ spectra within interval (0.1 to 1.3 GeV/c) for three different rapidity ranges with two temperature Boltzmann and Hagedorn functions.

| Fitting functions | Rapidity Interval | $A_1$(1/GeV) | $T_1$(MeV) | $A_2$(1/GeV) | $T_2$(MeV) | $\chi^2/n.d.f.$ | $R^2$ |
|---|---|---|---|---|---|---|---|
| Hagedorn | $y_{cm.} \leq -0.3$ | 6961±31 | 57±7 | 280±114 | 121±71 | 1.08 | 0.99 |
| | $\lvert y_{cm.} \rvert \leq 0.3$ | 1040±105 | 103±3 | $2\times10^{-5}\pm10$ | $1.37\times10^{8}\pm1.4\times10^{14}$ | 0.95 | 0.99 |
| | $y_{cm.} \geq 0.3$ | 8061±16 | 45±21 | 1374±47 | 92±4 | 1.77 | 0.98 |
| Boltzmann | $y_{cm.} \leq -0.3$ | 5536±18 | 52±5 | 190±67 | 112±6 | 1.06 | 0.99 |
| | $\lvert y_{cm.} \rvert \leq 0.3$ | 1114±26 | 73±17 | 227±328 | 111±17 | 1.02 | 0.99 |
| | $y_{cm.} \geq 0.3$ | 835±30 | 86±4 | 6222±59 | 44±11 | 1.71 | 0.98 |

The following figure 4.4 presents experimental $p_T$ spectra and their fitting with two temperatures Boltzmann function in the range (0.1 to 1.3 GeV/c), for three regions of rapidity in Alpha + Carbon collision. We normalized $p_T$ spectra of negative pions in different rapidity ranges, per one pion, since pions generated in one event may correspond to different regions of rapidity, means that same events may have contribution for $p_T$ spectra from these three rapidity intervals.

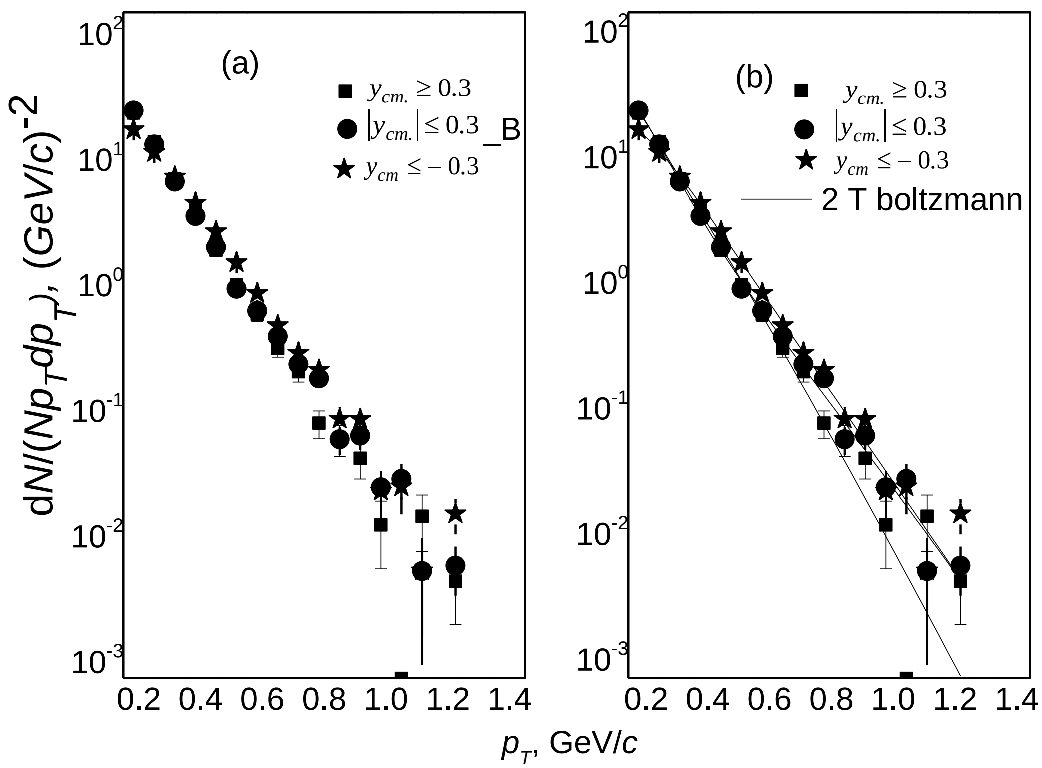


Figure 4.4. Experimental $p_T$ spectra of negative pions within interval (0.1 to 1.3 GeV/c), for all tree rapidity intervals (a), and fitted with two temperature Boltzmann function (shown by solid line (b)).

### 4.3 $p_T$ and Rapidity $y_{c.m}$ Analysis for One temperatures in Alpha ─ Carbon collisions.

It can be observed from Table 4.6, the fitting with the two temperatures Hagedorn functions of $p_T$ spectra from mid-rapidity range ($|y_{cm.}| \leq 0.3$) resulted in almost zero value of the parameter $A_2$ and too large value of $T_2$ with the values of uncertainties much greater than the absolute values of these parameters. Also, for fitting with two temperatures Boltzmann function of $p_T$ spectra of the negative pions coming from mid-rapidity range, fitting error of $A_2$ proved to be larger than its absolute value. Therefore, it is natural to study the rapidity range and centrality dependence of the $p_T$ spectra of negative pions by fitting their corresponding spectra also with one temperature Boltzmann and Hagedorn functions.

Following Table 4.7 shows extracted parameters from fitting results of transverse momentum spectra within interval (0.1 to 1.3 GeV/c), of negative pions in central, semi-central, and peripheral Alpha + Carbon collisions with one temperature Boltzmann and Hagedorn functions.

Table 4.7. Extracted parameters from fitting (with one temperature Boltzmann and Hagedorn functions) results of $p_T$ spectra (0.1 to 1.3 GeV/c), in central, semi-central and peripheral collisions.

| Fitting Function | Collision Type | Type | ***A***(GeV)$^{-1}$ | ***T***(MeV) | $\chi^2/n.d.f.$ | $R^2$ |
|---|---|---|---|---|---|---|
| Hagedorn function | Peripheral | Exper. | 828±79 | 90±2 | 2.91 | 0.96 |
| | | QGSM | 949±63 | 83±3 | 1.64 | 0.99 |
| | Semicentral | Exper. | 1431±124 | 96±3 | 3.11 | 0.97 |
| | | QGSM | 2690±115 | 83±2 | 0.92 | 0.99 |
| | Central | Exper. | 2754±288 | 94±1 | 1.46 | 0.98 |
| | | QGSM | 4645±359 | 84±2 | 1.31 | 0.99 |
| Boltzmann function | Peripheral | Exper. | 727±64 | 79±1 | 3.88 | 0.95 |
| | | QGSM | 792±44 | 74±1 | 1.91 | 0.99 |
| | Semicentral | Exper. | 1240±91 | 86±1 | 4.41 | 0.96 |
| | | QGSM | 2188±89 | 74±1 | 1.99 | 0.99 |
| | Central | Exper. | 2346±230 | 84±2 | 2.07 | 0.97 |
| | | QGSM | 3882±293 | 75±1 | 1.69 | 0.99 |

Table 4.8 shows rapidity dependence of extracted parameters from fitting the $p_T$ spectra within interval (0.1 to 1.3 GeV/c) for three different intervals of rapidity with one temperature Boltzmann and Hagedorn functions.

It is observed from values of $\chi^2/n.d.f.$ and $R^2$ in Tables 4.7 and 4.8, that fitting results of $p_T$ spectra in the range 0.1 to 1.3GeV/$c$, with one temperature Boltzmann and Hagedorn functions, are quite satisfactory for three groups of collision centrality and the three rapidity regions. It is also observed from Table 4.7 that the absolute values of extracted spectral temperatures proved to be noticeably and consistently smaller in case of peripheral collisions as compared to central and semi-central collision.

Table 4.8. The extracted parameters from fitting $p_T$ spectra within interval (0.1 to 1.3 GeV/c) for different rapidity intervals with one temperature Boltzmann and Hagedorn functions.

| Fitting | Rapidity | Type | ***A***(GeV)$^{-1}$ | ***T***(MeV) | $\chi^2/n.d.f.$ | $R^2$ |
|---|---|---|---|---|---|---|

| function | Interval | | | | | |
|---|---|---|---|---|---|---|
| Hagedorn function | $y_{cm} \leq -0.3$ | Exper. | 1451±133 | 93±2 | 4.69 | 0.95 |
| | | QGSM | 3008±157 | 79±1 | 1.98 | 0.99 |
| | $\lvert y_{cm}\rvert \leq 0.3$ | Exper. | 986±79 | **105±2** | 1.01 | 0.99 |
| | | QGSM | 1423±75 | **95±1** | 1.68 | 0.99 |
| | $y_{cm} \geq 0.3$ | Exper. | 2057±186 | 86±2 | 1.97 | 0.98 |
| | | QGSM | 3000±165 | 79±1 | 0.805 | 0.99 |
| Boltzmann function | $y_{cm} \leq -0.3$ | Exper. | 1217±107 | 83±1 | 6.14 | 0.93 |
| | | QGSM | 2491±122 | 71±1 | 3.31 | 0.99 |
| | $\lvert y_{cm}\rvert \leq 0.3$ | Exper. | 851±65 | **93±2** | 1.47 | 0.98 |
| | | QGSM | 1222±60 | **85±1** | 1.12 | 0.99 |
| | $y_{cm} \geq 0.3$ | Exper. | 1653±144 | 78±1 | 2.59 | 0.97 |
| | | QGSM | 2442±126 | 71±1 | 0.73 | 0.99 |

It is observed from Table 4.8 that extracted spectral temperatures of negative pions in Alpha + Carbon collisions proved to be considerably higher for pions coming from mid-rapidity range as compared with those from fragmentation region of target and projectile, both for experiment and QGSM data. A similar kind of behavior was found for spectral temperature of the negative pions in Carbon + Carbon and Carbon +Tantalum collisions [28, 32]. This is due to the fact that pions coming from midrapidity range are generated mostly in hard head-on nucleon-nucleon collisions, in which the two colliding nucleons nearly stop in their nucleon-nucleon cms, and, hence, the maximum collision energy is spent on creation of pions and the kinetic energies of these produced particles. Naturally, pions coming from midrapidity range will have, on the average, larger transverse momenta in comparison with those of pions coming from fragmentation region of target and projectile.  In reference [107] it is shown form analyses of rapidity distribution of pions for Magnesium -Magnesium interaction at 4.3*A* GeV/*c* that central region of rapidity contains the pions with significantly higher transverse momenta in comparison with fragmentation region of colliding nuclei. By analyses of rapidity spectra of negative pions in various hadron-nuclear and nuclear collisions at 4.2*A* GeV/*c*, it was found that, in central region of rapidity the fraction of negative pions got increased with higher transverse momentum and in fragmentation region of projectile and target the corresponding fraction is decreased. Major concentration of negative pions with high $p_T$ was found in central rapidity region.

To check the effect of $p_T$ fitting range on extracted spectral temperatures of negative pions for different centralities of Alpha + Carbon collisions and the three different regions of rapidity, are also fitted by $p_T$ spectra in range (0.1 to 0.8 GeV/c) with one temperature Boltzmann and Hagedorn function. A similar analysis for $p_T$ spectra of negative pions has been carried out for Carbon-Carbon and Carbon-Tantalum interactions [28, 32].

Table 4.9.Extracted parameters from fitting result of $p_T$ spectra in range (0.1 to 0.8 GeV/c) with one temperature Boltzmann and Hagedorn function in central, semi-central and peripheral collisions.

| Fitting function | Collision Type | Type | ***A***(GeV)$^{-1}$ | ***T***(MeV) | $\chi^2/n.d.f.$ | $R^2$ |
|---|---|---|---|---|---|---|
| Hagedorn | Peripheral | Exper. | 1025±121 | 86±2 | 2.28 | 0.98 |
| | | QGSM | 954±77 | 83±1 | 2.29 | 0.99 |
| | Semicentral | Exper. | 1767±189 | 92±2 | 1.88 | 0.99 |
| | | QGSM | 2660±150 | 83±1 | 1.26 | 0.99 |
| | Central | Exper. | 3032±373 | 92±3 | 1.58 | 0.98 |
| | | QGSM | 4841±374 | 83±1 | 1.61 | 0.99 |
| Boltzmann | Peripheral | Exper. | 867±89 | 76±1 | 3.16 | 0.97 |
| | | QGSM | 823±47 | 73±1 | 2.64 | 0.99 |
| | Semicentral | Exper. | 1487±129 | 81±1 | 3.18 | 0.98 |
| | | QGSM | 2242±98 | 73±1 | 2.87 | 0.99 |
| | Central | Exper. | 2694±294 | 81±2 | 2.30 | 0.97 |
| | | QGSM | 4141±299 | 74±1 | 1.87 | 0.99 |

From comparison of fitting results of $p_T$ spectra in range (0.1 to 0.8 GeV/c) and (0.1 to 1.3 GeV/c) Carbon + Carbon collisions, it was observed [32] that high $p_T$ ( $p_T > 0.8$ GeV/$c$) and large temperature region of pion spectrum with high statistical uncertainties significantly effects the extracted spectral temperature, and thus centrality dependence of spectral temperature is suppressed. Values of extracted parameters from fitting results of transverse momentum spectra in the interval $0.1 \leq p_T \leq 0.8$GeV/$c$ fitted with considered one temperature function for different centralities and for three rapidity intervals are presented in Tables 4.9 and 4.10, respectively.

Comparative observation of Tables 4.7 and 4.9, and Tables 4.8 and 4.10 shows that, extracted spectral temperatures $T$ for experimental data is found to be slightly smaller for the case of $p_T$ fitting interval (0.1 to 0.8 GeV/c) in comparison with that of (0.1 to 1.3 GeV/c). On the contrary, the comparative observation of Tables 4.7 and 4.9, and Tables 4.8 and 4.10 shows that, extracted spectral temperatures $T$ using the QGSM data have no dependence on fitting interval. It is also observed from Table 4.9, that mod value of spectral temperature are found to be consistently smaller for case of peripheral collisions as compared with central and semi-central collisions, as was also observed in Table 4.7 for fitting range (0.1 to 1.3 GeV/c). The extracted temperatures using QGSM data, as observed in Table 4.9, again have no dependence on centrality of collision, as was for the case of fitting interval (0.1 to 1.3 GeV/c) (given in Table 4.7). As observed from Table 4.10, extracted spectral temperatures of the negative pions in Alpha + Carbon collisions again found to be significantly higher for pions coming from mid-rapidity range as compared with those coming from fragmentation region of target and projectile, both for the experimental and QGSM data, which confirms the same trend, as observed in Table 4.8.

Table 4.10. Extracted parameters from fitting result of $p_T$ spectra in range $0.1 \leq p_T \leq 0.8$GeV/$c$ with one temperature Boltzmann and Hagedorn function in different rapidity regions

| Fitting function | Rapidity Interval | Type | ***A***(GeV)$^{-1}$ | ***T***(MeV) | $\chi^2/n.d.f.$ | $R^2$ |
|---|---|---|---|---|---|---|
| Hagedorn | $y_{cm} \leq -0.3$ | Experiment | 1901±192 | 87±2 | 4.05 | 0.97 |
| | | QGSM | 3120±171 | 78±1 | 2.64 | 0.99 |
| | $\|y_{cm}\| \leq 0.3$ | Experiment | 1068±101 | **102±2** | 0.05 | 0.99 |
| | | QGSM | 1355±80 | **97±1** | 1.92 | 0.99 |
| | $y_{cm} \geq 0.3$ | Experiment | 2149±220 | 85±2 | 1.53 | 0.99 |
| | | QGSM | 2883±170 | 80±1 | 0.27 | 0.99 |
| Boltzmann | $y_{cm} \leq -0.3$ | Experiment | 1591±150 | 78±2 | 5.60 | 0.95 |
| | | QGSM | 2592±132 | 70±1 | 4.42 | 0.99 |
| | $\|y_{cm}\| \leq 0.3$ | Experiment | 957±83 | **90±2** | 0.31 | 0.99 |
| | | QGSM | 1209±65 | **85±1** | 1.42 | 0.99 |
| | $y_{cm} \geq 0.3$ | Experiment | 1795±171 | 76±1 | 2.46 | 0.98 |
| | | QGSM | 2413±132 | 71±1 | 0.50 | 0.99 |

The experimental $p_T$ spectrum of negative pions for three different Alpha + Carbon collision centralities (central, semi-central and peripheral collisions) and fitting results in the interval (0.1 to 0.8 GeV/c), using one temperature Hagedorn fitting functions are presented in Figure 4.6. It can be observed from Figure 4.6 that, one temperature Hagedorn function gives satisfactory fitting results for experimental $p_T$ spectra in this $p_T$ range.

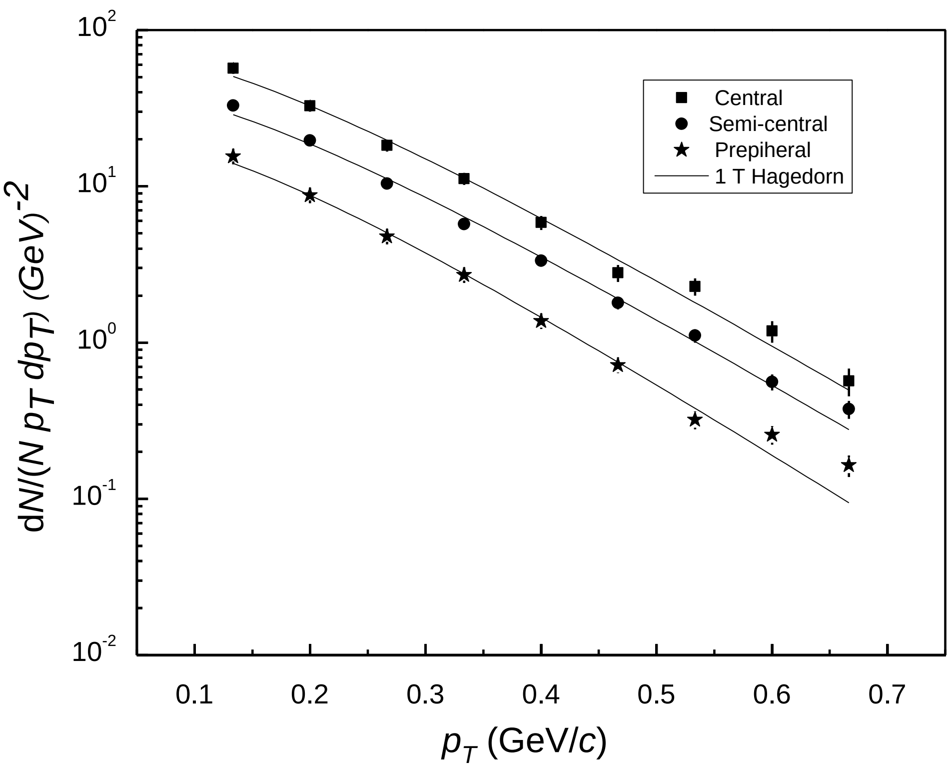


Figure 4.5. The experimental $p_T$ spectra of negative pions in region (0.1 to 0.8 GeV/c) fitted one temperature Hagedorn functions (shown by solid line).

The $p_T$ spectra of negative pions, calculated using QGSM data, for central, semi-central and peripheral Alpha + Carbon collisions and corresponding fitting results in the interval (0.1 to 0.8 GeV/c) with one temperature Hagedorn fitting function are given in Figure 4.5.

It can be seen from Figure 4.6 that, one temperature Hagedorn fitting function gives satisfactory fitting results for $p_T$ spectra of negative pions, obtained from QGSM data, for three different Alpha + Carbon collision centralities in the range (0.1 to 0.8 GeV/c).

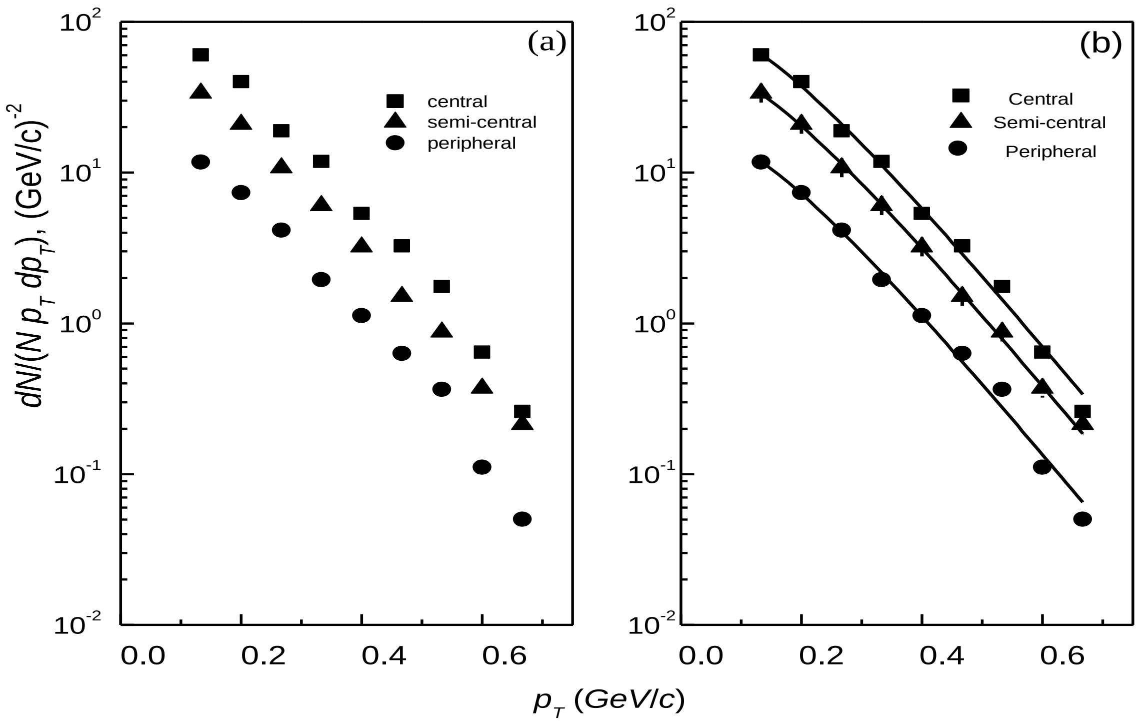


Figure 4.6. QGSM model $p_T$ spectra of negative pions, in central, semi-central and peripheral Alpha + Carbon collisions (a), also fitted in the range (0.1 to 0.8 GeV/c), with one temperature Hagedorn function (shown by solid lines line in (b)).

### 4.4 Rapidity distributions of $\pi^-$─mesons in *AA* interactions

We plan to consider the dependences of negative pions in experimental rapidity spectra distributions. These π− pions are obtained in $d^{12}C$, $^{12}C^{12}C$, and $^{12}C^{181}Ta$ interactions at incident projectile (deuteron, carbon) with momentum of 4.2GeV/*c* per nucleon. It is of great importance to investigate the dependences of $\pi^-$─mesons, on the mass numbers of target and projectile particles, various centralities of collisions and on $p_T$ distribution of $\pi^-$─mesons [108]. The extracted experimental data of $\pi^-$ will be compared with theoretical models (QGSM) [17]. It is very important to mention that extracting such kind of useful information on degree of stopping power of target nuclei such as dependence on collision centrality and the masses of target and projectile nuclei. Results are obtained from the experimental data might be beneficial to describe the relevant data on high energy heavy ion collisions.

Table 4.11. The number of participant protons and mean multiplicities per event of $\pi^-$-mesons, $p_T$ and the average values of $\langle y_{c.m.s} \rangle$ of $\pi^-$ in $d^{12}C$, $^{12}C^{12}C$, and $^{12}C^{181}Ta$ collisions in present analysis.

| Type | | $\langle n_{part.prot.} \rangle$ | $\langle n(\pi^-) \rangle$ | $\langle p_T(\pi^-) \rangle$, GeV/$c$ | $\langle y_{c.m} \rangle$ |
|---|---|---|---|---|---|
| $d+^{12}C$ | Exp. | 1.95±0.02 | 0.66±0.01 | 0.252±0.003 | –0.12±0.01 |
| | QGSM | 1.86±0.01 | 0.64±0.01 | 0.222±0.002 | –0.17±0.01 |
| $^{12}C+^{12}C$ | Exp. | 4.35±0.02 | 1.45±0.01 | 0.242±0.001 | –0.016±0.005 |
| | QGSM | 4.00±0.02 | 1.59±0.01 | 0.219±0.001 | 0.007±0.005 |
| $^{12}C+^{181}Ta$ | Exp. | 13.3±0.2 | 3.50±0.10 | 0.217±0.002 | –0.34±0.01 |
| | QGSM | 14.4±0.2 | 5.16±0.09 | 0.191±0.001 | –0.38±0.01 |

In figure 4.7 it shown a comparison between experimental and QGSM for negative mesons in present nucleus-nucleus collisions. In the figure 4.7 (a), it is shown these negative mesons are obtained from collision of Deuteron+Carbon, Carbon+Carbon, Carbon+Tantalum interactions at 4.2GeV/$c$ momentum per nucleon. In the figure 4.7 all the rapidity spectra are obtained at center of mass system ($y_{cms} \approx 1.1$) in present *AA* interactions, while the rapidity spectra distribution for Carbon+Carbon collision at c.m.s ($y_{cm}= 0$ due to symmetric C-C system with respect to midrapidity) are extracted. It can be seen from the figure 4.7 (a) the experimental data are very nicely fitted with the model data (QGSM) in Carbon+Tantalum, Deuteron+Carbon, and Carbon+Carbon interactions at 4.2*A* GeV/$c$ momentum. The number of participant protons, the mean multiplicity of $\pi^-$mesons, average value transverse momentum and the average values for rapidity distribution in Carbon+Tantalum, Deuteron+Carbon, and Carbon+Carbon interactions are presented in Table 4.11.

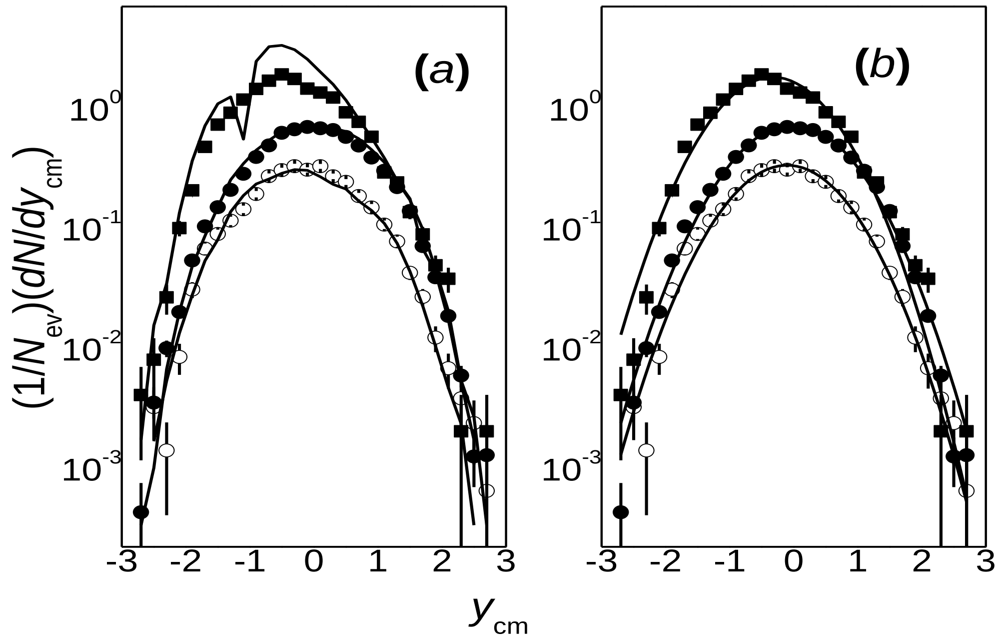


Figure 4.7. The experimental rapidity distribution of $\pi^-$ in $^{12}$CTa (■),$^{12}$C$^{12}$C (●), and $d^{12}$C (○) interactions at the present analyzed interaction. The corresponding experimental data is fitted by QGSM spectra (a) and Gaussian function (b) presented by solid lines.

The experimental rapidity distribution of $\pi^{-}$– pions fitted by Gaussian distribution function is presented in figure 4.7 (b), the equation for Gaussian function (2.16) is already explained in chapter 2.

$$F(y) = \frac{A_0}{\sigma} \exp\left( \frac{-(y-y_0)^2}{2\,\sigma^2} \right) ---------- \quad (4.1)$$

Where $y_0$ is represented by center of Gaussian spectra, $A_0$ is the fitting parameter and ($\sigma$) is the standard deviation, which presents width of spectra in the present work.

All parameters are obtained from fitting the experimental rapidity distributions of π–- mesons in *AA* (Deuteron+Carbon, Carbon+Carbon, and Carbon+Tantalum) collisions by Gaussian function in Equation (2.16) are presented in Table 4.12.

Table 4.12. It is presented the experimental and QGSM rapidity distribution of $\pi^-$–mesons fitted by Gaussian function and different parameters are extracted in $d^{12}$C, $^{12}$C$^{12}$C, and $^{12}$C$^{181}$Ta collisions.

| Type | | $A_0$ | $\sigma$ | $y_0$ | $\chi^2/$n.d.f. | $R^2$ |
|---|---|---|---|---|---|---|
| $d$+$^{12}$C | Exp. | 0.260±0.004 | 0.78±0.01 | –0.10±0.01 | 2.88 | 0.983 |
| | QGSM | 0.250±0.003 | 0.80±0.01 | –0.17±0.01 | 5.13 | 0.986 |
| $^{12}$C+$^{12}$C | Exp. | 0.575±0.004 | 0.793±0.003 | –0.016±0.005 | 8.93 | 0.992 |
| | QGSM | 0.624±0.004 | 0.786±0.003 | 0.009±0.005 | 14.21 | 0.983 |
| $^{12}$C+$^{181}$Ta | Exp. | 1.36±0.02 | 0.75±0.01 | –0.33±0.01 | 7.66 | 0.971 |
| | QGSM | 1.78±0.02 | 0.71±0.01 | –0.30±0.01 | 53.43 | 0.878 |

In case of very small deviation of theoretical fitting data from experimental data, then the $R^2$ factor approaches to one, and thus this shows a better quality fit between theoretical and experimental data. It is presented in the Table 4.12, the widths (cross section) of rapidity spectra distribution for negative pions are coincided with in errors for Deuteron+Carbon and Carbon+Carbon interactions, but values for standard deviation slightly lower in experimental and QGSM for Carbon+Tantalum collisions. The values of width of experimental rapidity distribution for negative mesons in the present collisions are little lower than values obtained in Ref. [44]. i.e. $\sigma_{\mathrm{C+Ta}} = 0.75 \pm 0.01$ and $\sigma_{\mathrm{C+C}} = 0.793 \pm 0.003$ in present analysis and $\sigma_{C+Ta} \approx 0.79$ and $\sigma_{C+C} \approx 0.82$ are values obtained in Ref. [44] for Carbon+Tantalum and Carbon+Carbon collisions for projectile at 4.2*A* GeV/*c*. In Ref. [44] they used experimental statistics were less than half as compare to our present collisions statistics. Values of $y_0$ obtained from the fitting of Gaussian function on negative mesons rapidity spectra have shown in Table 4.12 and these values proved to be equal to ( $y_{cms}$ within errors) values shown in Table 4.11 in the present analyzed data. The QGSM shows very nicely the widths and the $y_0$ of rapidity distribution for $\pi^-$–mesons in Carbon+Tantalum, Deuteron+Carbon, and Carbon+Carbon interactions in Table 4.12.

# Chapter 5 SUMMERY AND CONCLUSIONS

In Carbon+Tantalum interactions it was analyzed the dependences of characteristics of the charged pions at 4.2*A* GeV/*c*on centrality of collisions. Collisions centrality was characterized by the number of participant protons. There is a qualitative change in the average kinematical characteristic of charged pions on the basis of increasing the overlap region of target and projectile nuclei in Carbon+Tantalum interactions. There was a significant increase of the multiplicities of both positive and negative pions with increasing the overlap region of colliding Carbon+Tantalum nuclei. For all the three $^{12}$C+$^{181}$Ta collision centrality groups, we observed that multiplicity of positive pions was smaller as compared to that of the negative pions. This is likely due to the significant excess of the number of neutrons over protons in the target $^{181}$Ta nuclei (108 neutrons versus 73 protons), whereas number of neutrons is equal to the number of protons in the incident projectile $^{12}$C nuclei. Using the simple model, we estimated the multiplicity ratio $<n(\pi^-)>/<n(\pi^+)>$ is about 1.22 in $^{12}$C+$^{181}$Ta collision system. On the basis of Wounded Nucleon Model (WNM), we obtained the ratio $<n(\pi^-)>/<n(\pi^+)>$for C─Ta interactions at 4.2*A*GeV/*c* is about ≈1.24. So both ratios agree well on the basis of two different models. In Carbon+Tantalum collisions events, the experimental $<n(\pi^-)>/<n(\pi^+)>$ratios obtained for central, semicentral and peripheral collisions proved to be 1.04 ± 0.03, 1.08 ± 0.04, and 1.20 ± 0.05, respectively, decreasing noticeably with increasing (from peripheral to central) the degree of collision centrality. It can be seen there is a suppression of the $<n(\pi^-)>/<n(\pi^+)>$ratios in central and semicentral collisions events for Carbon+Tantalum collisions as compared to the calculated ratio obtained from the model ($<n(\pi^-)>/<n(\pi^+)>\approx1.22$).The main reason behind such suppression of the ratio $<n(\pi^-)>/<n(\pi^+)>$ in semicentral and central $^{12}$C+$^{181}$Ta collisions could be the higher absorption cross section of the slow negative pions produced on heavy $^{181}$Ta nuclei as compared to that of the slow positive pions. It is of great importance to present that, by increasing the collision centrality, the number of the produced slow negative pions produced in secondary interactions (rescatterings) on target $^{181}$Ta nucleons is expected to increase significantly. Hence, the suppression of the ratio $<n(\pi^-)>/<n(\pi^+)>$ should increase with increasing the $^{12}$C+$^{181}$Ta collision centrality. The average values of the full momentum distributions and their widths for the charged pions decreased significantly with an increase in $^{12}$C+$^{181}$Ta collision centrality. The observations confirm our finding, that the number of the relatively slow charged pions obtained in secondary collisions (rescatterings) on nucleons of target $^{181}$Ta nuclei increases significantly with increasing the collision centrality, which results in an increase of the average emission angle of $\pi^+$ and $\pi^-$ mesons. The results of the present collisions can be very helpful for investigation of production of charged pions and their dependences on degree of collisions centrality in heavy ion collisions at high energies.

The $p_T$ spectra of the negative pions extracted in C─Ta interactions at 4.2$A$GeV/$c$ were investigated by fitting with the four different functions i.e. Boltzmann, Hagedorn, Simple Gaussian, and Exponential functions. It was observed that $p_T$ spectra of $\pi^-$ ─ mesons are fitted much better by using the two-temperature Boltzmann and Hagedorn functions as compared to the fitting done by the one-temperature functions, and also it has very good agreement with the earlier works. In the given four fitting functions, Boltzmann and Hagedorn functions gives better fits of the experimental $p_T$ spectra and both functions give physically acceptable results of the spectral temperatures, compared to the other two functions. The fitting of the $p_T$ spectra of pions with Hagedorn function gives noticeably higher values of the spectral temperatures compared to that by Boltzmann function. It was observed that the fitting of the pion spectra by Gaussian function is not appropriate, since it gives unphysical large values of $T_1$ and $T_2$.

It is of great importance to investigate the correlations and characteristic of pions at intermediate collision energy. Therefore the correlation in the pions ($\pi^+$ and $\pi^-$) and light nuclei fragments production in the Oxygen-proton interactions at 3.25$A$GeV/$c$ was analyzed. The whole collision system was divided into two groups of charged pion for production of light nuclei fragments, (a) without charged pions and (b) with at least one charged pion. It was shown that mean multiplicities of light nuclei were higher for the second group with at least one charged pion. It was due those events in which at least one charged pion is produced, and also a large amount of energy momentum is transferred to the fragment of nuclei in present analyzed collision. For the interaction events with at least one charged pion, a large destruction of fragmented nuclei occurred as compared to those collisions where there is no charged pion. Total momentum and transverse momentum and there widths for production of light nuclei showed that they are independent on absence or availability of charged pions in the analyzed collisions events. The behavior of total momentum and transverse momentum distributions for light nuclei for two groups of the considered collision events showed satisfactorily coincidence. So, it can be concluded that light nuclei formation processes for these two groups do not depend on number of pions. The correlation observed between the absence/presence of charged pions and between light nuclei production is due small/large amount of momentum-energy transferred to the fragmenting nuclei.

We analyzed three collisions system (Carbon+Tantalum, Alpha+Carbon and Carbon+Carbon interactions) for $p_T$ spectra of $\pi-$ mesons. The experimental $p_T$ spectra were compared systematically with QGSM model calculations. We compared the experimental and model values of the mean multiplicities and average values of $p_T$ for negative pions, and the mean number of participant protons in the analyzed collision systems. We have shown that the QGSM model results underestimate the corresponding experimental results. This is due to neglecting the nuclear effect and use the production of heavy baryon resonances in the model. It was suggested that, if such effects are included in the model, then there will be a good agreement between QGSM and experiment. This comparison of model and experiment can be improved significantly.

The $p_T$ distributions of the $\pi^-$–mesons in three collision systems in experiment and QGSM model were fitted using one and two temperature Boltzmann and Hagedorn functions. Results of spectral temperatures were obtained from the fitting by (one and two temperature) Boltzmann and Hagedorn model functions in the whole range of $p_T$ spectra. The contribution of the lower temperature$T_1$to the total multiplicity of the negative pions was dominant (80 to 85) % while the contribution of the higher temperature$T_2$was low (10 to 15)%. Using Boltzmann and Hagedorn functions for two temperatures fit have much better and nice results as compare to one temperature fit of Boltzmann and Hagedorn functions. In the present work it was shown spectral temperatures ($T_1$, $T_2$) and their relative contributions ($R_1$, $R_2$) of $\pi^-$ – mesons and it was compared with results of previous works. Results extracted for present work have lower values of spectra temperatures as compared to previous results, because in previous works the temperatures were extracted from the kinetic energy spectra of pions as compared to the Lorentz invariant $p_T$ spectra analyzed by us.

The $p_T$ spectra of the negative pions for three different centralities of $^4$He─C collision system and also for three different ranges of rapidity were extracted and fitted for $p_T$ intervals $0.1 \leq p_T \leq 1.3$GeV/$c$ and $0.1 \leq p_T \leq 0.8$GeV/$c$. The values of the extracted temperatures were found lower in fitting range $0.1 \leq p_T \leq 0.8$GeV/$c$ in comparison with that of fitting range $0.1 \leq p_T \leq 1.3$GeV/$c$. In the range $0.1 \leq p_T \leq 0.8$GeV/$c$ the experimental $p_T$ spectra of the negative pions were fitted satisfactorily by one temperature Boltzmann and Hagedorn functions. In contrast with the QGSM extracted temperatures, the temperatures extracted from the experimental $p_T$ spectra were found quite sensitive to the considered $p_T$ fitting range. The extracted spectral temperatures of $\pi^-$─mesons weakly depend on the collisions centralities and were found compatible for the group of central, semi-central and peripheral Alpha + Carbon collision events. The extracted temperatures were found consistently higher for the $p_T$ spectra of negative pions at mid-rapidity range in comparison with extracted temperatures of the negative pions being produced in fragmentation regions of target and projectile.

We have used three collisions systems ($d$+$^{12}$C, $^{12}$C+$^{12}$C, and $^{12}$C+$^{181}$Ta) at incident momentum of nuclei of 4.2$A$GeV/$c$ to study rapidity distributions from negative pions. Using these systems, we obtained rapidity and $p_T$ spectra for $\pi^-$ ─ mesons. All the plots were obtained in center of mass system. The Rapidity for c.m.s is about ($\approx$1.1) in incident projectile. The Rapidity spectrum for C─C interaction is symmetric ($y_{c.m.s.} = 0$), as the projectile and target particle is same. The height of Rapidity spectra are increased as the masses of target and projectile increases and also the Rapidity spectra were shifted towards the target fragmentation region. This is because numbers of participant particles are increased as masses of overlapping particles are increased. It was observed that QGSM model shows satisfactory results with experimental data for negative pions. The Gaussian function also fit very nicely on the experimental data.

# REFERENCES


1. C. Amsler. *et. al*, *"Particle Data Group"*. Vol. 1. 2008.
2. D. Griffiths, *"Introduction to Elementery Particles"*. 2nd ed. 1987: John Wiley & Sons.
3. M. R. Stockmeier, *"Pion Production in Relativistic Heavy Ion Collision"*. 2002, University of Heidelberg, Germany. p. 18-19.
4. S. Teis. *et. al*, *"Pion-Production in Heavy-Ion Collision at SIS energies"*. arXive: nucl-th/9609009v1, 1996.
5. Steven Weinberg, *The First Three Minutes*. 1993, New York.
6. David Lindley, *The End of Physics*. 1993, New York.
7. Niclolas Solomey, *The Elusive Neutrino: A Subatomic Detective Story*. 1997: Scientific American Library, W. H. Freeman Co. .
8. J. W. Harris et. al., *"Pion production as a probe of the nuclear matter equation of state". Phys. Lett. B*, 1985. **153**: p. 377-381.
9. R. Stock, *"Particle production in high energy nucleus−nucleus collisions". Phys. Rep.*, 1986. **135**: p. 259-315.
10. E. L. Hjort *et. al.*, *Δ Resonance Production in $^{58}$Ni+Cu Collisions at E=1.97 AGeV.* Phys. Rev. Lett., 1997. **79**: p. 4345.
11. M. A. Lisa *et. al.* (EOS Collaboration), *Radial Flow in Au+Au Collisions at E=(0.25−1.15) A GeV.* Phys. Rev. Lett., 1995. **75**(14): p. 2662.
12. V.E. Fortov. and I.V. Lomonosov, *"Equations of State of Matter at High Energy Densities"* The Open Plasma Physics Journal, 2010. **3**: p. 122-130.
13. Aichelin J. and Werner K., *"A novel approach to rescattering in ultrarelativistic heavy ion collisions". Phys. Lett. B*, 1993. **300**: p. 158.
14. B. Abelev *et. al*, *Centrality determination of Pb-Pb collisions at sqrt $S_{NN}$ = 2.76 TeV with ALICE.* Phy. Rev. C., 2013. **88**(ALICECollaboration 044909 1301.4361).
15. Bao-An Li and Wolfgang Bauer, *Pion spectra in a hadronic transport model for relativistic heavy ion collisions.* Phys. Rev. C., 1991. **44**: p. 450.
16. P. K. Netrakanti and B. Mohanty, *The width of rapidity distribution in heavy ion collisions.* Phys. Rev. C., 2005. **71**(4): p. 047901.
17. N. S. Amelin *et. al.*, *Strangness production in proton and heavy ion collisions at 14.6 A GeV.* Phys. Rev. C, 1991. **44**: p. 1541.
18. Anton Adronic, *"An overview of the experimental study of quark-gluon matter in high energy nucleus-nucleus collisions". Int. J. Mod. Phys. A.*, 2014. **29**(1430047): p. 1430047-1.
19. F. Karsch, *Lattice QCD at high temperature and density*. *Lect. Notes Phys. A.*, 2002. **583**: p. 209-249.
20. Yasumichi Aoki Szabolcs Borsanyi *et. al.*, *The QCD transition temperature: results with physical masses in the continuum limit II.* J. High Energy Phys., 2009. **06**(088): p. 17.
21. H. H. Gan S. J. Lee and S. Das Gupta, *Applications of the extended Boltzmann-Uehling-Uhlenbeck model to participant and spectator dynamics.* Phy. Rev. C., 1987. **36**(6): p. 2365-2370.
22. L.P. Csernai, *"Introduction to Heavy Ion Collision"*. 1994, Chichester,: John & Wiley Sons England.

23. J. Kapusta, *“Particle production in the nuclear fireball model”,. phys. Rev. C.*, 1977. **16**: p. 1493-1498.
24. J. Gosset H. Gutbrod W. Meyer *et. al.*, *"Central Collisions of Relativistic heavy ions". Phy. Rev. C.*, 1977. **16**: p. 629.
25. P. Braun-Munzinger and J. Stachel, *Pion Production in Heavy Collisions.* Ann. Rev. Nucl. Part. Sci., 1987. **37**: p. 97-131.
26. B. Abelev *et. al.*, *Pion, Kaon, and Proton Production in Central Pb-Pb Collisions a* $\sqrt{s_{NN}} = 2.76$ *TeV.* Phys. Rev. Lett., 2012. **109**(25): p. 11.
27. P. Braun-Munzinger. and J. Stachel, *"Pion Production in Heavy Collisions". Ann. Rev. Nucl. Part. Sci.* , 1987. **37**: p. 97-131.
28. Kh. K. Olimov Akhtar Iqbal B. S. Yuldashev *et. al.*, *On transverse momentum spectra of negative pions in* $^{12}C+^{181}Ta$ *collisions at 4.2A GeV/c.* Int. J. Mod. Phys. E., 2014. **23**: p. 1450084-1-22.
29. Kh. K. Olimov Akhtar Iqbal V. V. Glagolev and Mahnaz Q. Haseeb, *Analysis of rapidity spectra of negative pions in* $d+^{12}C$, $^{12}C+^{12}C$, *and* $^{12}C+^{181}Ta$ *collisions at 4.2 GeV/c per nucleon. Phy. Rev. C.*, 2013. **88**: p. 11.
30. Kh. K. Olimov Akhtar Iqbal B. S. Yuldashev *et. al*, *CENTRALITY DEPENDENCES of SOFT and HARD COMPONENTS of* $p_t$ *DISTRIBUTIONS of NEGATIVE PIONS in* $^{4}He+^{12}C$ *COLLISIONS at 4.2A GeV/c.* Int. J. Mod. Phys. E., 2015. **24**(05): p. 24.
31. Kh. K. Olimov Akhtar Iqbal *et. al.*, *Centrality and system size dependences of temperatures of soft and hard components of* $p_t$ *distributions of negative pions in* $^{4}He+^{12}C$, $^{12}C+^{12}C$, *and* $^{12}C+^{181}Ta$ *collisions at sqrt.*$s_{NN} = 3.14$ *GeV. Phy. Rev. C.*, 2015. **92**: p. 16.
32. Akhtar Iqbal Khusniddin K. Olimov Imran Khan BS. Yuldashev Mahnaz Q. Haseeb, *On centrality and rapidity dependences of transverse momentum spectra of negative pions in 12 C+ 12 C collisions at 4.2 GeV/c per nucleon.* International Journal of Modern Physics E, 2014. **23**(09): p. 1450047.
33. M. Trzaska *et. al.*, *Excitation of the Δ (1232)-resonance in proton-nucleus collisions.* Z. Phys. A, 1991. **340**(3): p. 325-331.
34. J. Chiba *et. al.*, *Coincidence measurements of (p,n) reactions at 1.5 GeV/c on C and H in the Δ excitation region.* Phys. Rev. Lett., 1991. **67**(15): p. 1982.
35. T. Hennino *et. al.*, *Study of decay and absorption of the* Δ *resonance in nuclei with a 4π detector.* Phys. Lett. B, 1992. **B283**: p. 42-46.
36. C. Alt *et. al.*, *Energy dependence of lambda, Hyperon production in central Pb+Pb collisions at 20A, 30A, 40A, 80A, and 158A GeV measured at the CERN Super Proton Synchrotron.* Physical Review C, 2008. **78**(3).
37. S. Backovic *et. al.*, *Temperature of negative pions in inelastic (d, α, C) +(C, Ta) collisions at 4.2A GeV/c. Phy. Rev. C.*, 1992. **46, 04**: p. 1501-1506.
38. Kh. K. Olimov *et al*, *Rapidity and angular dependences of spectral temperatures of negatiove pions produced in* $^{12}C+^{12}C$ *collisions at 4.2 GeV/c. Int. J. Mod. Phy. E*, 2013. **22**(04): p. 1-14.
39. R. Brockmann, *“Pion and Proton "Temperatures" in Relativistic Heavy-Ion Reactions”. Phys. Rev. Lett.*, 1984. **53**(2012-2015).

40. Lida Chkhaidze *et al.*, *Temperatures of Λ Hyperons, K0 and Pi-mesons produced in C-C and Mg-Mg collisions at 4.2 ÷ 4.3 A GeV/c,.* Bull. Georg. Natl. Acad. Sci., 2010. **4**: p. 41-47.
41. R. Hagedorn and J. Rafelski, *"Hot hadronic matter and nuclear collisions",. Phys. Lett. B*, 1980. **97**: p. 136-142.
42. R. N. Bekmirzaev E. N. Kladnitskaya and S. A. Sharipova, *Rapidity distributions of protons in (p, d, alpha, C) C interactions at 4.2-GeV/c per nucleon (In Russian).* Phys. Atom. Nucl., 1995. **58**: p. 1548-1554.
43. R. N. Bekmirzaev E. N. Kladnitskaya M. M. Muminov and S. A. Sharipova, *Rapidity distributions of π- in (d, α, C)Ta collisions at 4.2 GeV/c per nucleon.* Physics of Atomic Nuclei, 1995. **58**(10): p. 1721-1727.
44. L. Simic S. Backovic D. Salihagic A. P. Cheplakov E. N. Kladnitskaya and R. R. Mekhdiy, *Centrality dependence of pion and proton spectra in C+C and C+Ta interactions at 4.2 GeV/c per nucleon.* phys. Rev. C., 1995. **52**: p. 356.
45. J. L. Klay *et. al.*, *Charged pion production in 2A to 8A GeV central Au +Au Collisions. Phys. Rev. C.*, 2003. **68**(054905).
46. B. Mohantyand J. Alam, *Velocity of sound in relativistic heavy-ion collions. Phys. Rev. C.*, 2003. **68**(064903).
47. A. I. Malakhov A. N. Sissakian *et. al.*, *Relativistic Nuclear Physics at the Joint Institute for Nuclear Research.* Physics of Elementary Particles and Nucle, 2007. **38**: p. 407.
48. I. B. Issinsky A. D. Kirillow A. D. Kovalenko and P.A. Rukoyatkin, *Beams of the Dubna Synchrophasotron and Nuclotron.* ACTA Physica Polonica B, 1994. **25**: p. 3.
49. Baldin *et. al.*, *Twenty years of the synchrophasotron of the JINR High-Energy Physics Laboratory.* Sov. atomic energy., 1977. **43**(6): p. 1146.
50. Veksler and Baldin, *JINR Annual Report 2003, Veksler and Baldin Laboratory of High Energies*. 2003.
51. Vladimir A. Nikitin, *Synchrophastron studies.* Physics - Uspekhi, 2007. **50**(8): p. 862.
52. Donald A. Glaser, *Some Effects of Ionizing Radiation on the Formation of Bubbles in Liquids.* Phys. Rev. , 1952. **87**(4): p. 665-665.
53. M. P. Balandin N. G. Borisov *et al*, *A 2-metre propane bubble chamber.* Nuclear Instruments and Methods, 1963. **20**: p. 110-113.
54. E. O. Abdrahmanov *et. al.*, *Joint Institute for Nuclear Research, Report P1-10779, Dubna 1977* Yad. Fiz, 1978. **27**: p. 1020.
55. E. O. Abdrahmanov *et. al.*, *Joint Institute for Nuclear Research, Report E1-11517, Dubna 1978.* yad. Fiz., 1978. **28**: p. 1304.
56. D. Armutlisky, *Multiplicity, momentum and angular distributions of protons from the interactions of p, d, α and C with carbon at 4.2 GeV/c/nucleon momentum. Z. Phys. A*, 1987. **328**: p. 455-461.
57. A. I. Bondarenko *et. al.*, *JINR Communications P1-98-292, Dubna, Russia,.* 1998.
58. H. N. Agakishiyev, *e.a.*, *"Multiplicity, momentum and angular characteristics of negative pi-mesons for pC, dC, αC and CC interactions at 4.2 GeV/c per nucleon",. Z. Phys. C.*, 1985. **27**: p. 177.
59. Kh. K. Olimov and Mahnaz Q. Haseeb, *Production of $\Delta^0$(1232)-resonances in p+12C collisions at a momentum of 4.2 GeV/c.* Eur. Phys. J. A, 2011. **47**(79).

60. I. A. Bondarenko *et. al., Bondarenko A. I., Bondarenko R. A., Kladnitskaya E. N., Kuznetsov A. A., Toneeva G. P. and Yuldashev B. S. "The Ensemble of interactions on carbon and hydrogen nuclei obtained using the 2 m propane bubble chamber exposed to the beams of protons and H-2, He-4, C-12 relativistic nuclei at the Dubna Synchrophasotron"* JINR Communications. – Dubna, 1998., 1998. **№ P1-98-292.**
61. V. Flaminio G. W. Moorhead O. R. D. Morrison N. Rivoi, *Compilation of cross sections.* CERN-HERA Reports. - CERN (Geneva), 1983. **№ 83-02.**
62. Ts. Baatar, *Analyzing the Features of π– Mesons and Protons from AC Interactions at a Momentum of p = 4.2 GeV/c per Projectile Nucleon on the Basis of the FRITIOF Model.* Phys. At. Nucl., 2000. **63**: p. 839.
63. A. S. Galoyan E. N. Kladnitskaya O. V. Rogachevsky R. Togoo and V. V. Uzhinskii, *Features of pC Interactions at a Momentum of 4.2 GeV/c versus the Degree of Centrality of a Collisions between a Proton and a Carbon Nucleus: Kinematical Features of Secondaries.* Phys. At. Nucl., 2004. **67**: p. 256.
64. Alma *et. al., "Peripheral and central nucleus-nucleus collisions at 4.2 GeV/c per nucleon",.* JINR Communications E1-82-510, Dubna, Russia,, 1982.
65. A. I. Bondarenko *et. al, "Study of nucleus-nucleus interactions with complete destruction of the target nucleus with momentum 4.2-GeV/c per nucleon",. Phys. At. Nucl.*, 1997. **60**: p. 1833.
66. Kh. K. Olimov Mahnaz Q. Haseeb Imran Khan A. K. Olimov V. V. Glagolev, Phys. Rev. C, 2012. **85**(014907).
67. Kh. K. Olimov, and Mahnaz Q. Haseeb., *"Production of Δ0(1232)-resonances in p+12C collisions at a momentum of 4.2 GeV/c",. Eur. Phy. J. A.*, 2011. **47**: p. 79.
68. Kh. K. Olimov *et. al., "$\Delta^0$ (1232) production in d + 12C collisions at 4.2 A GeV/c",.* Phys. Rev. C., 2012. **85**(014907).
69. N. S. Amelin *et. al., "Further Development Of A Quark-Gluon String Model For Describing High-energy Collisions With A Nuclear Target".* Sov. J. Nucl. Phys., 1990. **52**: p. 172-178.
70. S. Nagamiya, *"Role of Mean Free Paths of Product Particles in High-Energy Nucleus-Nucleus Collisions",. Phys. Rev. Lett.*, 1982. **49**: p. 1383-1386.
71. J. Gosset *et. al., "Calculations with the nuclear firestreak model",. Phys. Rev. C.*, 1978. **18**: p. 844-855.
72. S. Nagamiya *et. al., "Single-Particle Spectra Associated with High-Multiplicity Events in 800 MeV/Nucleon Ar on KCl and Pb",. Phys. Rev. Lett.*, 1980. **45**: p. 602-605.
73. S. Bohrmann and J. Knoll, *"Finite number of effects in high-energy nuclear collision: Implications on pion spectra",. Nucl. Phys. A.*, 1981. **356**: p. 498-516.
74. R. Hagedorn, in Cargese Lectures in Physics VI, ed. E. Schatzman, Gordon and Breach, New York, 1973: p. 643.
75. Akhtar Iqbal Khusniddin K. Olimov Mushtaq Ahmad *et. al., Collision centrality dependencies of charged pion production in $^{12}C+^{181}Ta$ collisions at 4.2 A GeV/c.* International Journal of Modern Physics E, 2018. **27**(11): p. 12.
76. L. Ahle *et. al.* (E-802 and E-866 Collaborations), *Cantrality dependence of kaon yields in Si + A and Au + Au collisions at the AGS.* Phys.Rev. C., 1999. **60**: p. 18.
77. D. Krpic G. Skoro I. Picuric S. Backovic and S. Drndarevic, Phys. Rev. C, 2002. **65**(034909).

78. Bao-An Li and Che Ming Ko, *Formation of superdense hadronic matter in high energy heavy-ion collisions.* Phys.Rev. C., 1995. **52**(4): p. 2037.
79. W. Ehehalt W. Cassing A. Engel U. Mosel Gy. Wolf, *Effects of pion and delta selfenergies in nucleus-nucleus reactions.* Phys. Lett. B, 1993. **298**: p. 31-35.
80. M. Eskef *et. al*. (FOPI Collaboration), *Identification of baryon resonances in central heavy-ion collisions at energies between 1 and 2 AGeV.* Eur. Phys. J. A, 1998. **3**: p. 335-349.
81. J. Barrette *et. al.* (E814 Collaboration), *Measurement of pion enhancement at low transverse momentum and of the Δ resonance abundance in Si-nucleus collisions at AGS energy.* Phys. Lett. B, 1995. **351**: p. 93-98.
82. G. E. Brown J. Stachel and G. M. Welke, *Pions from resonance decay in Brookhaven relativistic heavy-ion collisions.* Phys. Lett. B., 1991. **253**(1-2): p. 19-22.
83. Kh. K. Olimov *et. al.*, *Production of* $\Delta^0$ *and* $\Delta^{++}$ *resonances in collisions of 4He nuclei with carbon nuclei at 4.2 GeV/c per nucleon.* Phys. Rev. C, 2007. **75**(067901).
84. L. Chkhaidze *et al.*, *The temperatures of protons and π– mesons in central nucleus-nucleus interactions at a momentum of 4.5 GeV/c per incident nucleon* Z. Phys. C, 1992. **54**: p. 179.
85. L. Chkhaidze *et al.*, *An isotropic collective flow of Λ-hyperons produced in C+C collisions at 4.2 A GeV/c* Nucl. Phys. A., 2009. **831**(1-2): p. 22-38.
86. A. Bialas M. BleszyńskiaW. Czyżb, *Multiplicity distributions in nucleus-nucleus collisions at high energies.* Nuclear Physics B, 1976. **111**(3): p. 461-476.
87. V. Butsev Yu. K. Gavrilo A. B. Kurepin, *THE PROBABILITY OF SINGLE-NUCLEON EMISSION IN* $\pi^-$*CAPTURE REACTIONS ON THE* $^{152}$*S m AND* $^{164}$*Dy NUCLEI* Physics of Particles and Nuclei, 1981. **11**: p. 900.
88. Heinz J Weyer, *Pion absorption in light nuclei.* Physics Reports, 1990. **195**(6): p. 295-367.
89. T.-S. H. Lee and R. P. Redwine, *Pions-Nucleus-Interactions.* Ann. Rev. Nucl. Part. Sci., 2002. **52**: p. 23-63.
90. A. Engel W. Cassing U. Mosel M. Sch¨afer Gy. Wolf, *Pion-nucleus reactions in a microscopic transport model*.* arXiv:nucl-th/9307008v1 7 Jul 1993, 1993.
91. R. D. McKeown *et al.*, *How Many Nucleons are Involved in Pion Absorption in Nuclei?* Phys. Rev. Lett., 1980. **44, 1033**(44).
92. I. Navon *et al.*, *True Absorption and Scattering of 125-MeV Pions on Nuclei.* Phys. Rev. Lett., 1979. **42, 1465**(22).
93. Y. M. Shabelsky, *On the Multiplicity of the Seconderies produced in collisions of relativistic nuclei* Acta Physica Polonica B, 1979. **10**: p. 1049-1056.
94. Kosim Olimov Khusniddin K. Olimov Sagdulla L. Lutpullaev Akhtar Iqbal Alisher K. Olimov Bekhzod S. Yuldashev KG. Gulamov, *Correlations between production of charged pions and formation of light nuclei in* $^{16}$*Op collisions at 3.25 A GeV/c.* International Journal of Modern Physics E, 2017. **26**(06): p. 1750033.
95. Kh. K. Olimov, *Experimental investigation of charge-exchange processes involving a target proton in 16Op collisions at a momentum of 3.25 GeV/c per nucleon.* Phys. At. Nucl. , 2008. **71**: p. 405.
96. V. V. Glagolev *et. al.*, *isotope composition of fragments produced in high-energy 0-16 p interaction.* JETP *Lett.*, 1993. **58**: p. 497.

97. V. V. Glagolev *et. al.*, *Formation of the mirror nuclei 3H and 3He in 16Op collisions at a momentum of 3.25 GeV/c per nucleon.* Phys. At. Nucl., 2007. **70**(3): p. 421-426.

98. Khusniddin K. Olimov Qasim Ali Mahnaz Q. Haseeb Atif Arif Sagdulla L. Lutpullaev BS. Yuldashev, *Phenomenological analysis of rapidity distribution of negative pions in central $^{12}C$+ $^{12}C$ collisions at Sqrt. $S_{NN}$=3.14GeV.* International Journal of Modern Physics E, 2015. **24**(06): p. 1550049.

99. M. Anikina, *The analysis of π– mesons produced in nucleus-nucleus collisions at a momentum of 4.5 GeV/c nucleon in light front variables* Eur. Phys. J. A, 2000. **7**: p. 139.

100. L. Bravina, *Fluid dynamics and quark gluon string model: What we can expect for Au+Au collisions at 11.6 A GeV/c* Nucl. Phys. A, 1994. **566**: p. 461.

101. Akhtar Iqbal Khusniddin Olimov Mushtaq Ahmad Ali Zaman Obaidullah Jan B. S. Yuldashev, *Centrality and rapidity dependences of negative pions in He-C collisions at 4.2 A GeV/c.* Modern Physics Letters A, 2019. **33**: p. 19.

102. NA44 Collaboration (I. G. Bearden et al.), *Collective Expansion in High Energy Heavy Ion Collisions.* Phys. Rev. Lett., 1997. **78**: p. 2080.

103. L. Chkhaidze *et. al.*, *Collective flow of protons and negative pions in nucleus–nucleus collisions at momentum of 4.2–4.5 A GeV/c.* Nucl. Phys. A., 2007. **794**(1-2): p. 115-131.

104. L. Chkhaidze T. Djobava A. Galoyan, *Collective flows of protons and π− mesons in 2H+ C,Ta and He+C, Ta collisions at 3.4 GeV/nucleon.* Phy. Rev. C., 2011. **84**(6).

105. L. Chkhaidze T.D. Djobava L. L. Kharkhelauri E. N. Kladnitskaya A. A. Kuznetsov, *Study of collective flow effects in CC collisions at a momentum of 4.2 GeV/c per nucleon.* Phys. At. Nucl., 2004. **67**: p. 693-702.

106. KH. K. Olimov and M. Q. Haseeb, *On spectral temperatures of negative pions produced in $d^{12}C$, $^{4}He^{12}C$, and $^{12}C^{12}C$ collisions at 4.2 A GeV/c* Phys. At. Nucl., 2013. **76**: p. 595-601.

107. L. Chkhaidz T. Djobava L. Kharkhelauri and M. Mosidze, *The comparison of characteristics of pi- mesons produced in central Mg-Mg interactions with the quark gluon string model predictions.* Eur. Phy. J. A., 1998. **1**: p. 299-306.

108. D. Armutlisky *et. al.*, *"Multiplicity, momentum and angular distributions of protons from the interactions of p, d, α and C with carbon at 4.2 GeV/c/nucleon momentum",. Z. Phys. A*, 1987. **328**: p. 455-461.

***List of Publications of Akhtar Iqbal***

This thesis is based on the following publications.


[1] Akhtar Iqbal, Khusniddin Olimov, Mushtaq Ahmad, Ali Zaman, Obaidullah Jan, B. S. Yuldashev, *Centrality and rapidity dependences of negative pions in He-C collisions at 4.2 A GeV/c*. Modern Physics Letters A, 2019. **33**, p. 19.
doi.org/10.1142/S0217732319500925

[2] Akhtar Iqbal, Khusniddin K. Olimov, Mushtaq Ahmad,Sh. Z. Kanokova,Sagdulla L. Lutpullaev, Alisher K. Olimov, Kadyr G. Gulamov, Sh. D. Tojimamatov, Bekhzod S. Yuldashev, "*Collision centrality dependencies of charged pion production in $^{12}C$+$^{181}Ta$ collisions at 4.2 A GeV/c".* International Journal of Modern Physics E, 2018. **27**, p. 12.
DOI:10.1142/S0218301318500921

[3] Kosim Olimov,Akhtar Iqbal**,**Khusniddin K. Olimov, Sagdulla L. Lutpullaev, Alisher K. Olimov, Bekhzod, S. Yuldashev, KG. Gulamov, "*Correlations between production of charged pions and formation of light nuclei in $^{16}Op$ collisions at 3.25AGeV/c".* International Journal of Modern Physics E, 2017. **26,** p. 1750033.
DOI: 10.1142/S0218301317500331

[4] Akhtar Iqbal**,** Khusniddin K. Olimov, Imran Khan, BS. Yuldashev, Mahnaz Q. Haseeb, *On centrality and rapidity dependences of transverse momentum spectra of negative pions in $^{12}C$+ $^{12}C$ collisions at 4.2 GeV/c per nucleon.* International Journal of Modern Physics E, 2014. **23**(09): p. 1450047.
DOI:10.1142/S0218301314500475

[5] Kh. K. Olimov Akhtar Iqbal, B. S. Yuldashev *et. al.*, *On transverse momentum spectra of negative pions in $^{12}C$+$^{181}Ta$ collisions at 4.2A GeV/c.* Int. J. Mod. Phys. E., 2014. **23**: p. 1450084-1-22.
DOI:10.1142/S0218301314500840

[6] Kh. K. Olimov Akhtar Iqbal, V. V. Glagolev and Mahnaz Q. Haseeb, *Analysis of rapidity spectra of negative pions in d+$^{12}C$,$^{12}C$+$^{12}C$, and $^{12}C$+$^{181}Ta$ collisions at 4.2 GeV/c per nucleon.* Phy. Rev. C., 2013. **88**: p. 11.
DOI:10.1103/PhysRevC.88.064903

[7] Kh. K. Olimov,Akhtar Iqbal, B. S. Yuldashev *et. al*, *Centrality Dependences Of Soft and Hard Components Of $P_t$ Distributions Of Negative Pions In $^4He$+$^{12}C$ Collisions At 4.2A GeV/c.* Int. J. Mod. Phys. E., 2015. **24**(05): p. 24.

DOI:10.1142/S0218301315500366

[8] Kh. K. Olimov, Akhtar Iqbal *et. al.*, *Centrality and system size dependences of temperatures of soft and hard components of $p_t$ distributions of negative pions in $^4He+^{12}C$, $^{12}C+^{12}C$, and $^{12}C+^{181}Ta$ collisions at $\sqrt{s_{NN}}$ = 3.14 GeV.Phy. Rev. C.*, 2015. **92** p. 16.
DOI:10.1103/PhysRevC.92.024909